SHEET FORMING AND FORGING OF

Zn-Al ALLOYS.

TO MY PARENTS

SHEET FORMING AND FORGING OF Zn-Al ALLOYS

by

J. A. Forster, B.Sc.

A Thesis

Submitted to the Faculty of Graduate Studies

in Partial Fulfilment of the Requirements

for the Degree

Master of Engineering

McMaster University

June 1974

MASTER OF ENGINEERING (1974)
(Production)

McMASTER UNIVERSITY
Hamilton, Ontario

TITLE: SHEET FORMING AND FORGING OF Zn-Al alloys.

AUTHOR: James Allam Forster, B.Sc. (Hons.)
University of Manchester Institute of Science and Technology.

SUPERVISOR: Dr. J.L. Duncan

NUMBER OF PAGES: xiv, 152

SCOPE AND CONTENTS:

A brief introduction to superplasticity is presented.

The forming of superplastic sheet into a rectangular trough is examined and the thickness distribution theoretically determined. Figures, dependent on the height to width ratio of the trough, are presented of the thickness variation against a suitable geometric parameter.

Experiments have been performed on the forming of superplastic Zn-Al into a flat bottomed cylindrical cavity. A semi-empirical analysis based on the theoretical work of Cornfield and Johnson is presented and the theoretical and experimental thickness distributions compared.

The closed die forging of superplastic and conventional Zn-Al eutectoid alloys is examined. The results of experiments are presented and a two phase forging cycle, suitable for rate dependent materials, is presented.

ACKNOWLEDGEMENTS

I wish to acknowledge the assistance, guidance and continual encouragement of my supervisor, Dr. J.L.Duncan.

The help of John Grach and numerous other people at Noranda Research Centre is gratefully acknowledged in connection with the sheet forming work performed during the summer of 1973.

The material for the forging experiments was supplied by Cominco Limited to whom I extend my appreciation.

The financial support granted by the National Research Council is gratefully acknowledged.

A public word of thanks is extended to John Stannard for his diligent proof-reading of the original manuscript and to Laurie Jacobson for her typing of the same.

Thanks are also due to fellow students for making this period at McMaster University a very happy experience.

TABLE OF CONTENTS

LIST OF FIGURES

LIST OF SYMBOLS

b - half the width of a long rectangular trough

c_m - edge thickness constant

c_m' - pole thickness constant

h_o - original depth of die

k - constant in constitutive equation $\sigma = k\dot{\varepsilon}^m$

m - strain rate sensitivity

$\bar{p}$ - mean extrusion pressure

P_c - steady state extrusion pressure when cross-sectional area is that of the container

P_p - steady state extrusion pressure when cross-sectional area is that of the punch

r - radius of cylindrical die

R_o' - radius of deforming membrane when material first starts adhering to the sides and bottom of a rectangular die

s_e - edge thickness

s_p - pole thickness of a hemispherical dome when forming into a cylindrical die

s_o' - uniform sheet thickness when deforming membrane first starts adhering to the sides and bottom of a rectangular die

$\bar{s}$ - mean hemispherical dome thickness when forming into a cylindrical die

s - uniform current thickness of deforming membrane when forming into a rectangular trough

s_o - original sheet thickness

T - absolute temperature

u - distance, measured from the centre-line of a rectangular trough to the point of contact of the sheet when material is adhering to the bottom of the die only

v_o - punch velocity

x - current height

ϕ - extrusion parameter

$\dot{\epsilon}$ - strain rate

σ - flow stress

α_o - tangent angle when material first touches the bottom of a shallow trough $(h_o/b \quad 1)$

α - current tangent angle when material is adhering to the bottom of a rectangular die only

CHAPTER ONE

INTRODUCTION

1.1 Definition

Superplasticity has been defined by various authors to be "the unusual ability of metals to flow with the fluid-like characteristics of hot polymers and glasses".[1] Perhaps a less glamorous but more rigorous definition is that given by Duncan[2], "Superplasticity is a hot metal working phenomenon exhibited by certain alloys; it is characterized by an unusually low plastic flow stress and high rate sensitivity."

The rate sensitivity may be a new term to some readers but will be explained in detail under a separate heading.

Regardless of the definition, the pronounced property of these alloys is their ductility which is well in excess of conventional metals as shown in Fig. 1.1.

1.2 Historical Background

Rosenhain et al[3] in 1920 noted that heavily worked Zn-Al-Cu tertiary eutectic alloy ceased to behave like a normal crystalline material but more like a viscous solid such as pitch. This observation was followed in 1934 by an extensive paper on the properties of some Pb-Sn alloys by Pearson.[4] He noted that under certain conditions extremely large

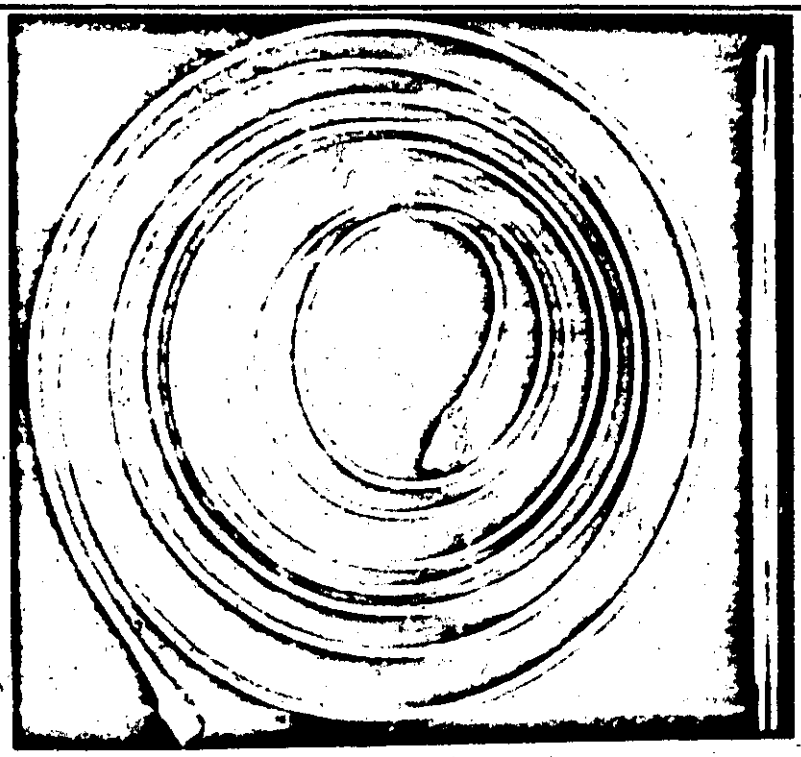

FIGURE 1.1
Photograph showing the extraordinary extensions possible with the superplastic alloys, from ref 4.

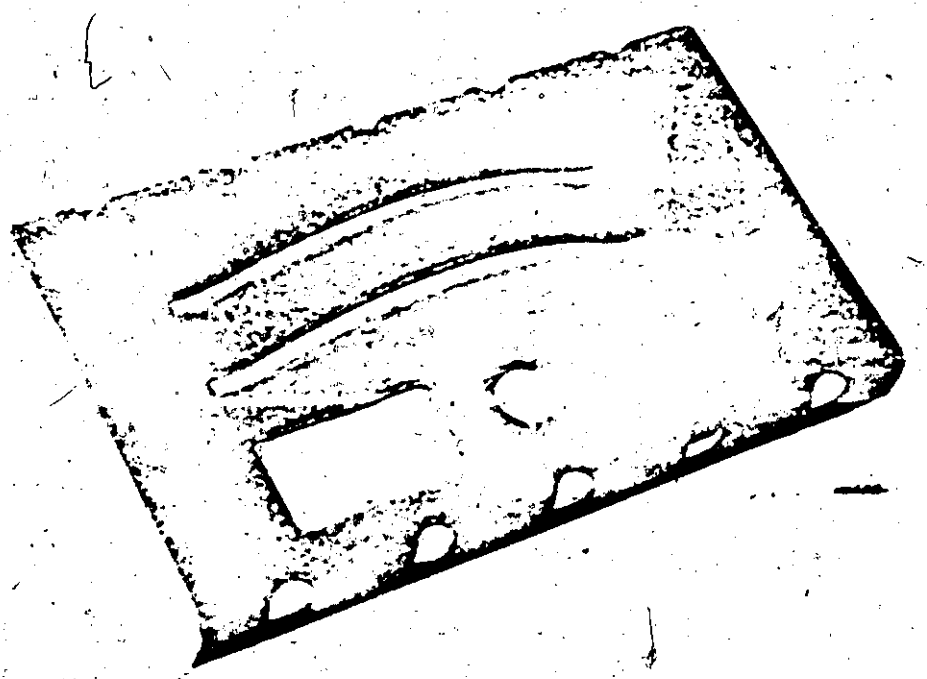

FIGURE 1.3

One of 1400 control plates manufactured by I.S.C. Alloys for Scammell lorries, from ref.39.

elongations were possible.

In the nineteen-forties and fifties, little attention was paid to the observations of either Rosenhein or Pearson by investigators in the western world. The Russians, however, were examining the characteristics and reasons for this observed phenomenon and a number of papers were published, in Russian, concerning this work.[5-8]

In 1962, Underwood[9] published a review of the previous investigators' work and in the course of translation from the Russian papers, the rather ambiguous term 'superplasticity' was adopted. Since polymers, phenolics, polyesters, polyurethanes and many other organic materials are grouped together and termed 'plastics', the term 'superplastic' can obviously lead to confusion since it defines a phenomena which is metallic in origin.

Following the review by Underwood, considerable interest was focused on the subject by both academics and industrialists. Backofen[1,10-13] and his co-workers did much of the basic research to determine a mathematical model to describe the material behaviour and more important, to determine the necessary conditions for superplasticity. In an early paper, Avery and Backofen[10] proposed some metallurgical reasons for the phenomenon.

In the last ten years, superplasticity went through a phase of being a 'popular' research area and as a consequence

the subject is now well documented, the review paper by Johnson[14] in 1970 quoted 191 references.

Much of this early work dealt with superplasticity in the lower melting point alloys, especially the Pb-Sn systems.[4,10,15-18] While these alloys are truly superplastic and useful model materials, they are too soft at room temperature to be of industrial significance. The eutectoid Zinc-Aluminium (78% Zn - 22% Al) has also been studied extensively[1,19-22] and is the most promising of the superplastic alloys.

1.3 Commercial Applications

Following the work of Backofen mentioned earlier, I.B.M. began investigating the commercial applicability of superplastic alloys, resulting in the use of the Zn-Al alloy for some production components, Figure 1.2

This alloy is readily available on the American continent in sheet or billet form and costs $1.00 a pound; the alloy is produced in Canada by Noranda and Cominco, although each concern markets its own 'variety' of the alloy. The European markets seem to have been captured by Imperial Smelting Corporation in England who market an alloy called SPZ. This company has met with some commercial success on a production basis, Figure 1.3 shows one of 1400 control panels manufactured for Scammell lorries. Figure 1.4 shows some of the components which this firm have made on a

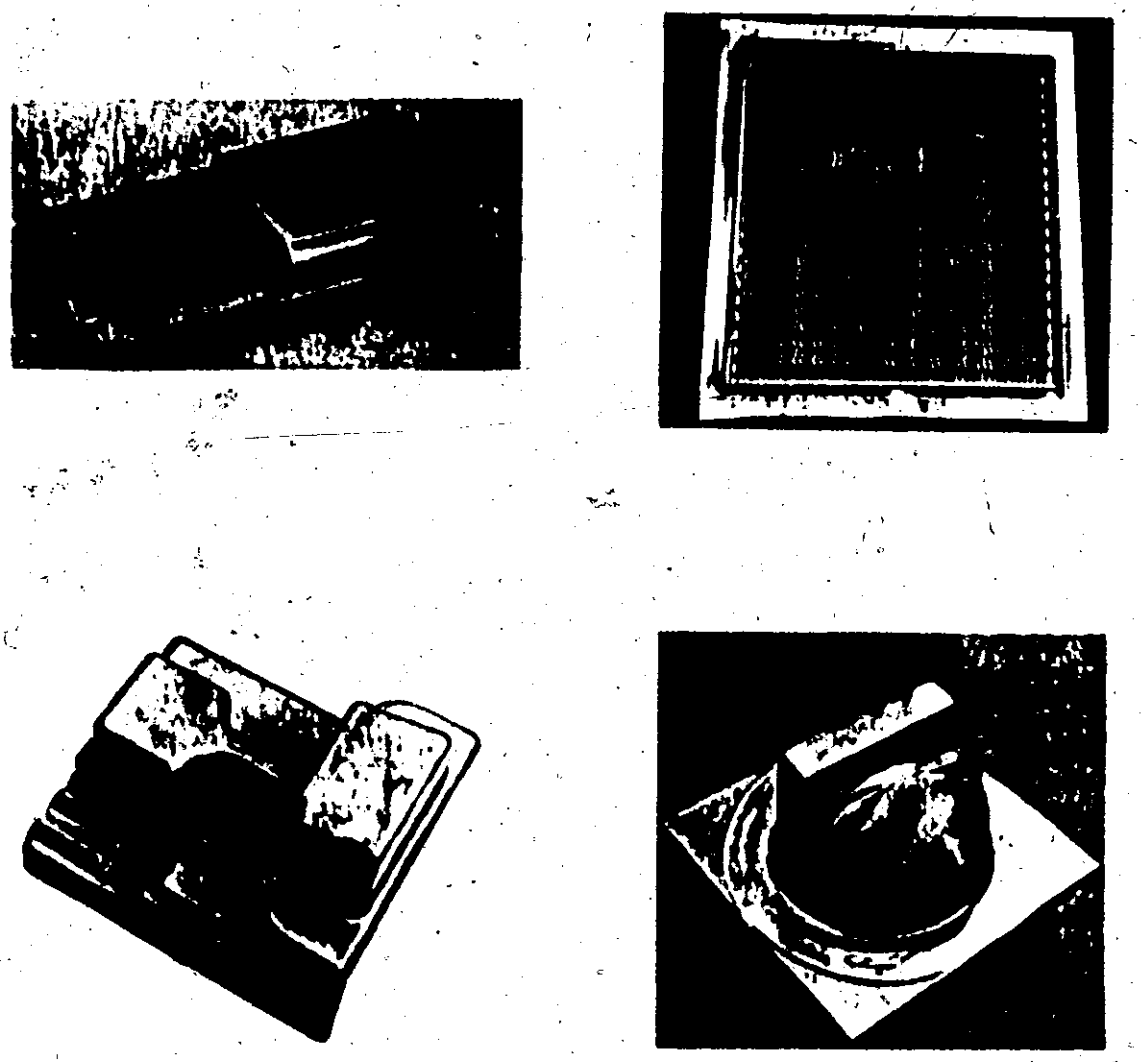

FIGURE 1.2
Some parts made by I.B.M. from superplastic Zn-Al sheet, from ref. 40

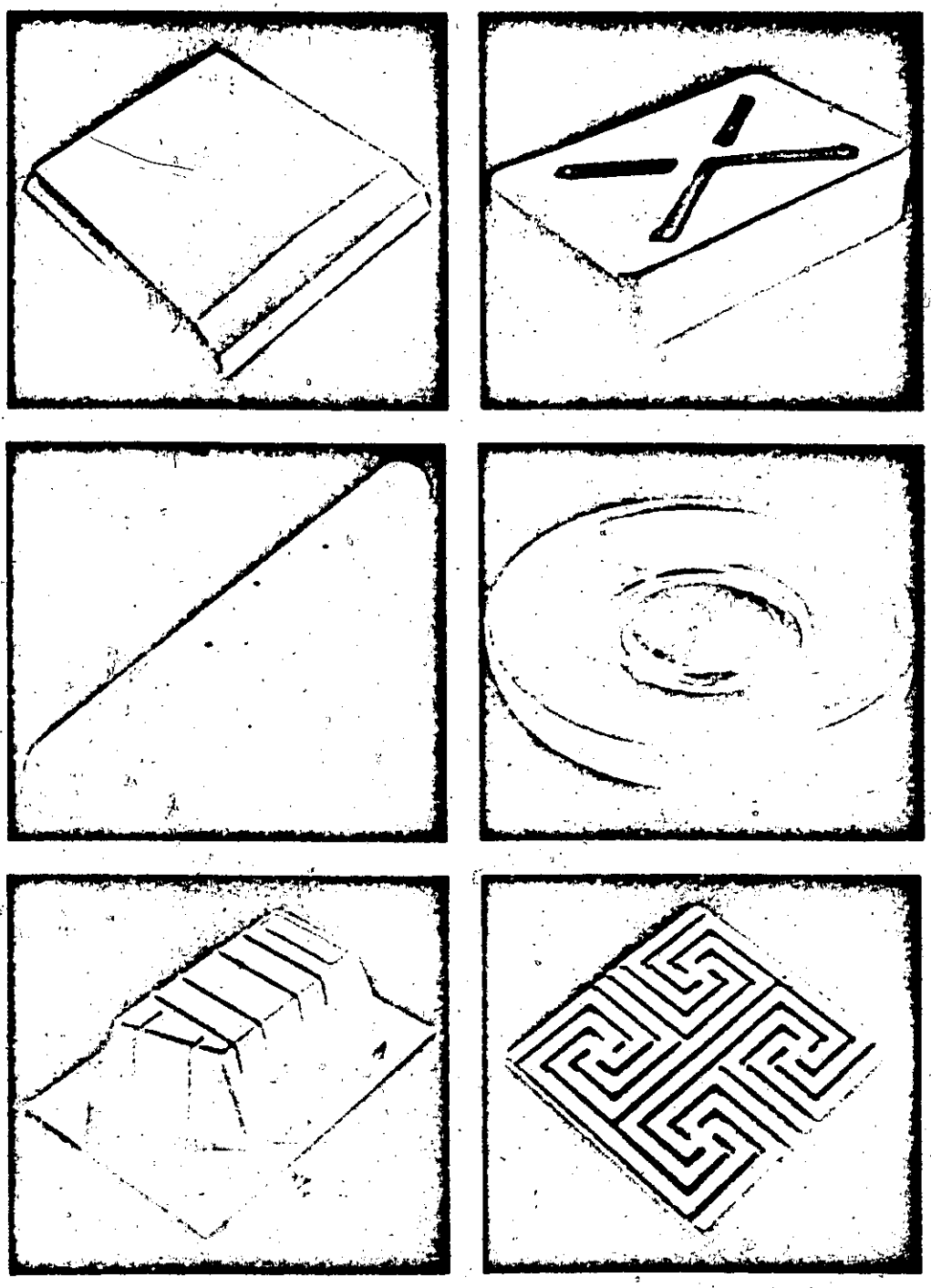

PIGURE 1.4

Some parts produced by I.S.C. Alloys Ltd. Great Britain, from ref 39.

prototype scale.

One field of application which is currently making substantial use of superplastic alloys is that of prototype evaluation. A recent project undertaken by the Centre of Applied Research and Engineering Development at McMaster University and McMaster Medical Centre, indicates the significant savings which can result from the use of this alloy [23]. Figure 1.5 shows one of the 150 units manufactured from a superplastic Zn-Al alloy.

The industrial applications seem to have been concerned primarily with the forming of superplastic sheet, by either vacuum or pressure forming techniques and processes somewhat similar to those used in the plastics industry. Until recently, little commercial or academic attention has been focused on bulk forming techniques, ie. forging, compression molding. An excellent paper on superplastic forging has been published by Stewart[36], Figure 1.6 shows the part he manufactured to demonstrate the possibilities and, as can be seen, this part has sharp corners and thin webs.

Again I.B.M. seems to have led the industrial research centres in examining the possible applications by manufacturing a number of prototype parts, as shown in Figure 1.7.

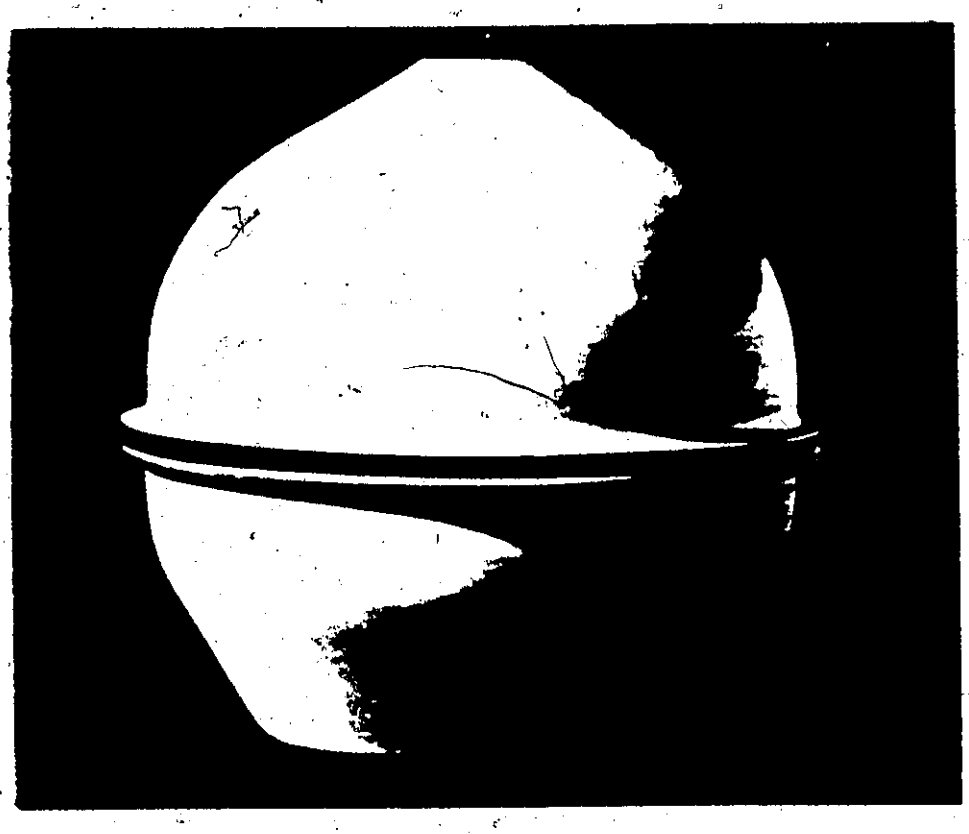

Figure 1.5

Prototype medication monitor made from Zn-Al, from ref. 23.

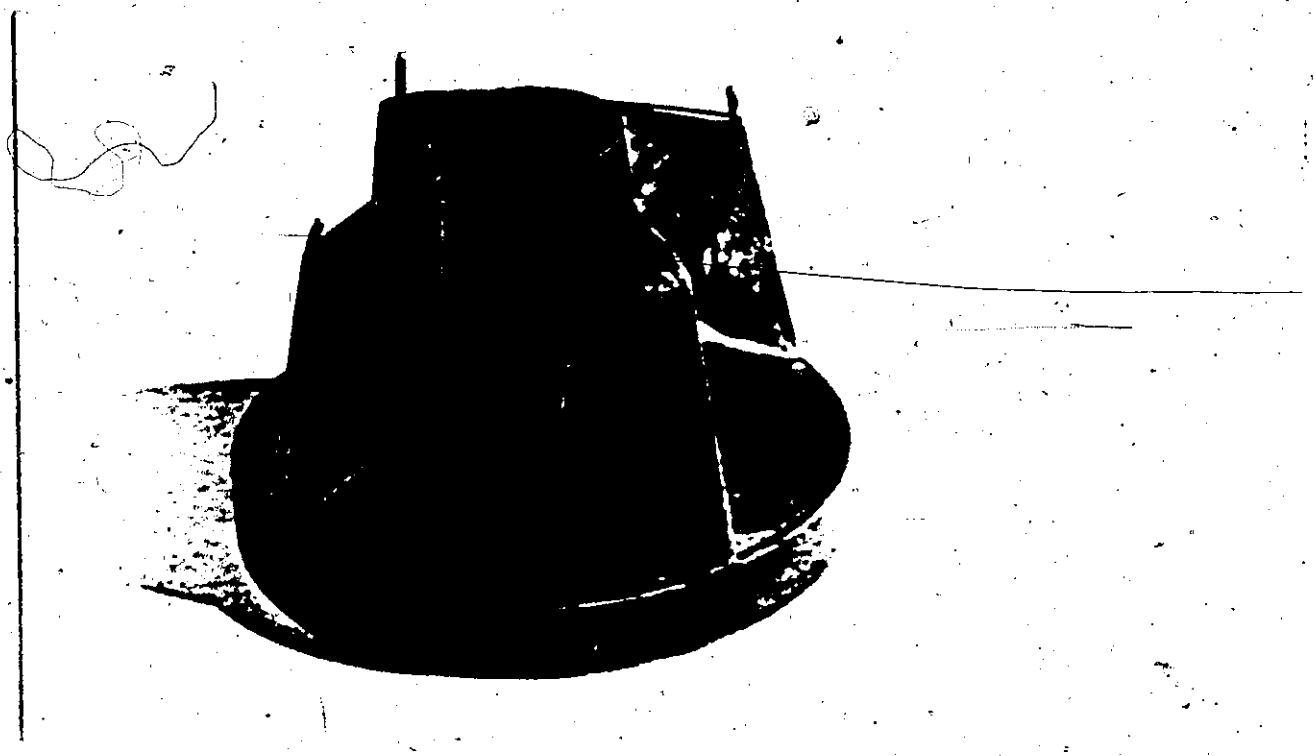

Figure 1.6

Demonstration part forged in Zn-Al, from ref. 36.

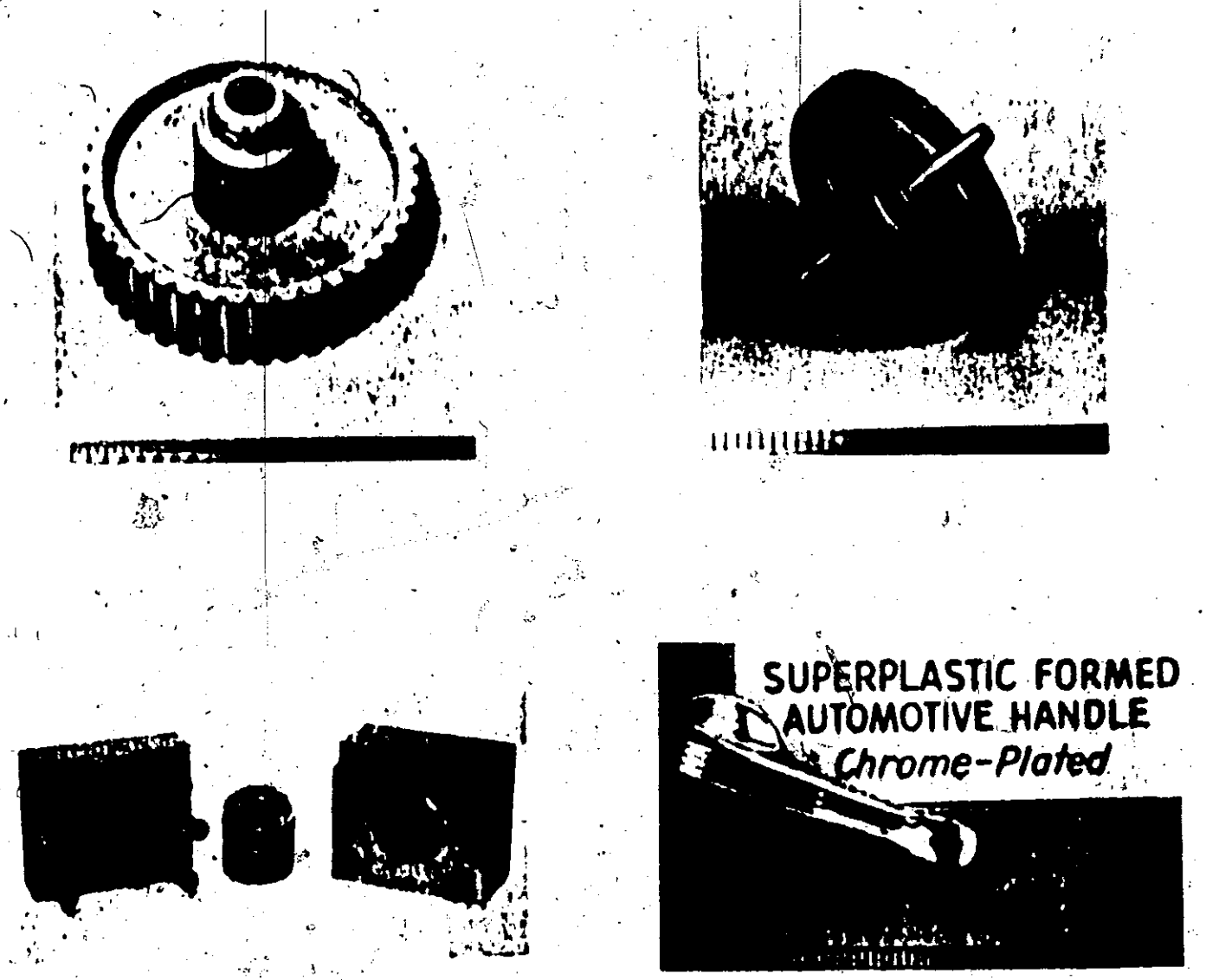

FIGURE 1.7

Some parts forged by I.B.M. from superplastic Zn-Al, from ref. 40

1.4 Scope of Present Work

From the preceeding it will be appreciated that superplastic forming techniques are now commercially viable. The processes used are primarily tensile in nature, making use of the large neck free elongations possible with these alloys. The thickness can thus vary from point to point in the formed part. The thickness distribution is consequently of prime importance and a simple method of prediction is of obvious industrial value.

In this thesis, an elementary analysis is presented for the forming of superplastic alloy sheet into two commonly encountered geometric shapes,

1) the forming into a long rectangular trough

2) the forming into a flat bottomed cylindrical die.

Experiments were then performed to compare the theoretical results with experimental findings.

To examine the bulk forming properties of superplastic alloys, experiments were performed which examined some aspects of closed die forging. This work is presented in the ensuing chapters of this thesis. It is, however, necessary to give a brief background to the subject and this is done in the next chapter.

CHAPTER TWO

SUPERPLASTICITY

2.1 Types of Superplasticity

Two basic mechanisms of superplastic behaviour have been recognized;

i) Environmental Superplasticity

Environmental superplasticity is observed in certain alloys which are thermally cycled about a phase transformation temperature. The most common example of this form of superplasticity is the thermal cycling of steel between the ferrite and austenite phases at 900°C. Elongations of 500% have been obtained using this technique.[24]

ii) Micrograin Superplasticity

Superplastic behaviour is associated with a stable, ultra-fine equiaxed grain structure, usually less than 10 microns ($m \times 10^{-6}$). This is an isothermal process at approximately half the absolute melting point of the material. This type of superplasticity is of greater industrial importance since there is no need to cycle the temperature, consequently, the majority of the published work deals with this type of superplasticity.

The work presented in this thesis deals only with micrograin superplasticity. Table 2.1 is a list of materials

MATERIAL	REPORTED VALUES m	% elong.	TEMPERATURE °C
Cd-Zn eutectic	-	400	20
Sn-Pb eutectic	0.6	700	20
Sn-2%Pb	0.5	-	20-80
Sn-81%Pb	0.5	-	20-80
Sn	0.5	-	20
Sn-bi eutectic	0.2	1950	20
Sn-1%Bi	o.48	500	22
Sn-5%Bi	0.68	1000	20
Pb-5%Cd	0.35	-	20
Zn comercial)	0.2	400	20-70
Zn-0.2%Al	0.8	450	23
Zn-0.4%Al	0.43	550	20
Zn-ZnO_2 particles	-	120	26
Zn-W particles	-	100	26
Zn-4.9%Al eutectic	0.5	300	200-360
Zn-22%Al eutectoid	0.7	1500	200-300
Zn-40%Al	0.48	700	250
Mg (comercial)	-	80	-
Mg-0.5%Zr	0.3	150	500
Mg-6%Zn-0.5%Zr	0.6	1000	270-310
Mg-Al eutectic	0.8	2100	350-400
Al-Cu eutectic	0.9	500	440-520
Cu-38%Zn	0.5	300	450-550
Cu-10%Al-3%Fe	0.6	720	800
Cu-71.9%Ag	0.53	500	675
Ni	-	225	820
Ni-39%Cr-10%Fe	0.5	1000	810-980
Fe-25%Cr-6%Ni	-	600	870-980
Fe-C alloys	0.57	350	700
Low alloy steels	0.65	400	800-900
Cr-30%Co	-	160	1200
Co-10%Al	0.47	850	1200
Ti-5%Al-2.5%Sn	0.72	450	900-1200
Ti-4%Al-2.5%O	0.6	-	950-1050
Ti-6%Al-4%V	0.85	1000	800-1000
Ti-0.3% impurity.	0.8	-	900
Zircalloy	0.5	200	900
W-15% to 30%Re	0.46	200	2000

TABLE 2-1

Materials for which micrograin superplasticity has been observed, from ref. 49.

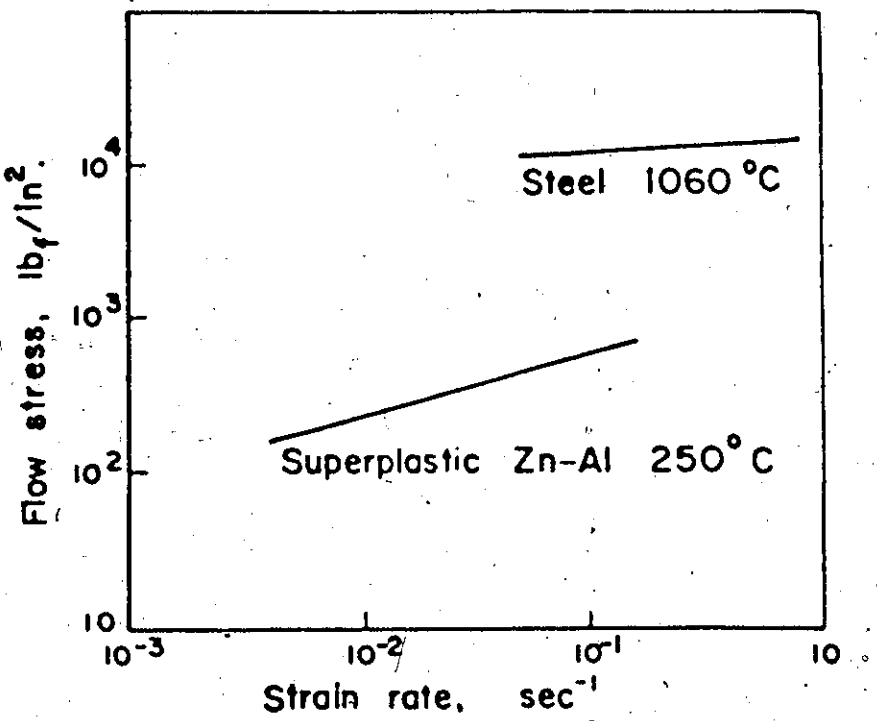

PIGURE 2.1

Flow stress, strain-rate curves for the hot working of steel and the forming of a superplastic alloy.

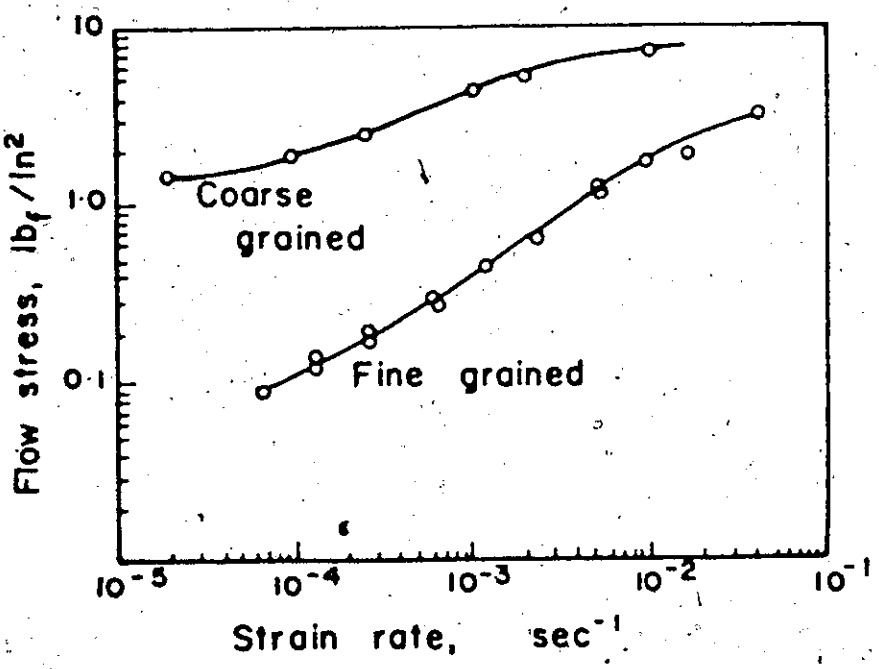

PIGURE 2.2

Stress, strain-rate behaviour for a coarse and fine grained material.

which have been rendered superplastic. Also indicated are those alloys which can be obtained commercially.

2.2 Constitutive Equation

In hot working processes, the stress strain behaviour of conventional alloys can be represented by an equation of the form

$$\sigma = k \varepsilon^{n} \dot{\varepsilon}^{m} \qquad \text{.....} (2.1)$$

where $\dot{\varepsilon}$ is the strain-rate and

m is the strain-rate sensitivity.

The value of m is usually small, 0.1 or less.

The deformation of superplastic alloys at the appropriate temperature, however, is remarkably independent of strain and Equation 2.1 reduces to

$$\sigma = k \dot{\varepsilon}^{m} \qquad \text{.....} (2.2)$$

where m is in the range

$$0.3 < m < 0.8$$

Figure 2.1 compares the behaviour of a superplastic alloy and a conventional alloy at the superplastic forming and hot working temperatures respectively.

2.3 Factors Affecting Superplasticity

Equation 2.2 indicated previously to describe the material behaviour of a superplastic alloy is very simple

and is only really true for an isothermal process where the value of the constant k and the strain-rate sensitivity are known. The temperature is not the only variable and the following is a brief discussion of the variables and their significance.

2.3.1 Grain Size

The grain size and shape are important aspects of a superplastic material. The grains must be small, usually less than 10 microns, and the structure must be equiaxed.

At constant strain-rate and temperature , the flow stress σ is given by

$$\sigma \propto L^{b} \qquad \text{..... (2.3)}$$

where L is the grain size. The exponent b has been reported as lying in the range 0.7 to 1.2.[26,27]

For the cold working of conventional materials the equation governing the deformation is that suggested by Petch[28],

$$\sigma \propto (L)^{-\frac{1}{2}} \qquad \text{..... (2.4)}$$

It will be seen that from this relationship as the grain size is reduced, the flow stress increases. This trend is very different from that indicated by Equation 2.3. and Figure 2.2.

2.3.2 Temperature

Superplastic deformation occurs at approximately 40% of the absolute melting point of the material.

Figure 2.3 shows the variation of the flow stress with temperature for a superplastic Zn-Al alloy. The flow stress decreases as the temperature increases, however, at 276°C., the transformation temperature, there is a marked increase in flow stress.

The behaviour of the same Zn-Al alloy in the annealed state is also shown in Figure 2.3.

2.3.3 Strain-Rate Sensitivity, m

The strain-rate sensitivity or 'm' value of an alloy is one method of alloy clarification, if $m>0.3$, the material is considered to be superplastic. The 'm' value is determined experimentally from the slope of a log stress vs. log strain-rate curve.

The strain rate sensitivity is the controlling parameter in the growth of an instability and it is this fact which enables the characteristically large neck free elongations of the superplastic alloys. Figure 2.4 shows the effect of m on the deformation of a tensile specimen. Two materials are considered having strain-rate sensitivities of $m=0.1$ and $m=0.6$ corresponding to the hot working of a

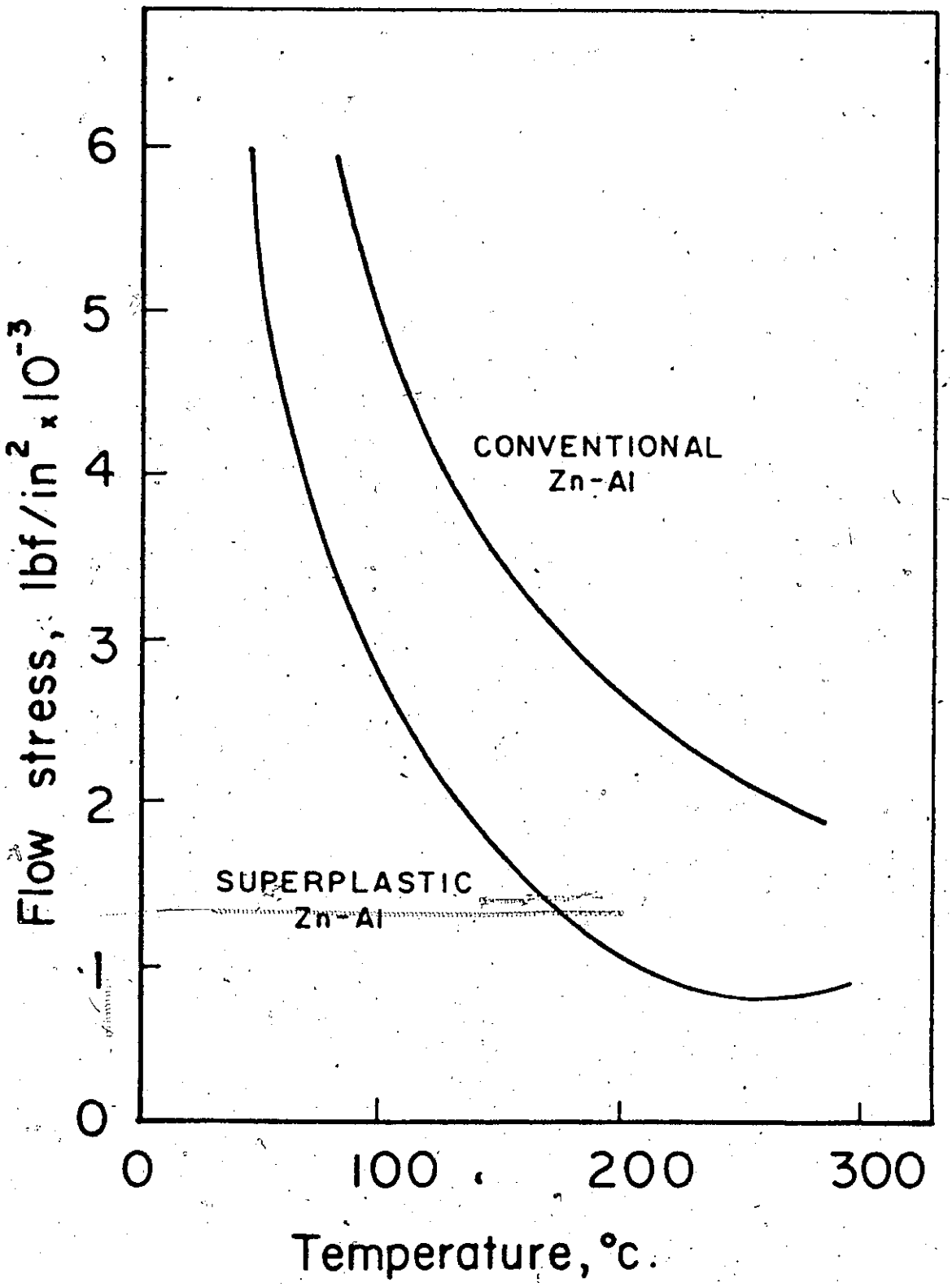

FIGURE 2.3

Variation of flow stress with temperature for Zn-Al in the superplastic and annealed states, derived from ref. 43.

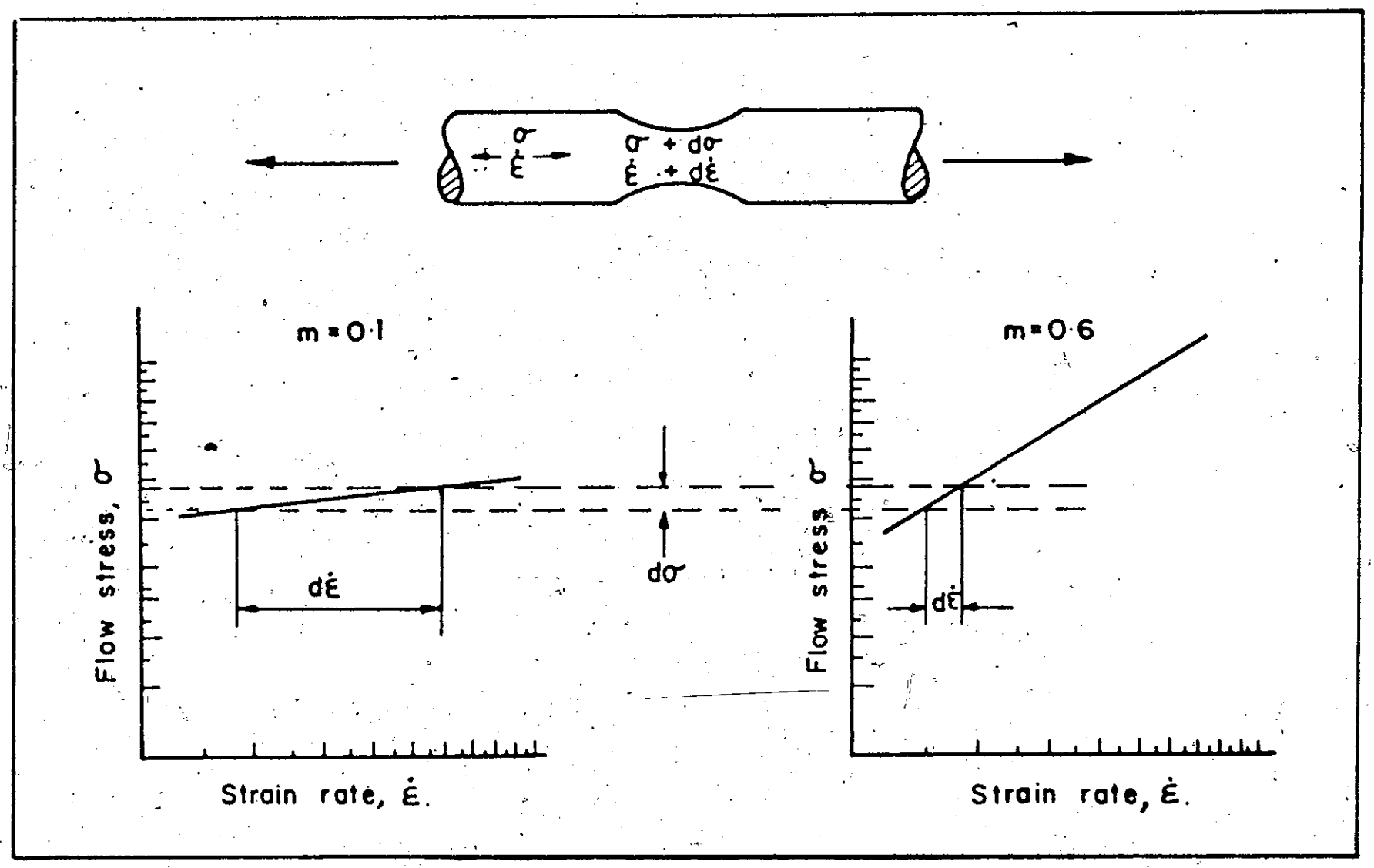

FIGURE 2.4

Schematic figure indicating the effect of 'm' on the growth of instabilities.

steel and a superplastic material respectively. Both materials are assumed to have no strain hardening capacity.

In the tensile bar, necking will be initiated at some point and within the necking region the stress will increase by an amount $d\sigma$ due to the difference in the cross-sectional area dA.

For an equal difference in area, the difference in stress will be the same for both materials. The increase in strain-rate $d\dot{\varepsilon}$, however, will be different depending on the slope of the $\log \sigma$, $\log \dot{\varepsilon}$ curve, ie. on m.

When m is small, as in hot working, $d\dot{\varepsilon}$ is large and the instability grows quickly, failure occurs for small total strains of the specimen. For a superplastic material with a high 'm' value, the increase of strain rate $d\dot{\varepsilon}$ is smaller and the growth of the instability is consequently smaller enabling large total elongations before failure.

As m approaches unity, the growth of instabilities is reduced until finally a small difference in area has no effect on the strain-rate gradient along the bar. This is a viscous fluid.

The industrial manufacturers of superplastic alloys are consequently interested in producing an alloy with a high m value. Unfortunately the strain-rate sensitivity is dependent upon a number of variables,

a) Strain-rate

The variation of the m value with strain rate is shown in Figure 2.5 and it is clear from this graph why superplastic forming processes are confined to a certain strain-rate regime if full use is to be made of the superplastic property. If the strain-rate is increased to normal metal forming rates, the m value decreases and the material behaves like a conventional alloy. If the strain-rate is decreased and we approach strain-rates common in creep forming, then again the m value decreases. Table 2-2 indicates a number of common metal working processes and an approximate strain-rate for the process.

b) Temperature

It was indicated in Section 2.3.2, and Fig. 2.3, that the flow stress of a superplastic alloy is temperature dependent. Figure 2.6, from the work of Backofen et al shows the dependence of the strain-rate sensitivity upon temperature. The step change of the m value at the transition temperature is clearly indicated.

From the preceeding paragraphs it is clear that Equation 2.2 is a very simple expression when one considers the variables involved. More complex equations have been proposed, for example

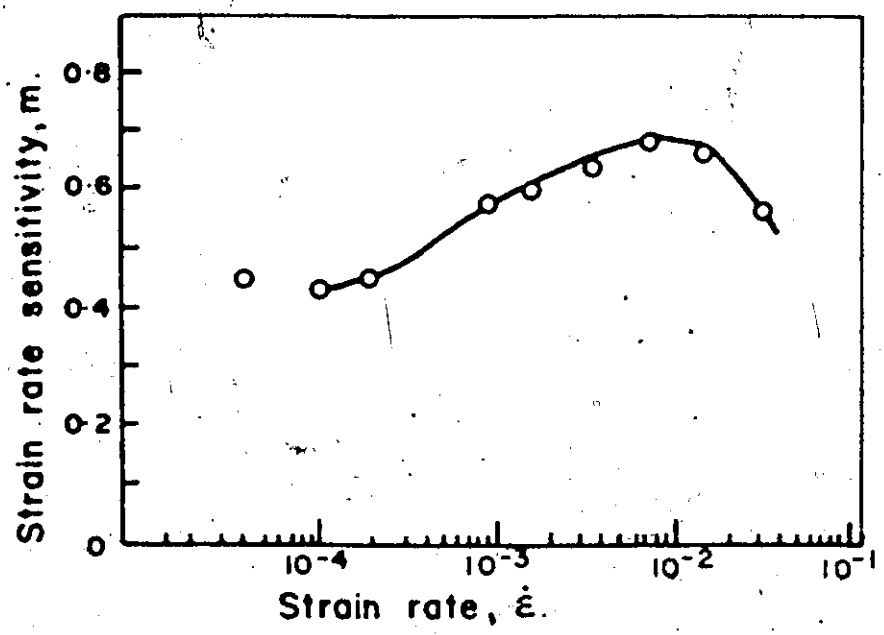

FIGURE 2.5

Variation of strain-rate sensitivity, m, with strain-rate, from ref. 11.

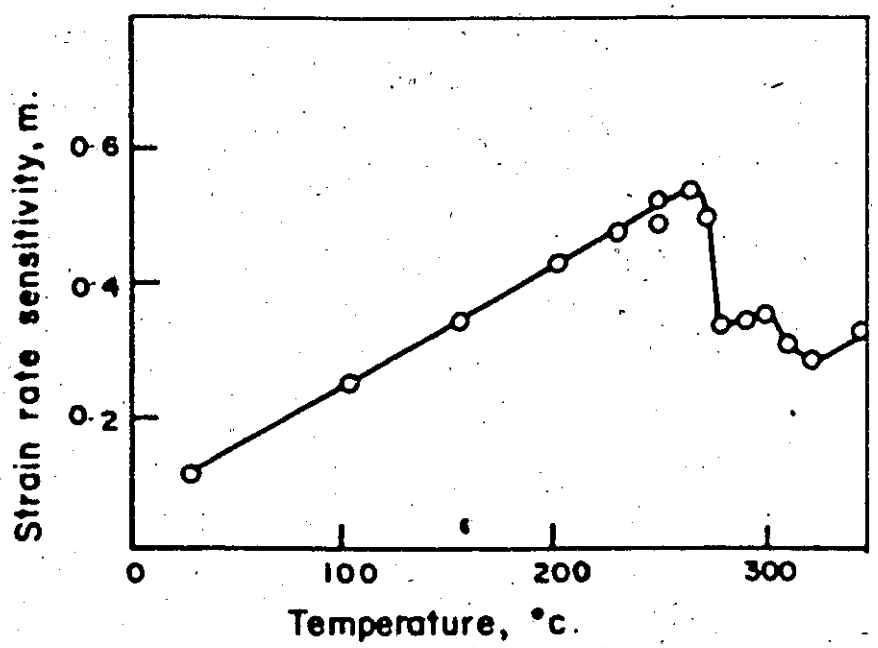

FIGURE 2.6

Variation of strain-rate sensitivity, m, with temperature, from ref. 48.

PROCESS	STRAIN RATE (per sec.)
Superplastic deformation	10^{-4} to 10^{-1}
Creep	10^{-10} to 10^{-5}
Normal hot working process	1 to 10^{2}
Machining, (cutting speed 80 ft/sec).	10^{4}
Explosive forming	10 to 10^{2}
Explosive welding	10^{5}

TABLE 2-2.

Table indicating the strain rates in a number of common metalworking process, from ref. 38.

$$\dot{\varepsilon} = c \cdot \frac{\sigma^n}{L^a} \exp\left\{\frac{-Q}{KT}\right\}$$

where, c is a constant,

n is the strain rate sensitivity ($\frac{1}{m}$),

L is the grain size,

Q is the activation energy,

K is the Boltzmann constant,

T is the temperature.

However, Equation 2.2 is a simple and useful engineering relationship in the analysis of the deformation of superplastic alloys.

2.4 Mechanisms of Superplastic Deformation

In spite of intensive efforts, the basic mechanism of superplastic flow is not yet fully understood. Any proposed mechanism must be capable of explaining the low value of m in regions I and III of Figure 2.7, which is a schematic representation of the material behaviour.

A number of mechanisms have been proposed and the more important of these are,

1) grain boundary sliding
2) diffusional creep
3) dynamic recrystallization.

It would appear, however, that none of these mechanisms

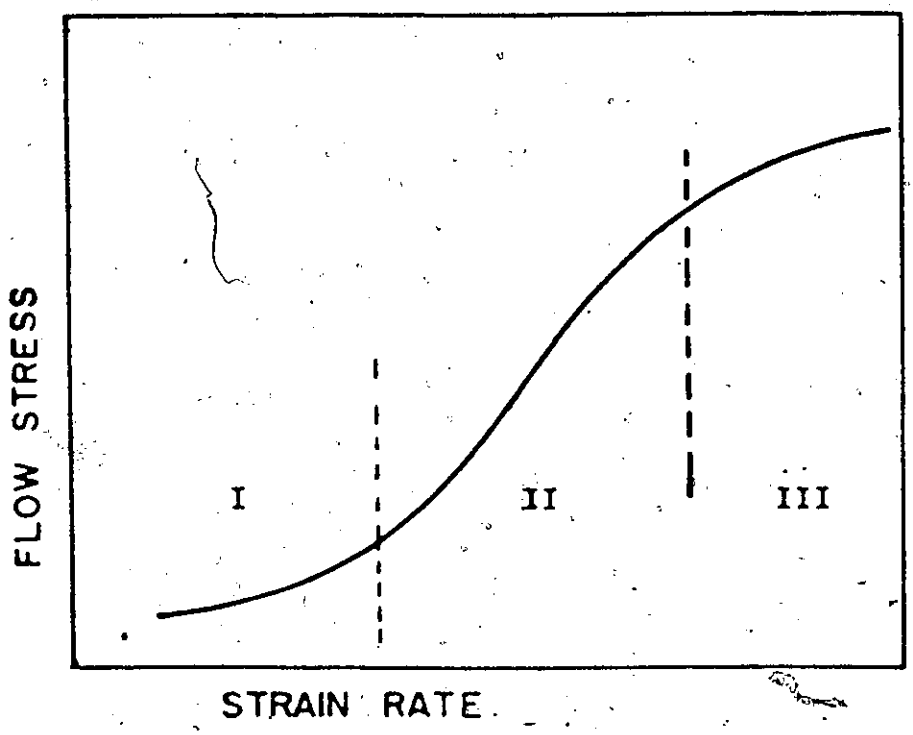

FIGURE 2.7

Schematic log. stress v's log. strain-rate for a superplastic alloy.

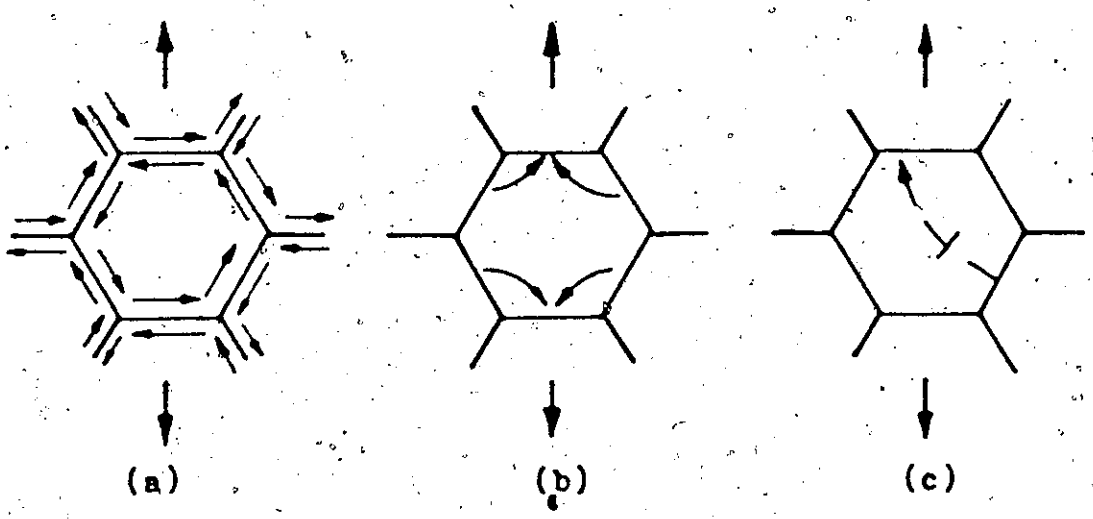

FIGURE 2.8

Mechanisms of deformation; a) Grain boundary sliding b) Vacancy diffusion, c) Dislocation climb.

is capable of completely explaining the phenomena and that a combination of two or more is likely. Which mechanism is dominant in a particular condition is not clear and there has been much discussion concerning this subject.[10,11,44,45]

The basic mechanisms listed above are described briefly:

1) Grain Boundary Sliding

Deformation of this type is by the relative motion of grains by shear along their boundaries, as in Figure 2.8 a). A mathematical relationship of the form

$$\dot{\varepsilon} = c\,\frac{\sigma}{L}$$

has been suggested, where c is a constant, σ is the applied stress and L is the grain size.

The strain rates predicted by this equation are, however, much higher than experimentally observed values.

The characteristic lack of marked changes in either the grain size or shape in superplastically deformed alloys suggests that a high proportion of the strain is due to grain boundary sliding. It is clear, however, that the grains cannot rotate relative to one another without causing voids in the structure. It is thus necessary that any deformation by grain boundary sliding must be accompanied by some form of accomodating mechanism such as diffusion or slip. The question which now arises from a combination of deformation modes, is which mechanism controls the deformation rate?

2) Diffusional Creep

Under the action of an applied tensile stress, there is a vacancy migration as indicated in Figure 2.8 b). Vacancy migration can occur either through the body of the grain (Nabarro-Herring) or along the grain boundaries (Coble) and the controlling equations are:

Nabarro-Herring $$\dot{\varepsilon} = \frac{B_1}{L^2} \left\{\frac{V\sigma}{RT}\right\} D_l$$

Coble $$\dot{\varepsilon} = \frac{B_2}{L^3} \left\{\frac{V\sigma}{RT}\right\} D_{gb}$$

where B_1 and B_2 are constants, L is the grain size, V is the atomic volume and D_l and D_{gb} are the lattice and grain boundary diffusion constants.

Both equations predict a value of the strain rate sensitivity equal to unity which has never been observed experimentally. Also, it is implicit in both types of diffusion that the grains would tend to elongate in the direction of the applied tensile stress. There is, however, no grain elongation when alloys are deformed superplastically.

These discrepancies between the experimentally observed phenomena and the theoretical mechanism tend to indicate that this mechanism is not the controlling one for superplastic flow.

3) Dynamic Recrystallization

Based on the experimental observation that after

superplastic deformation there is little work hardening and the material appears to be in a fully recovered state, it has been proposed that a controlling mechanism could be that of dynamic recrystallization or recovery.

One possible mechanism of recovery is that of dislocation climb, indicated in Figure 2.8 c), where the dislocations climb through the structure of the grain to the grain boundary. At the grain boundary these dislocations are absorbed with the aid of vacancies, possibly formed by grain boundary diffusion.

It has been suggested that dynamic recrystallization is the softening mechanism and that it is initiated at regions of high local lattice strain. However, the characteristic periodic cycle of flow stress observed in the dynamic recrystallization during hot working has not been observed in superplastic deformation.

The foregoing paragraphs are a very brief summary of the major mechanisms now thought to be important in the study of superplastic flow. A more thorough survey is to be found in an excellent review paper by Johnson[46].

2.5 Room Temperature Properties

The majority of the research work on superplastic

alloys has been conducted at the forming temperature, which, for the Zn-Al system, is approximately 250°C. There has been a serious shortage of information however, on the room temperature properties of these alloys. Nuttall[20] has recently performed an extensive study on the room temperature properties of the Zn-Al eutectoid alloy and has shown that there is a significant decrease in hardness and flow stress with rolling reduction of the as-quenched alloy. After annealing there was an increase of hardness and, presumably, flow stress. This is clearly opposite to that normally observed in metals. Unfortunately, no table was presented by Nuttall which compared the mechanical properties of the material in various states.

The improvement of the creep resistance of the Zn-Al eutectic by additions of copper has been the subject of a paper by Naziri and Pearce[43] who concluded that an addition of 1% copper improved the room temperature creep resistance by a factor of 140. The majority of commercial alloys based on the Zn-Al system thus have small additions of copper to improve the creep properties.

Table 2-3 is a technical data sheet indicating some of the room temperature mechanical properties of a typical Zn-Al alloy in both the superplastic (rolled) condition and the annealed condition.

Properties		
Mechanical	**As-Rolled**	**Annealed and Air-Cooled**
Tensile Strength (psi)[a]	30,000 (approx.)	45,000 (approx.)
% Elongation [a]	100-200 %	10 %
Yield Strength (psi)[a]	20,000 (approx.)	40,000 (approx.)
Design Strength (psi)[b]	200	2,200
"m" Value	0.45 - 0.53	-
"R" Value (psi-min)	950 - 1,150	-
Rigidity	Superior to Plastics	

(a) With initial strain rate of 0.2 in./min. at room temperature

(b) 0.1% elongation in 10,000 hours. Alloy modifications can be made to provide higher design strengths.

Physical	**As-Rolled**	**Annealed and Air-Cooled**
Density	0.187 lb/in^3	0.187 lb/in.^{3}
Thermal Conductivity	-	85 BTU/hr/ft^2/°F.
Specific Heat	-	0.13 BTU/lb/°F.
Electrical Resistivity	-	5μ Ω-cm
Coefficient of Thermal Expansion (70°F - 200°F)	-	13.5μ in/in/°F.

TABLE 2-3

Technical data sheet indicating some of the room temperature properties of a comercial Zn-Al.

CHAPTER THREE

THEORETICAL ANALYSIS OF SHEET FORMING

3.1 Introduction

The forming of superplastic sheet material has been the subject of numerous experimental studies,[29,33] while the free forming of a circular sheet, clamped around the edge, has been analyzed theoretically.[30-32]

Processing techniques similar to those used within the plastics industry may be used to form superplastic alloys and Figure 3.1 illustrates some techniques suggested by Johnson et al.[35] Many of these are large strain tensile processes and the thickness can vary from point to point within the formed part. The thickness distribution is consequently of prime importance and in designing tooling and forming equipment it is an advantage to be able to predict this distribution.

This chapter is a theoretical analysis of the forming of superplastic sheet into two basic shapes;

i) the two dimensional forming of a sheet into an infinitely long rectangular cavity

ii) the axisymmetric forming of a sheet into a flat bottomed cylindrical die.

It was considered that these two shapes were the basis for

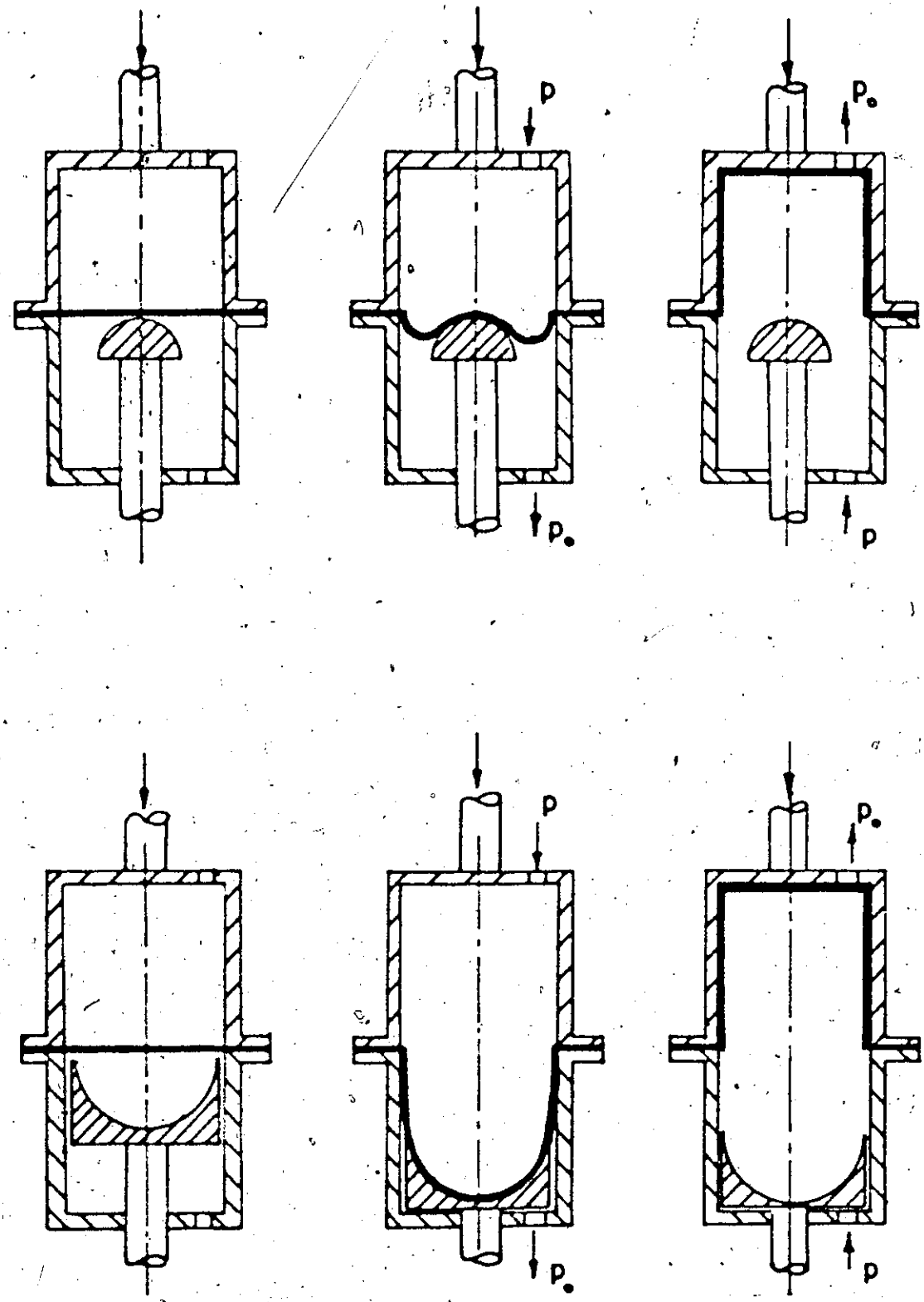

FIGURE 3.1

Some techniques suggested to form superplastic alloys, from ref. 35.

a majority of parts and that by a suitable combination of both theories the thickness distributions for many practical parts could be evaluated.

The thickness distribution for these parts are presented in the form of graphs of thickness ratio against an appropriate geometric parameter.

3.2 Forming Into an Infinitely Long Rectangular Trough

The case of a thin sheet being deformed into a long rectangular trough is examined and the following assumptions are made,

i) plane strain conditions exist

ii) the flexural strength is negligible

iii) after contacting the walls, the sheet does not slip or deform

iv) at any instant the unsupported membrane forms part of a circular arc of uniform thickness

v) the material is incompressible

vi) the material is isotropic

The sheet is consequently in one of two possible modes,

a) rigid material adheres to the die wall

or b) material is part of a cylindrical membrane deforming uniformly.

The transition from mode of deformation to the other is clearly at the point where the deforming membrane

contacts the die wall, as shown in Figure 3.2.

From the above it may be concluded that the thickness distribution of the formed part is a function only of die geometry.

3.2.1 Mechanics of Deformation

An examination of the deformation process indicates that there are three possible deformation modes dependent on the height to width ratio (h_o/b) of the die. These are,

i) The height is greater than half the width. ($h_o/b>1$)

The sheet forms a cylindrical membrane as shown in Figure 3.3 with successively smaller radii until it reaches a radius equal to b. Deformation continues with material adhering to the walls of the die as the cylindrical membrane, now of constant radius b, moves down. This continues until the membrane touches the bottom of the die, the point of contact of the sheet with the die wall being given by

$$h = h_o - b$$

As the deformation continues, the sheet adheres to both the wall and the bottom of the die as the radius of the membrane decreases. This situation is examined in case (ii).

ii) The height is equal to half the width. ($h_o/b=1$)

This is equivalent to the bulging of a sheet into a 90° v-groove as analyzed by Holt.[31] The cylindrical membrane touches the bottom of the die when it has formed to a radius

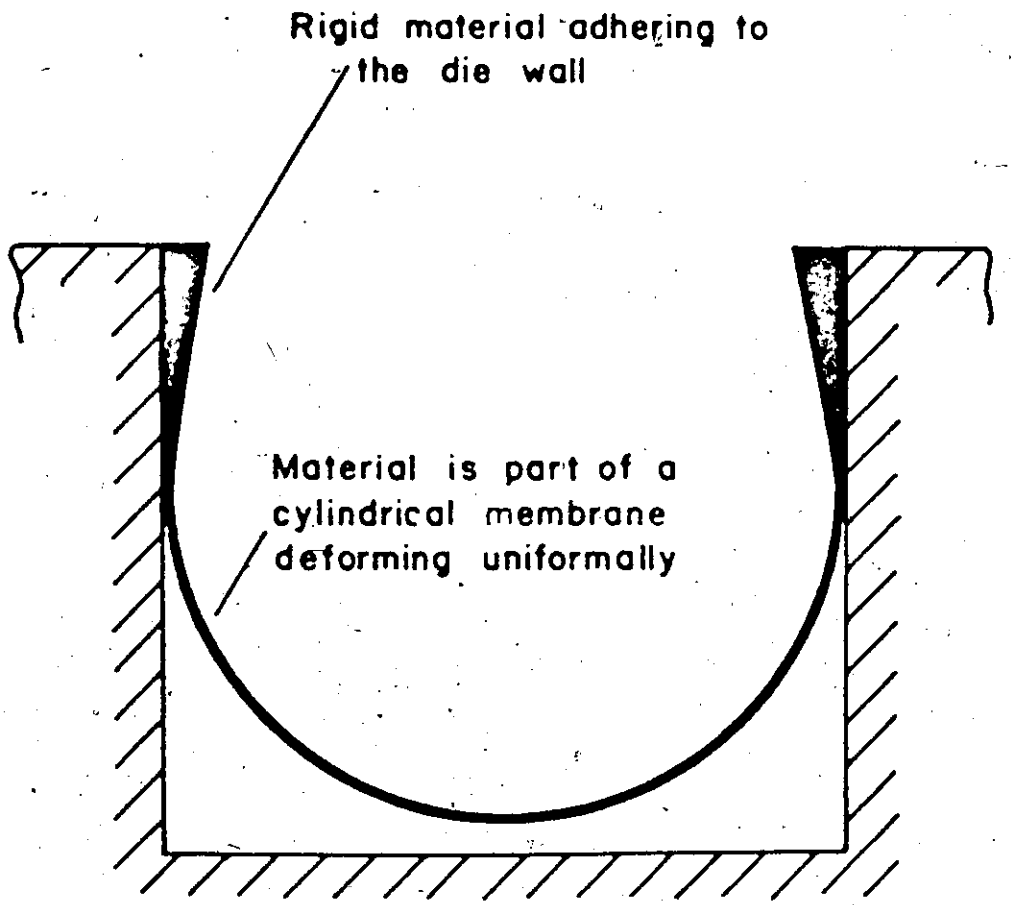

PIGURE 3.2

The two modes of deformation when forming into a long rectangular trough.

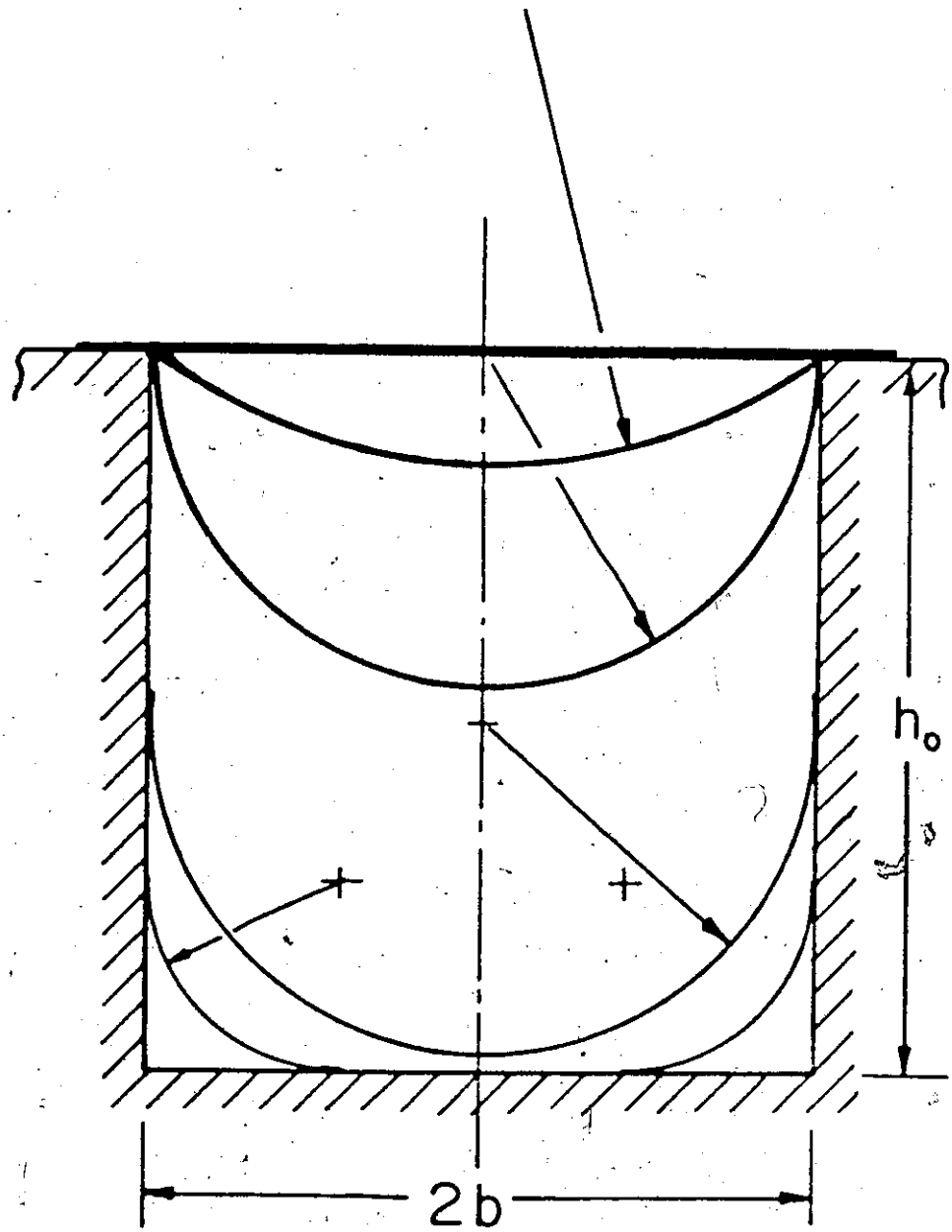

FIGURE 3.3
Schematic diagram of forming into a long rectangular trough with $h_o/b>1$.

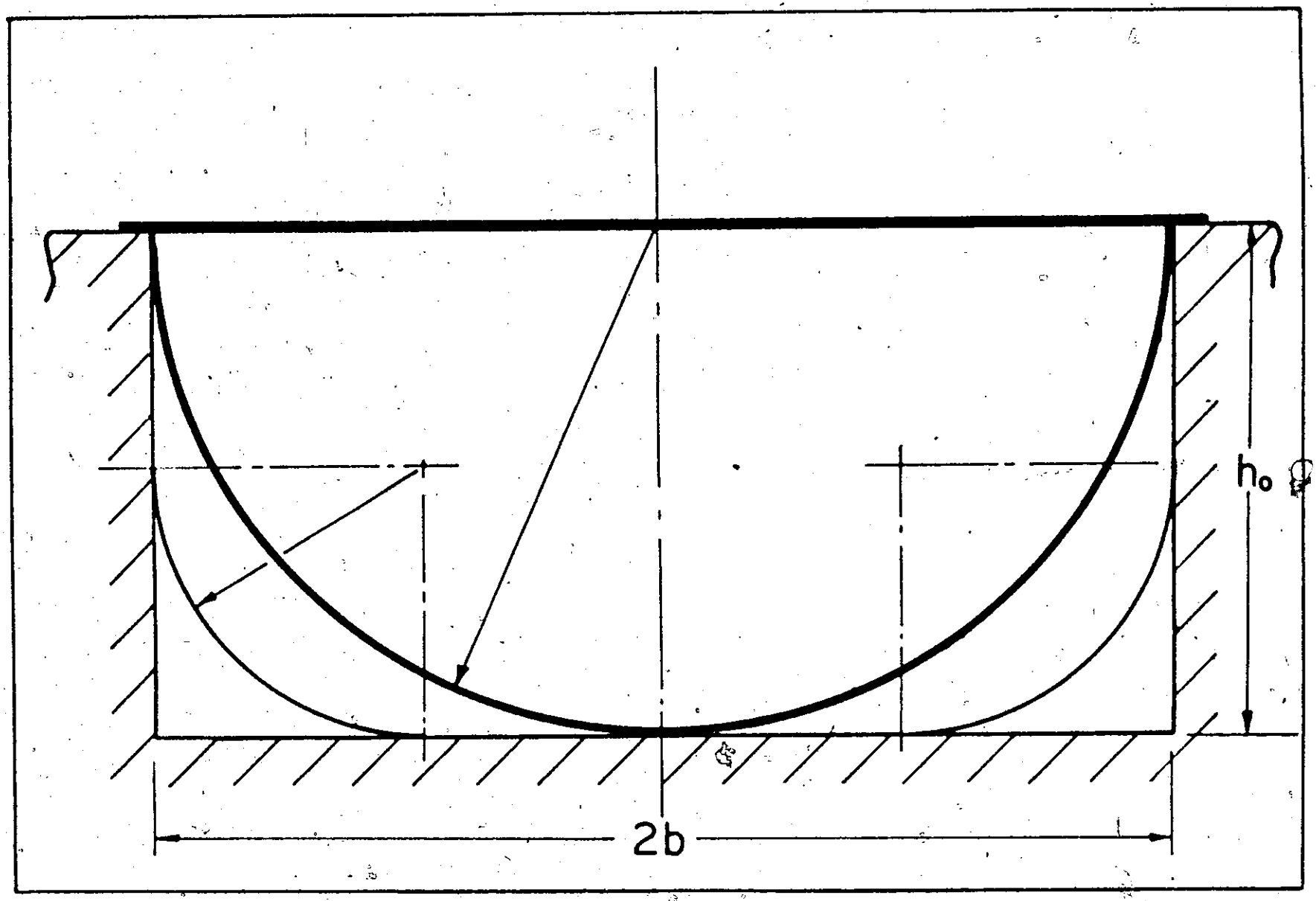

FIGURE 3.4

Schematic diagram of the mechanics of forming into a long rectangular trough with $h_o/b=1$.

of b and forming into the corners starts. The deforming sheet adheres to the sides and to the bottom as the radius of the free membrane approaches zero, as shown in Figure 3.4.

iii) The height is less than half the width. ($h_o/b<1$)

The sheet as before forms a cylindrical bulge of successively smaller radii, however, before the radius is equal to b, the deforming sheet touches the bottom of the die as shown in Figure 3.5. The process continues as material adheres to the bottom of the die and the radius of the deforming membrane decreases. This continues with the sheet adhering to the bottom of the die and 'pivoting' at the point of contact 'A' in Figure 3.5, until the radius is equal to h_o. At this point forming into the corners starts as the sheet adheres to the side and to the bottom of the die and we have the situation indicated in (ii) above.

3.2.2 Theoretical Thickness Distribution

From the previous section it is apparent that the thickness distribution is dependent upon the height to width ratio of the die and that there are three cases which must be analyzed separately. The thickness distribution for each of the cases indicated previously is given below.

a) Case (i) $h_o>b$

Initially, a cylindrical bulge is formed and this continues to deform uniformly until the radius is equal to

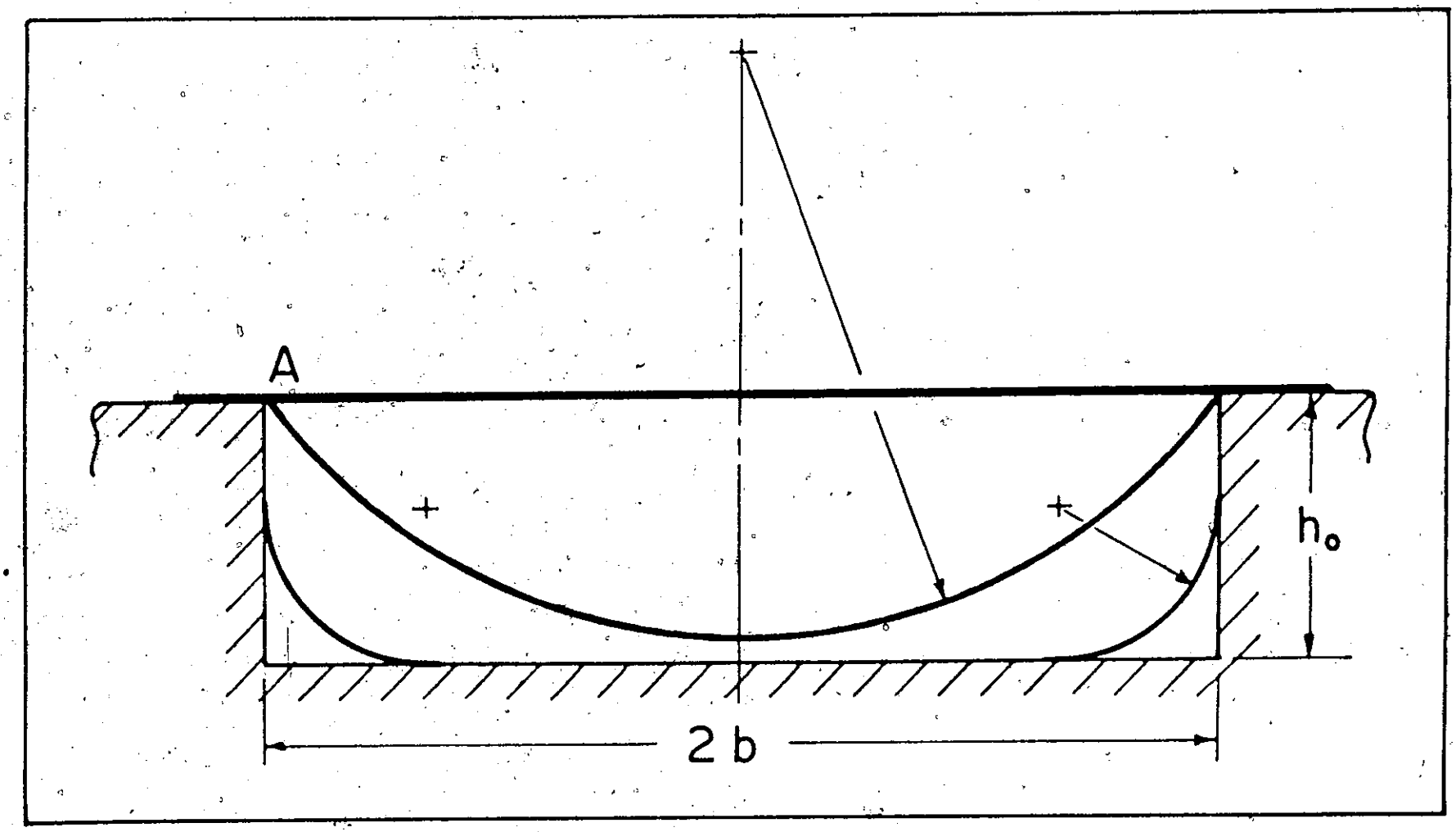

FIGURE 3.5

Schematic diagram of the mechanics of forming into a long rectangular trough with $h_o/b < 1$.

b, as indicated previously. The formed cylindrical membrane then moves down into the die.

If the deformed sheet has adhered to the side to a depth 'x', as in Figure 3.6, while the remainder is a circular arc of uniform thickness; then, assuming the thickness in the interval dx is constant, the thickness is obtained from the condition of constant volume,

$$\pi \frac{2bs}{2} = \left\{\pi \frac{2b}{2} + 2dx\right\} (s + ds) \qquad \text{..... (3.1)}$$

Neglecting second order derivatives

$$dx = \frac{-\pi b ds}{2s} \qquad \text{..... (3.2)}$$

Integrating and simplifying

$$\frac{s}{s_{x=o}} = e^{-\left(\frac{2x}{\pi b}\right)} \qquad \text{..... (3.3)}$$

Where $s_{x=0}$ is the uniform bulge thickness at x=0, ie. when the cylindrical bulge is first formed, and is given by

$$s_{x=o} = \frac{2}{\pi}.s_o \qquad \text{..... (3.4)}$$

Therefore

$$s = \frac{2}{\pi}.s_o e^{-\left(\frac{2x}{\pi b}\right)} \qquad \text{..... (3.5)}$$

This is the thickness variation in the height range

$$(h_o - b) > x > 0$$

b) <u>Case (ii) $h_o = b$</u>

This is the situation when material begins to adhere simultaneously to both the sides and to the bottom of the

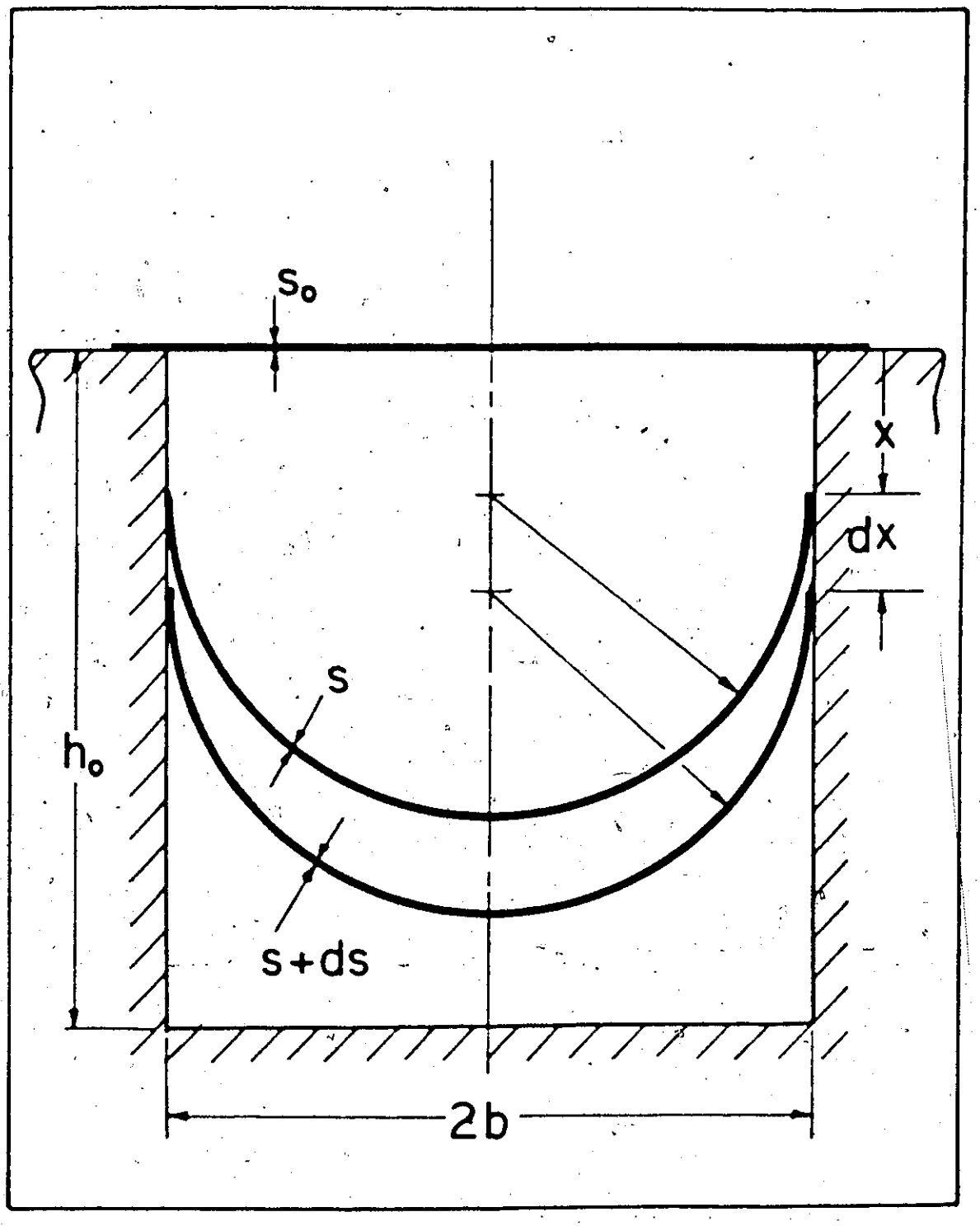

FIGURE 3.6

Schematic of two successive stages for forming into a very deep trough when material is adhering to the sides of the die only.

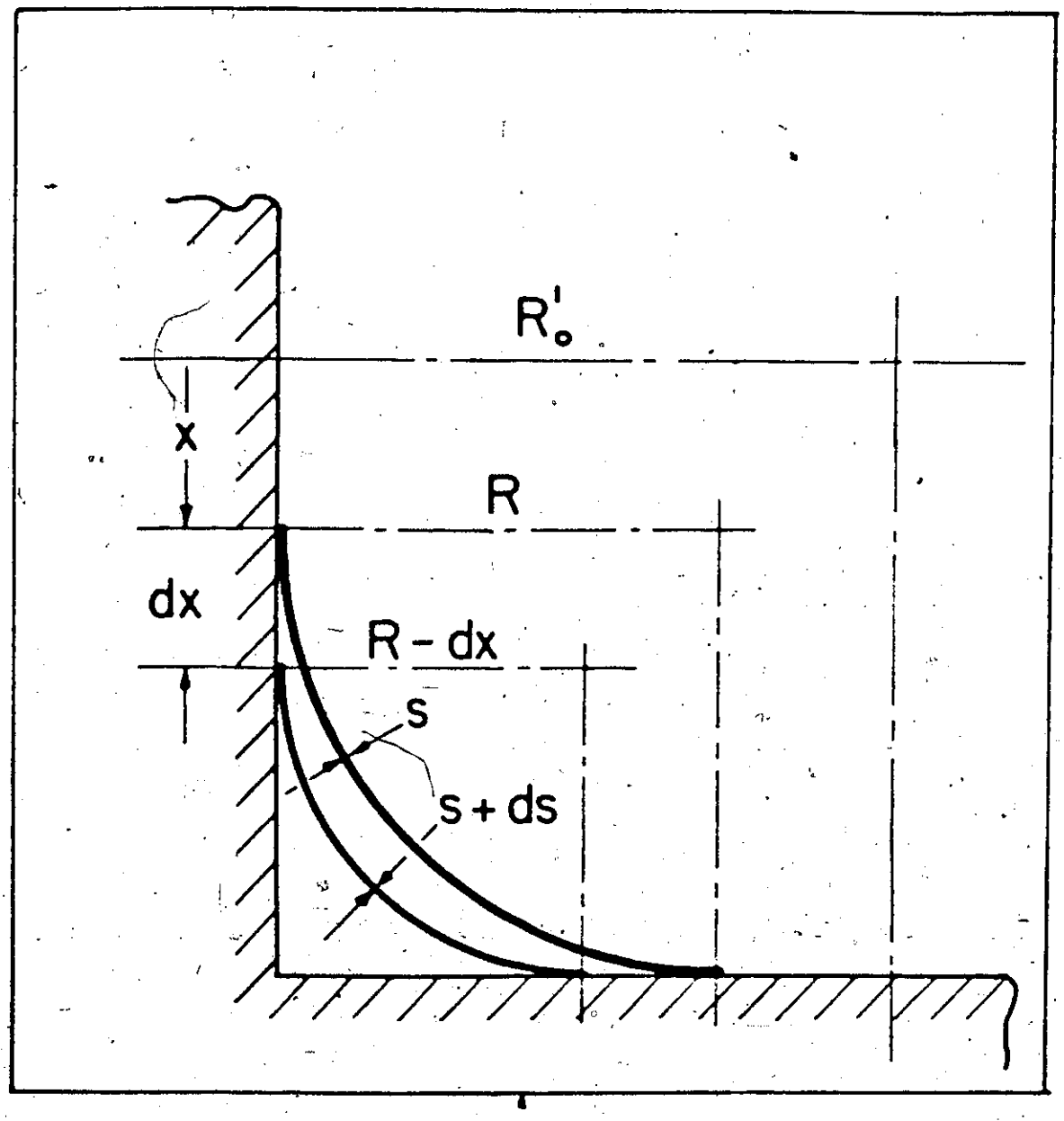

FIGURE 3.7

Schematic of two successive stages for forming into the corners of the die when material is adhering to both the bottom and sides of the die.

die, as shown in Figure 3.7.

For constant volume and assuming that the thickness in the interval dx is constant, then the thickness is given by

$$\frac{\pi Rs}{2} = \left\{2dx + \frac{\pi}{2}(R - dx)\right\}(s + ds) \quad \ldots\ldots (3.6)$$

Simplifying and ignoring second order derivatives

$$\frac{ds}{s} = \frac{dx}{R}\left\{1 - \frac{4}{\pi}\right\} \quad \ldots\ldots\ldots (3.7)$$

where $$R = R_o' - x \quad \ldots\ldots\ldots (3.8)$$

and R_o' is the radius of the sheet when forming into the corners starts.

Substituting Eqn. 3.8 into Eqn. 3.7

$$\frac{ds}{s} = \left\{1 - \frac{4}{\pi}\right\}\left\{\frac{1}{R_o - x}\right\} dx \quad \ldots\ldots\ldots (3.9)$$

which upon integration yields

$$s = s_o' \left\{\frac{R_o' - x}{R_o'}\right\}^{\left(\frac{4}{\pi} - 1\right)} \quad \ldots\ldots\ldots (3.10)$$

where s_o' is the thickness of the sheet at the start of such a process, ie. at x=0. The general parameters R_o' and s_o' are introduced so that this equation is applicable for the cases $h>b_o$ and $h<b_o$ when the initial radius R_o' and thickness s_o' will be different.

The thickness variation when the sheet forms into the corners is consequently given by Eqn. 3.10.

c) <u>Case (iii) $h_o<b$</u>

The situation in this case is different to those

described previously because the material adheres to the bottom of the die before touching the sides, as shown in Figure 3.8. When the deforming sheet first touches the bottom of the die the thickness is obtained from the condition of constant volume,

$$2bs_o = 4\alpha_o R_o s_{u=o} \qquad \text{..... (3.11)}$$

therefore

$$s_{u=o} = \frac{bs_o}{2\alpha_o R_o} \qquad \text{..... (3.12)}$$

where R_o is the radius of the membrane and is given by

$$R_o = \frac{h_o}{2\sin^2\alpha_o} \qquad \text{..... (3.13)}$$

Substituting Eqn. 3.13 into Eqn. 3.12

$$s_{u=o} = \frac{b\sin^2\alpha_o s_o}{\alpha_o h_o} \qquad \text{..... (3.14)}$$

This is the uniform sheet thickness when the deforming membrane touches the bottom of the die.

As forming continues, material adheres to the bottom of the die and in the range

$$(b-h) > u > 0$$

the thickness variation is obtained in the following manner.

Consider a sheet which is suspended from the corner and contacts the base at a depth h_o below. The distance measured along the base, from the centre, is u as shown in Figure 3.9.

The chordal distance of the unsupported membrane is AP where

$$AP = \frac{h_o}{\sin\alpha} \qquad \text{..... (3.15)}$$

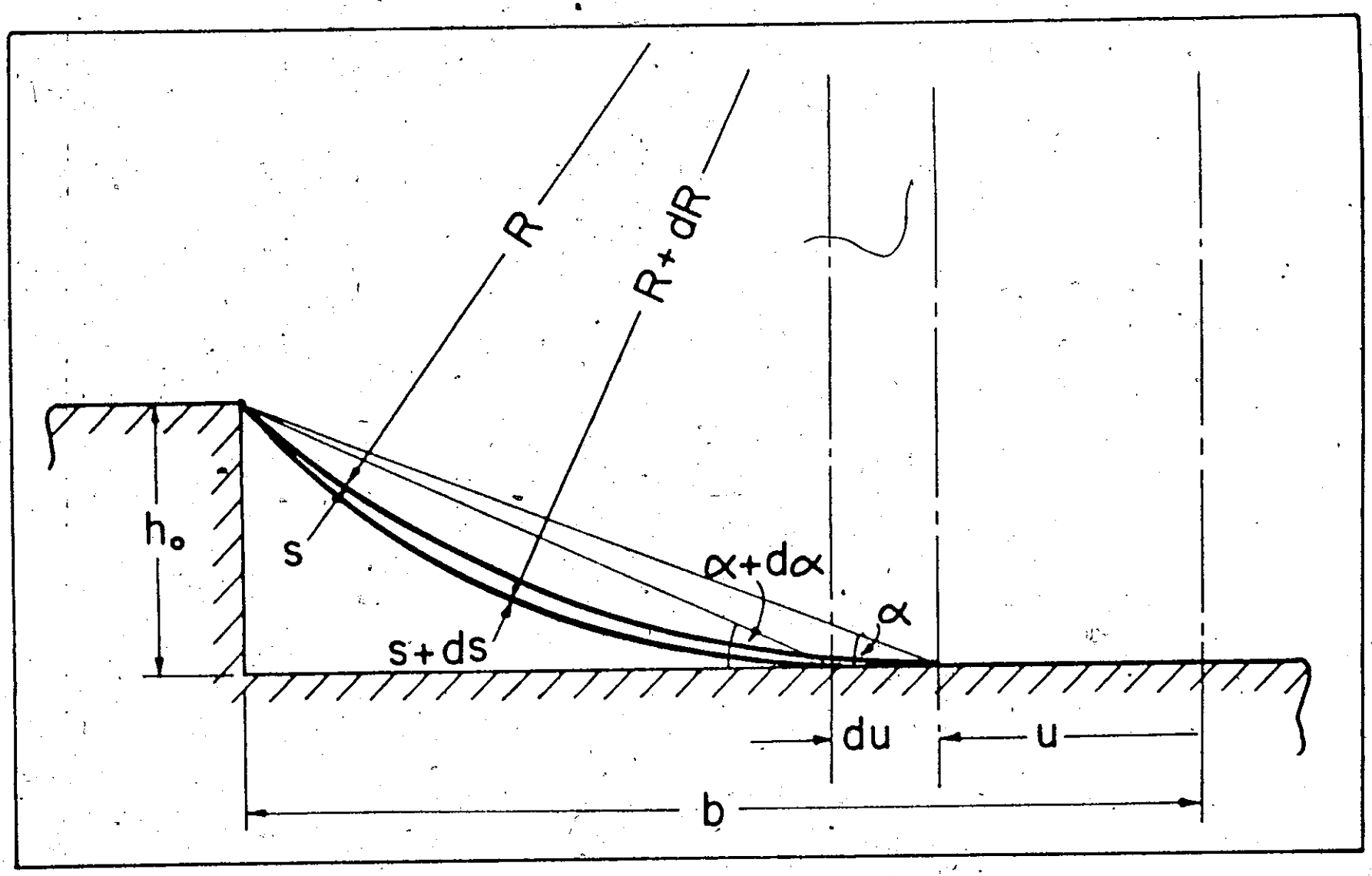

FIGURE 3.8

Schematic of two successive stages for forming into a very shallow trough when material is adhering to the bottom of the die only.

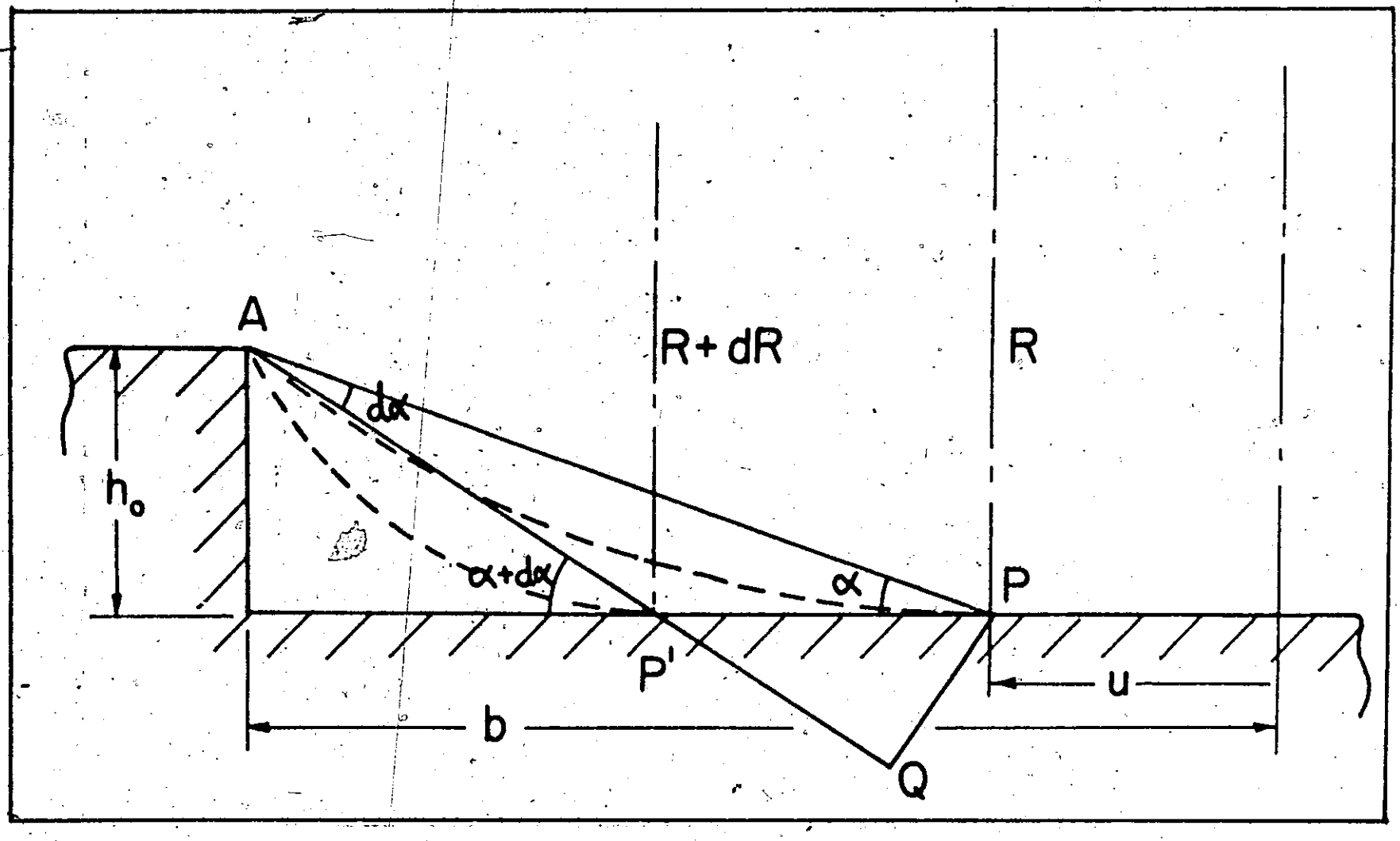

FIGURE 3.9

Geometry of deformation of two successive stages for forming into a very shallow trough.

During an increment in the forming process, the point of contact of the deforming sheet with the bottom of the die moves from P to P',

$$PP' = du = \frac{PQ}{\sin\alpha} \qquad \text{..... (3.16)}$$

but from the geometry

$$PQ = \frac{h_o}{\sin\alpha} d\alpha \qquad \text{..... (3.17)}$$

therefore

$$du = \frac{h_o}{\sin^2\alpha} d\alpha \qquad \text{..... (3.18)}$$

From Eqn. 3.13

$$R = \frac{h_o}{2\sin^2\alpha}$$

therefore $du = 2Rd\alpha$ ..... (3.19)

For constancy of volume then

$$R.2\alpha.s = s.du + 2(R+dR)(\alpha+d\alpha)(s+ds) \qquad \text{..... (3.20)}$$

Simplifying and ignoring second order derivates

$$\frac{du}{R} + \frac{d\alpha}{\alpha} + \frac{dR}{R} + \frac{ds}{s} = 0 \qquad \text{..... (3.21)}$$

Substituting Eqn. 3.19 and noting that

$$\frac{dR}{R} = \frac{-2d\alpha}{\tan\alpha} \qquad \text{..... (3.22)}$$

then

$$\frac{2d\alpha}{\alpha} + \frac{ds}{s} - \frac{2d}{\tan\alpha} = 0 \qquad \text{..... (3.23)}$$

$$\frac{ds}{s} = 2\left\{\frac{1}{\tan\alpha} - \frac{1}{\alpha}\right\}d\alpha \qquad \text{..... (3.24)}$$

Integrating and noting the boundary condition that

$s = s_{u=o}$ at $\alpha = \alpha_o$ we obtain

$$s = s_{u=o}\left\{\frac{\alpha_o}{\alpha}\,\frac{\sin\alpha}{\sin\alpha_o}\right\}^2 \qquad \text{..... (3.25)}$$

The thickness variation in the range $(b-h_o)>u>0$ is therefore given by Eqn. 3.25 where α, the angle of contact, is given by

$$\alpha = \tan^{-1}\left\{\frac{h_o}{b-u}\right\} \qquad \text{..... (3.26)}$$

When $\alpha = \frac{\pi}{4}$ or $u>(b-h_o)$ material begins to adhere to the sides and forming into the corners starts. The thickness variation is then predicted by Eqn. 3.10.

3.2.3 Summary

The thickness variation for the forming of a superplastic alloy sheet into a rectangular cavity can be described by the following equations dependent upon the initial die geometry, see Figure 3.13.

For $h_o>b$, that is, a deep trough, the thickness distribution is initially described by Eqn. 3.5

$$s = \frac{2}{\pi}\, s_o \exp\left\{\frac{-2x}{\pi b}\right\}$$

but when $x \geqslant (h_o-b)$

the sheet is forming into the corners and the appropriate conditions, ie. the thickness when $x=h_o-b$ and the width of the die are substituted into Eqn. 3.10.

$$s = s_o'\left\{\frac{b-x}{b}\right\}^{\left(\frac{4}{\pi}-1\right)}$$

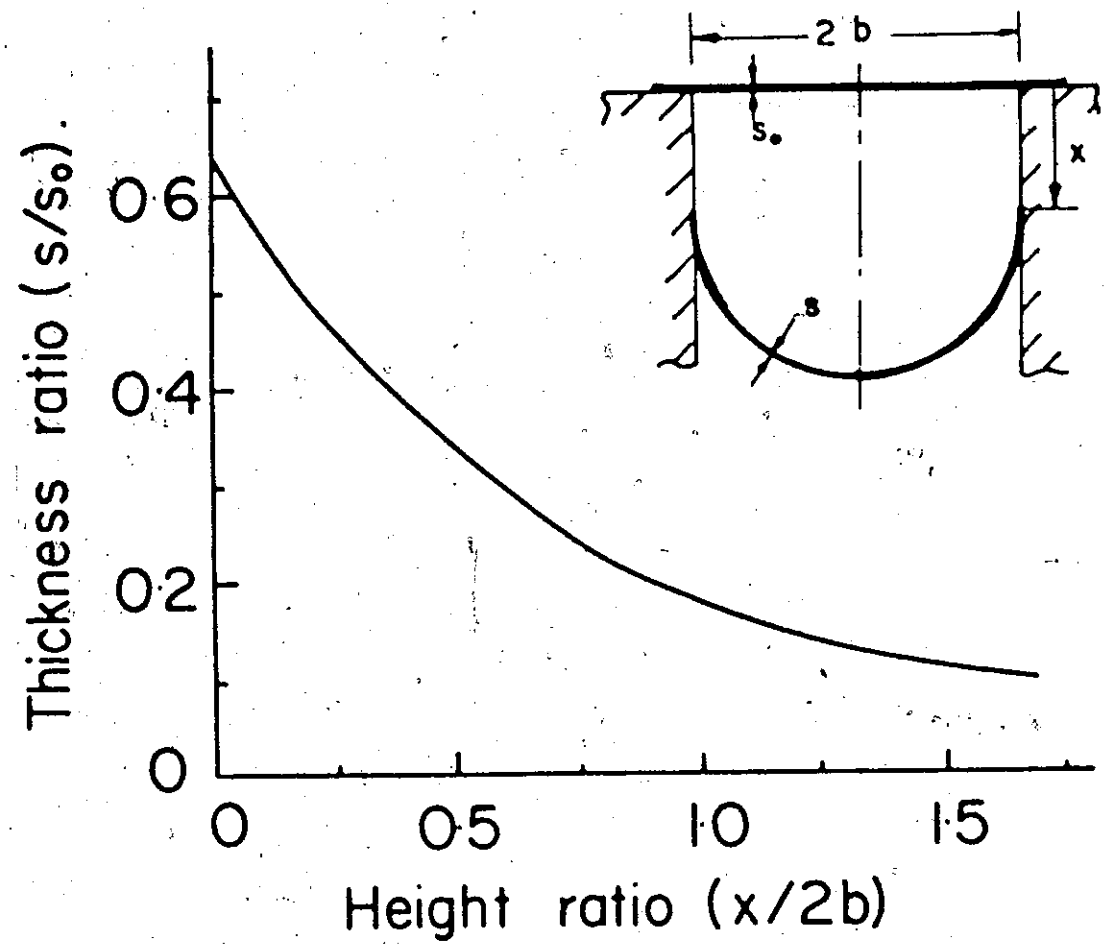

FIGURE 3.10

Theoretical thickness distribution for forming into a very deep trough.

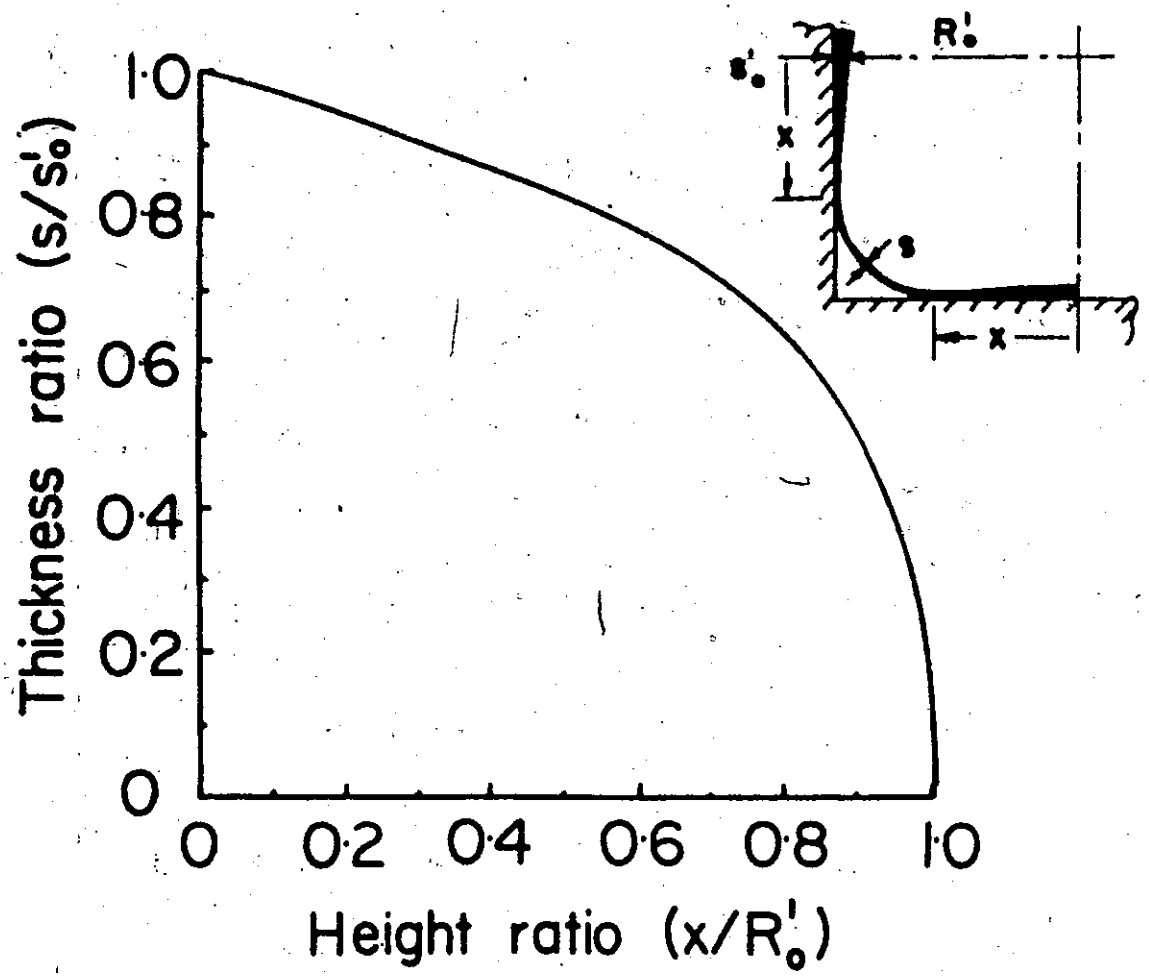

FIGURE 3.11

Theoretical thickness distribution when material is forming into the corners of a rectangular trough.

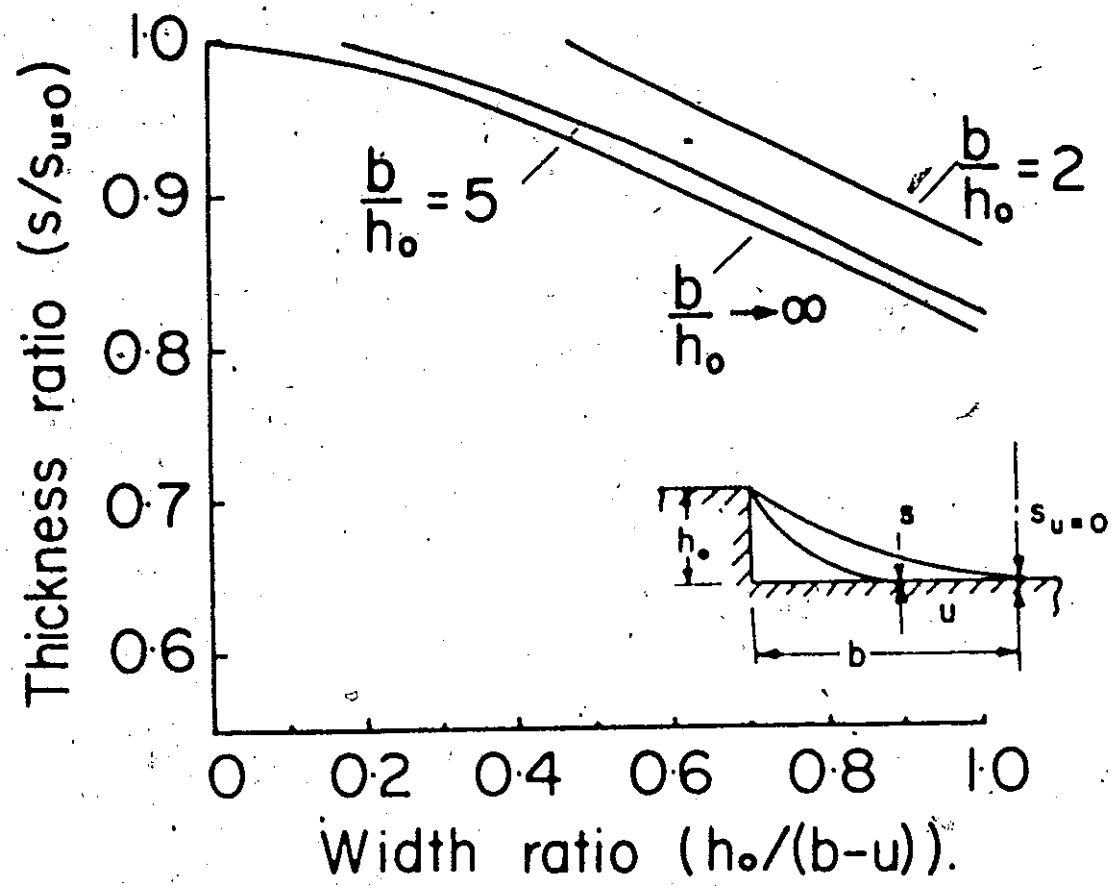

FIGURE 3.12

Theoretical thickness distribution along the bottom of the die for forming into a very shallow trough.

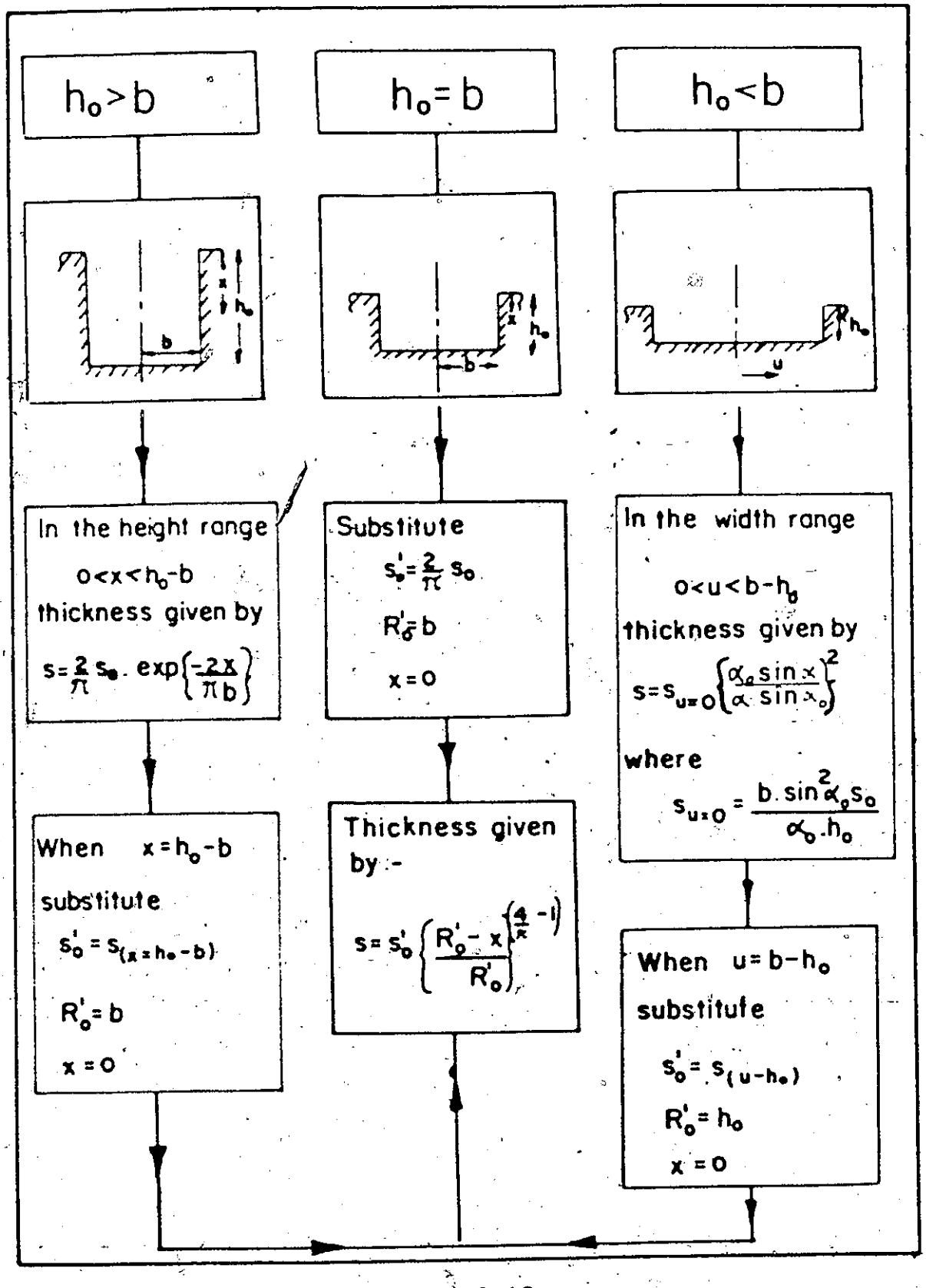

FIGURE 3.13

Thickness distribution flow diagram.

Note that x is now made equal to zero since it refers to the height from the position when forming into the corners is initiated.

For $h_o=b$, the material immediately forms into the corners of the die and the thickness distribution is described by a combination of Eqn. 3.10 and Eqn. 3.4.

$$s = \frac{2}{\pi} s_o \left\{\frac{b-x}{b}\right\}^{(\frac{4}{\pi}-1)}$$

For $h_o<b$, the material initially adheres to the bottom of the die and in the interval $(b-h_o)>u>0$ the thickness is defined by

$$s = s_{u=o}\left\{\frac{\alpha_o}{\alpha}\frac{\sin\alpha}{\sin\alpha_o}\right\}^2$$

where $s_{u=o}$ is given by Eqn. 3.14 and α is defined by Eqn. 3.26. When $u=(b-h_o)$, material begins to form into the corners and Eqn. 3.10 with a suitable value for s_o' is used.

$$s = s_o'\left\{\frac{h_o-x}{x}\right\}^{(\frac{4}{\pi}-1)}$$

The thickness distribution is thus described for every geometric configuration. Figures 3.10, 3.11 and 3.12 are graphs representing Equations 3.5, 3.10 and 3.25 respectively and from these figures the thickness distribution can be easily obtained.

3.3 Forming Into a Flat Bottomed Cylindrical Die

The bulging of a circular blank clamped at the edge

has been the subject of a number of papers. These analyses were concerned primarily with the free forming of a dome which, in the limit, became a hemispherical shell.

Jovane[30] in his, the first, analytic paper on the subject assumed that the deforming membrane was of uniform thickness. Subsequent experiments proved this assumption to be incorrect and there followed a number of papers examining the variation of thickness in the formed dome.

Cornfield and Johnson[32] showed that in the free forming of a circular blank, clamped at the edges, the thickness varied from point to point within the formed part. For a hemisphere they showed that the thickness decreases approximately linearly with height and that the rate of thinning was dependent upon m, the rate of thinning was less for higher values of m.

Experimental results have been presented by Johnson et al[35] for the forming of superplastic sheet into a flat bottomed cylindrical cavity and Al-Naib[34] has presented an analytical solution for this problem which is rather complicated.

In the following work, a rather rudimentary analysis for the forming into a flat bottomed cylindrical cavity is presented. The results of the work of Cornfield and Johnson are used and the assumption is made that the thickness profile of the hemispherical bulge remains constant.

3.3.1 Theoretical Thickness Distribution

The hemispherical dome advances down into the cylinder as shown in Figure 3.14. The thickness at the edge of the hemisphere is related to the mean or average dome thickness, $\bar{s}$, by

$$s_e = c_m \bar{s} \qquad \text{..... (3.27)}$$

where c_m is a constant dependent upon the 'm' value of the material, as shown in Figure 3.15. These curves were determined empirically from the results of the work by Cornfield and Johnson.

Assuming the thickness in the interval dx, in Figure 3.14, is constant, then for constant volume

$$2\pi r^2 \bar{s} = (2\pi r^2 + 2\pi r dx)(\bar{s} + d\bar{s}) \qquad \text{..... (3.28)}$$

Simplifying and ignoring second order derivatives

$$\frac{d\bar{s}}{s} = \frac{-dx}{r} \qquad \text{..... (3.29)}$$

which upon integration and substitution of the boundary condition that

$$(\bar{s})_{x=o} = \frac{s_o}{2}$$

gives

$$\bar{s} = \frac{s_o}{2} e^{\frac{-x}{r}} \qquad \text{..... (3.30)}$$

Substituting Eqn. 3.27 into Eqn. 3.30 gives

$$s_e = c_m \frac{s_o}{2} e^{\frac{-x}{r}} \qquad \text{..... (3.31)}$$

The thickness at the pole of the dome can similarly be

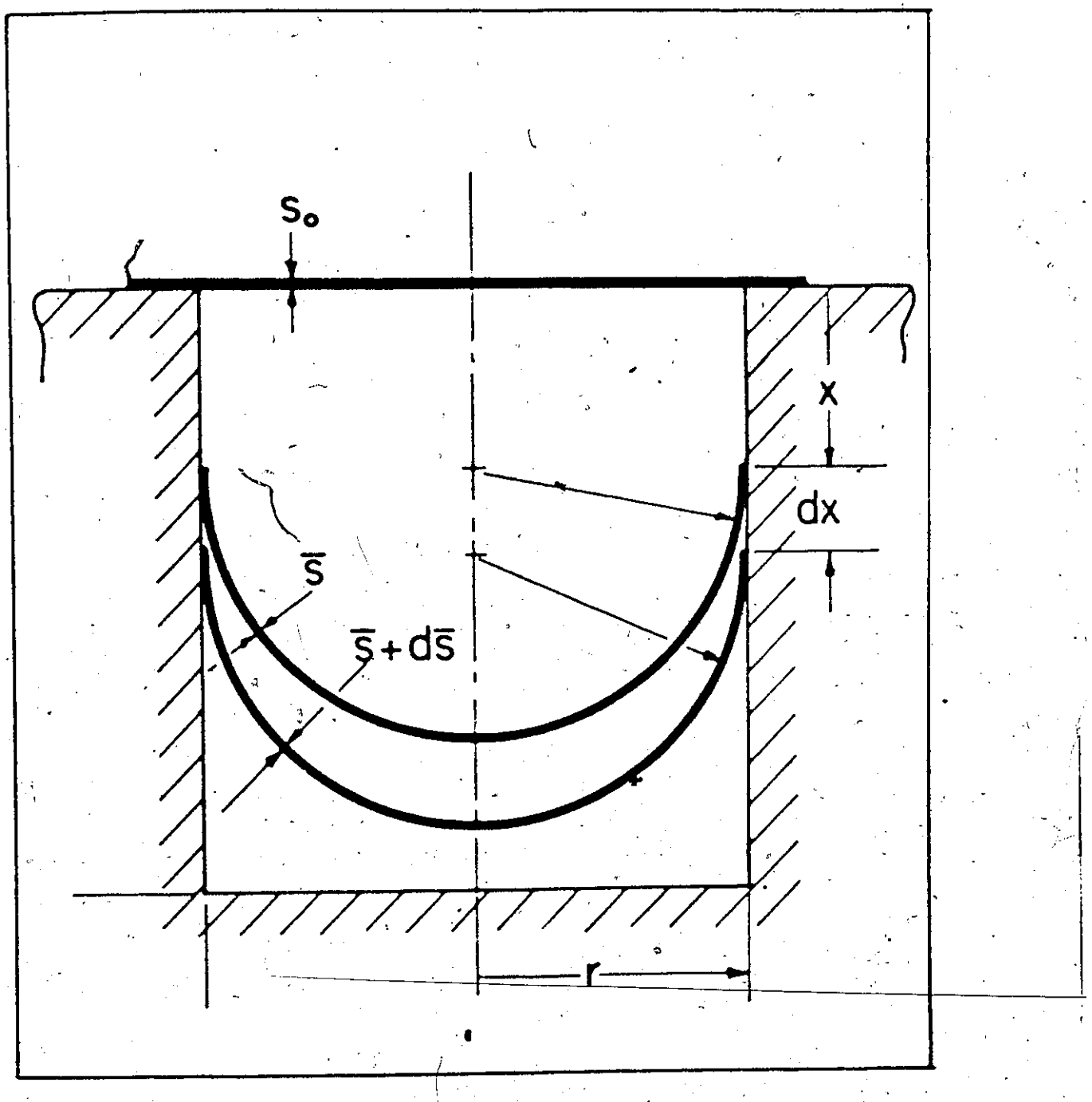

PIGURE 3.14

Schematic of two stages in the forming of a sheet into a cylindrical cavity as the hemispherical dome advances into the die.

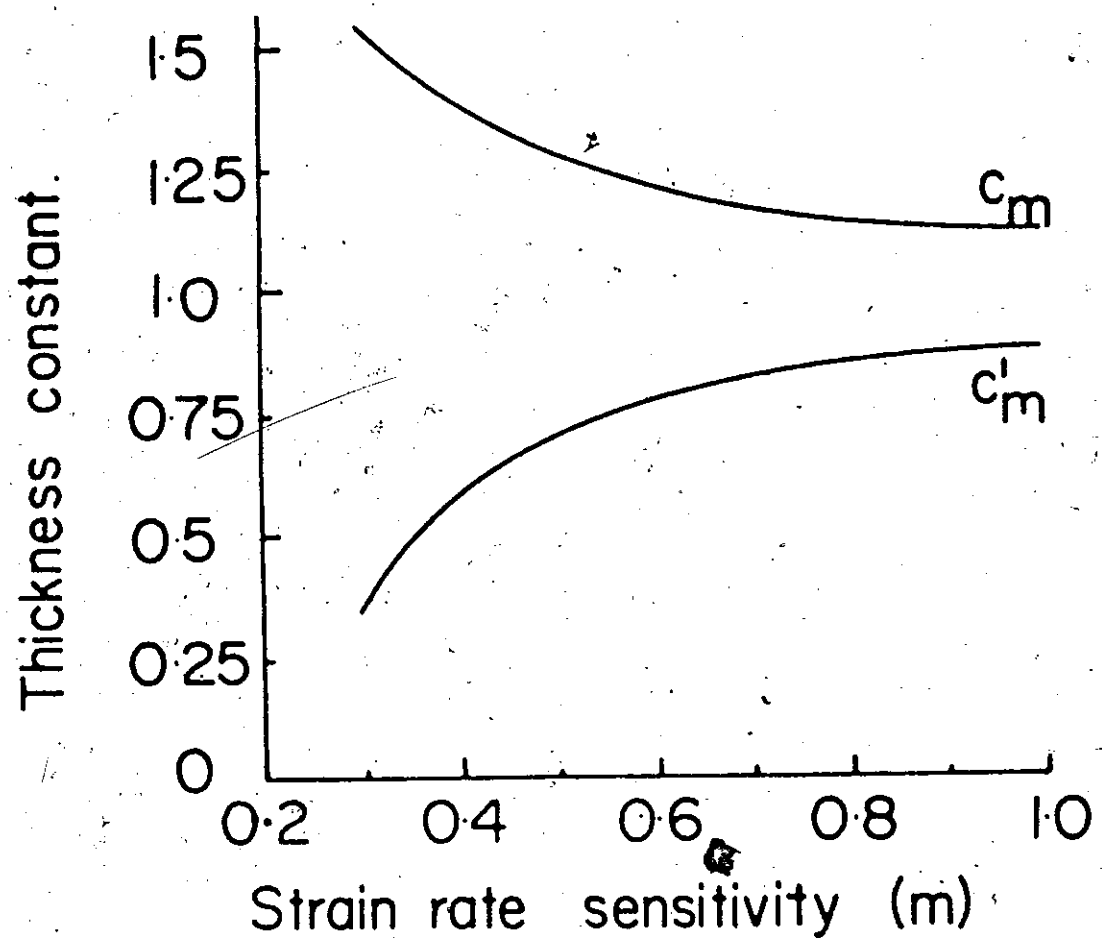

FIGURE 3.15

Variation of the constants c_m and c'_m with strain-rate sensitivity, m, derived from ref.32.

written as

$$s_p = c_m' \cdot \frac{s_o}{2} e^{\frac{-x}{r}} \qquad \text{..... (3.32)}$$

where c_m' is also given in Figure 3.15.

The thickness distribution along the sides of the formed part in the height range $(h_o-r)>x>0$ is defined by Eqn. 3.31.

If we now assume that, although material is adhering to the bottom and to the sides of the die, the deformation continues to vary in the same manner indicated by Eqn. 3.31, then the final edge thickness $(s_e)_{x=h_o}$ is given by

$$(s_e)_{h_o} = c_m \frac{s_o}{2} e^{\frac{-h_o}{r}} \qquad \text{..... (3.33)}$$

If the depth of the cavity is h_o, then the thickness when the hemispherical membrane first touches the bottom of the die is given by

$$(s_p)_{h_o} = c_m' \frac{s_o}{2} e^{\frac{-(h_o-r)}{r}} \qquad \text{..... (3.34)}$$

The thickness distribution across the base is assumed to vary linearly from $(s_p)_{h_o}$ at the centre to $(s_e)_{h_o}$ at the edge.

3.3.2 Summary

The thickness distribution down the side of the formed part is predicted by Eqn. 3.31. The thickness distribution along the bottom of the formed part is assumed to vary

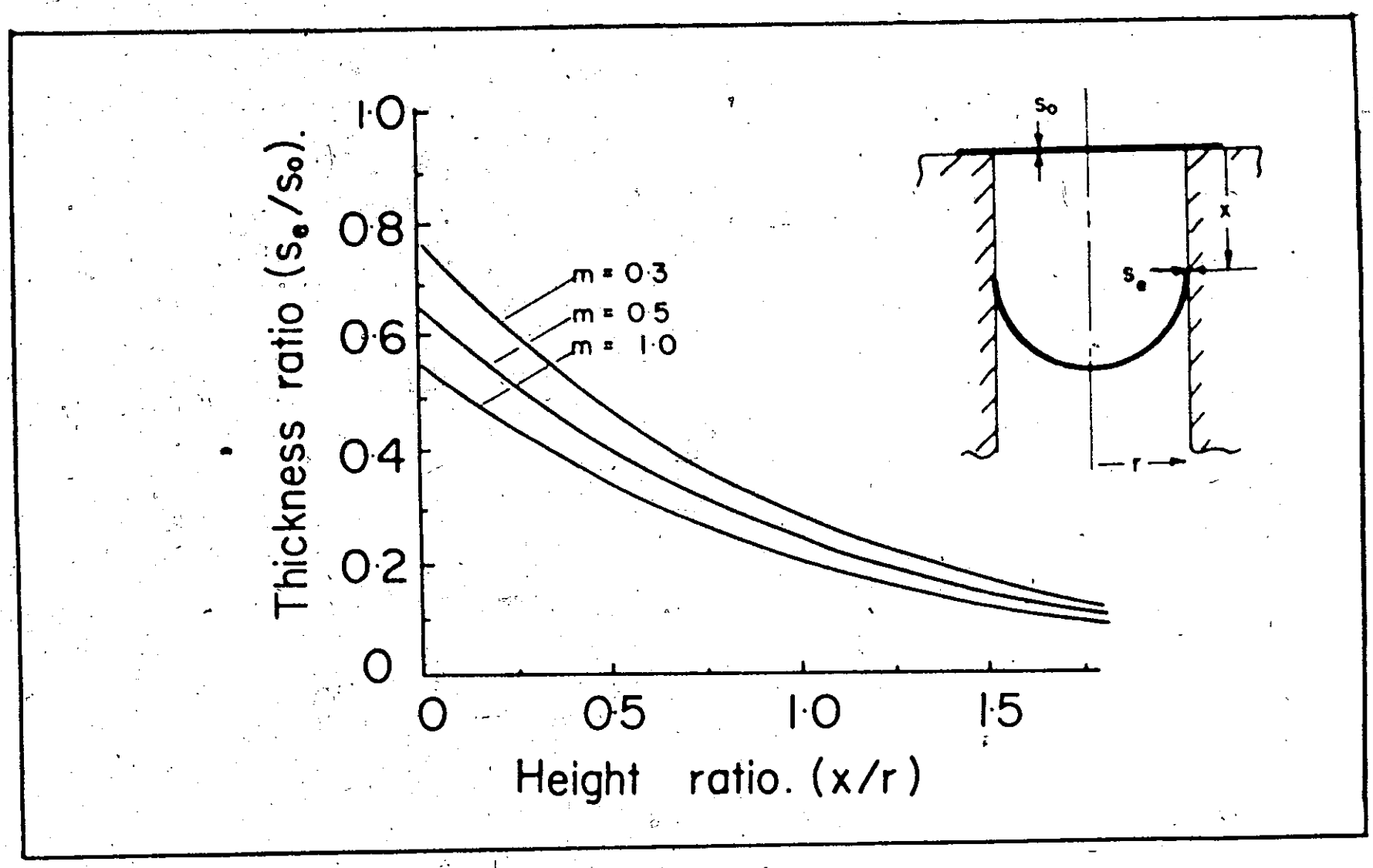

FIGURE 3.16

Theoretical thickness distribution along the sides for forming into a deep cylindrical cavity.

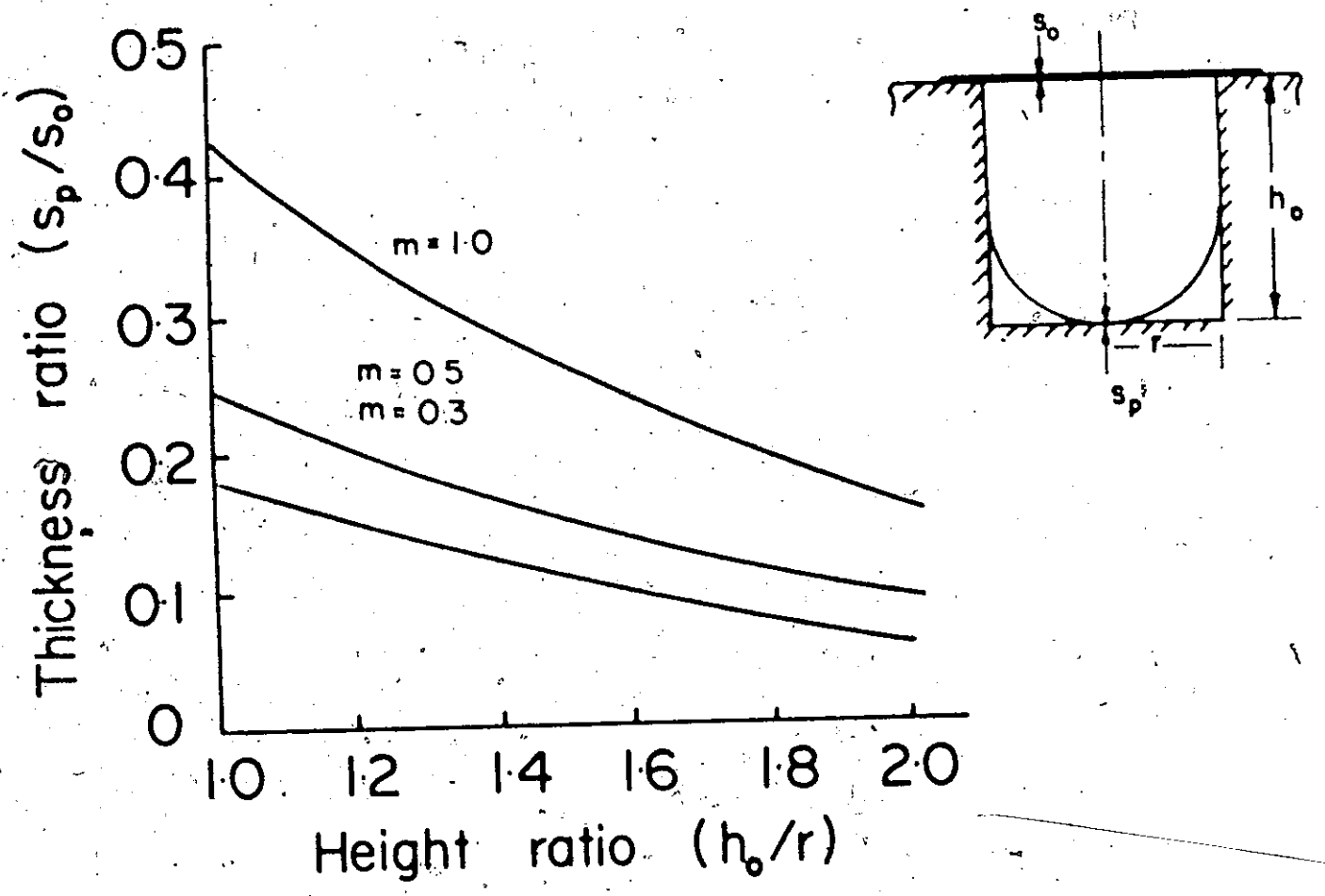

FIGURE 3.17

Theoretically determined pole thickness ratios when the deforming membrane first touches the bottom of the cylindrical cavity.

linearly from the pole thickness when the dome first touches the bottom, as predicted by Eqn. 3.34, to the edge thickness when the height is h_o as predicted by Eqn. 3.33.

The thickness profiles predicted by Eqn. 3.31 and Eqn. 3.33 are given in Figure 3.16 and Figure 3.17, for different values of 'm', the strain-rate sensitivity. For any given material and h_o/r ratio, the thickness distribution can be readily obtained from these figures.

It should be pointed out that this is only an approximate analysis and that the results of Cornfield and Johnson apply only to a hemisphere formed from a flat sheet. In the case indicated above, however, the advancing hemisphere is formed from material which is already non-uniform in thickness. Thus we may expect that the thickness distributions obtained from Figures 3.16 and 3.17 will be slightly greater than the experimental results.

CHAPTER FOUR

EXPERIMENTAL INVESTIGATION OF SHEET FORMING

4.1 Introduction

The experiments described in this chapter were performed in conjunction with Noranda Research Centre as part of a larger research project involving superplastic alloys. The main objectives of the work presented here were a preliminary investigation of forming times and thickness distribution for forming into a flat bottomed cylindrical cavity and to gain some practical experience with forming superplastic alloys.

The equipment, a thermoforming machine which is similar to that described by Al-Naib[34] was designed by Noranda in conjunction with the Metalworking Research Group at McMaster University. It should be pointed out, however, that the author did not participate in the design stage of this project. The thermoforming machine which will be described in a later section of this chapter is shown in Figure 4.1.

The author spent a period of three months working for Noranda Research Centre as a summer student and it was his responsibility to assemble, test and commission the thermoforming machine. Following this period of 'debugging', a

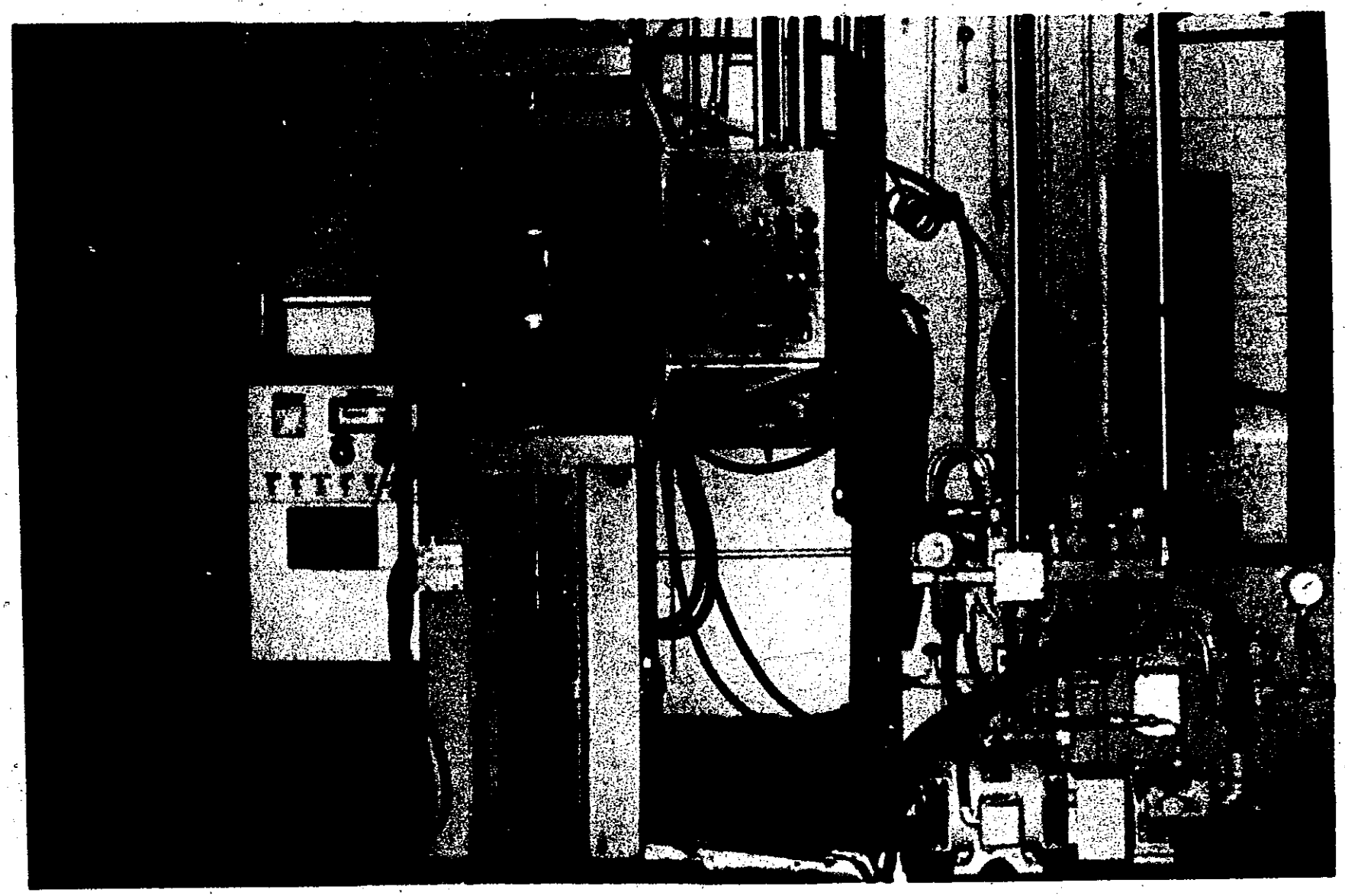

4.1 Photograph of the thermoforming machine

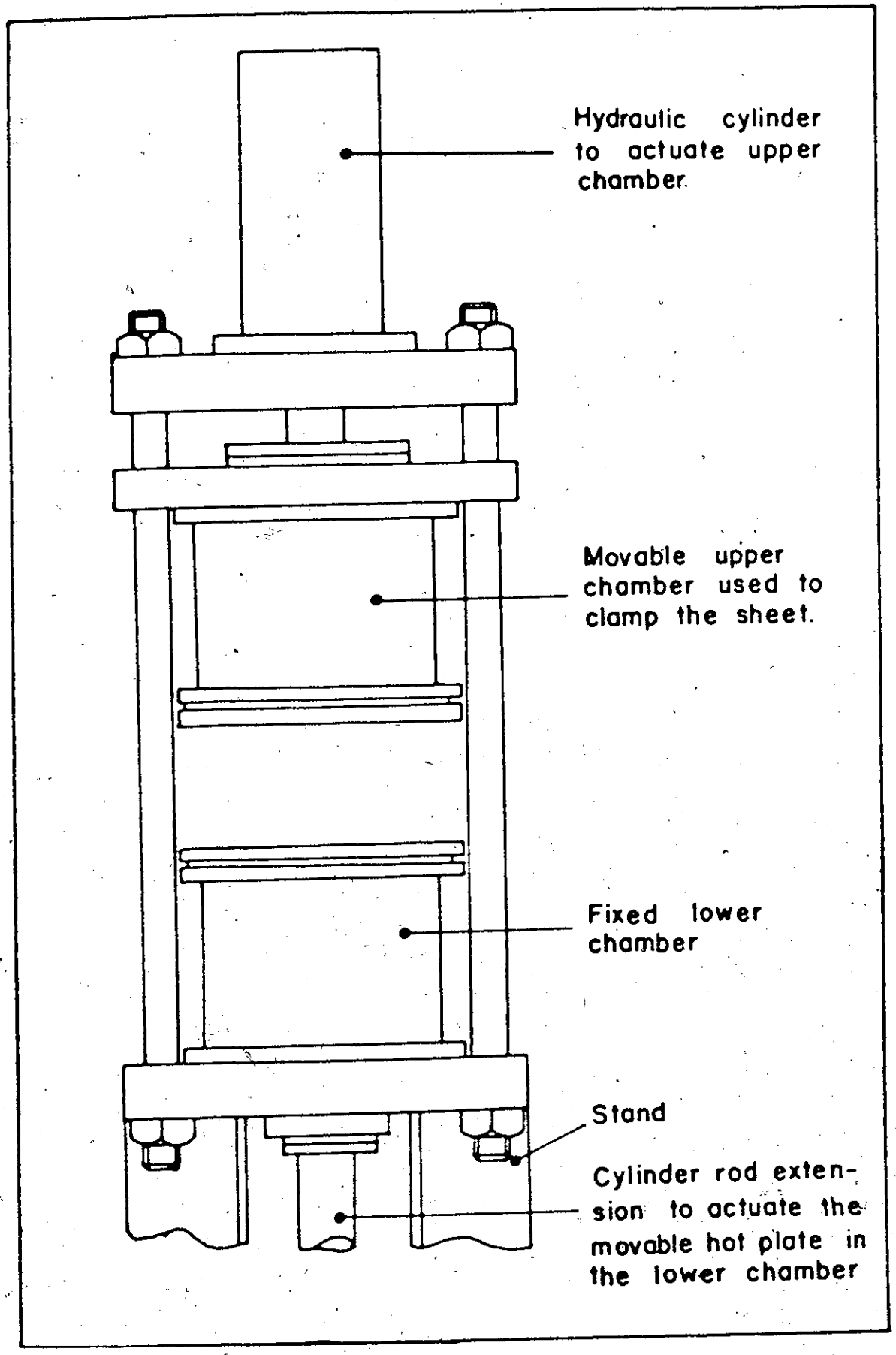

FIGURE 4.2

Schematic diagram of the forming machine.

number of tests were performed on the axisymmetric forming of a circular blank into a flat bottomed cylindrical cavity.

The results of these experiments are presented in this chapter with a summary of some of the practical difficulties encountered with thermoforming superplastic sheet material.

4.2 The Thermoforming Machine

General Description

The thermoforming machine and ancillary equipment is pictured in Figure 4.1 and the forming machine is shown schematically in Figure 4.2. The machine consists essentially of two forming chambers, a movable upper chamber and a fixed lower chamber. The chambers are identical and measure eight inches internal diameter and are approximately eight inches deep. The forming chambers are fabricated from steel while the removable chamber linings are aluminium. Inside the lower forming chamber there is a movable hot plate which is hydraulically controlled and can be raised or lowered at different speeds.

The hydraulic pump and associated equipment can be seen on the right of the thermoforming machine in Figure 4.1. Gas bottles will be seen behind the hydraulic unit. These bottles were used as the pressure supply for the forming operations and contain nitrogen. Nitrogen was chosen for

safety reasons although there was some concern about the weakening of the steel forming chambers by nitrogen embrittlement.

4.2.1 Heating Arrangement and Temperature Control

Heating of the forming chambers was accomplished using electrical resistance heaters as shown in Figure 4.3. A total of ten heaters were used within the machine, five in each chamber, and these were arranged as follows;

3 1200 w. heaters on the sides of the aluminium inner lining

1 650 w. heater in the hot plate

1 550 w. heater in the hot plate

The outer heating elements were controlled automatically by the thermocouples placed in the clamping rings. The remaining elements were controlled manually using simerstats which were placed in each circuit. The thermocouples indicated were connected via a simple switching circuit to a two pen chart recorder. It was usual to record the temperature of the middle of the lower forming chamber and the hot plate since the forming was into the lower chamber. As a secondary check, a surface pyrometer was used to observe the temperature distribution within the forming chamber.

The heat-up time to 250°C. was about one-half hour although an hour was usually allowed for the temperature to

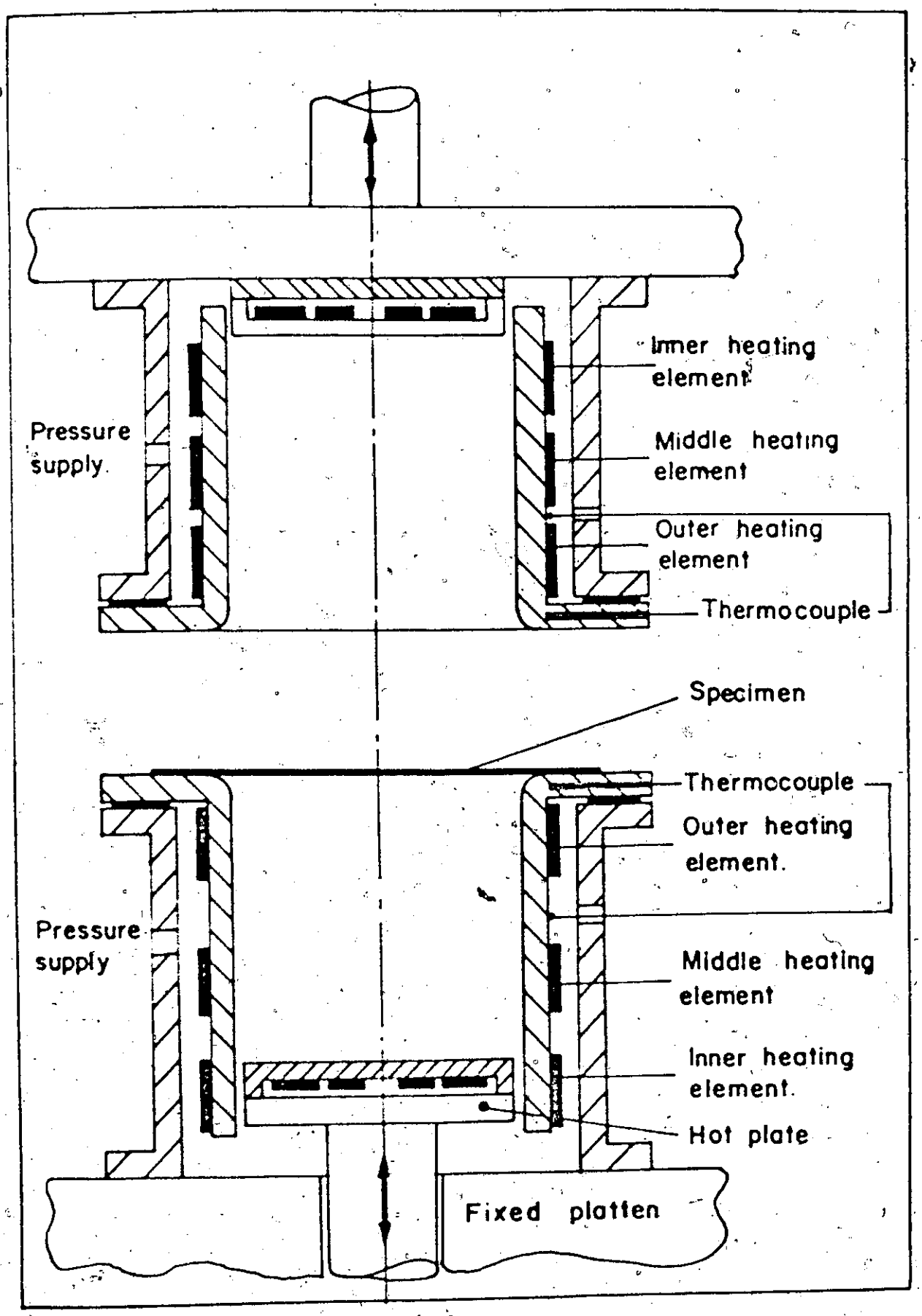

FIGURE 4.3

Schematic diagram of the internal arrangement of the forming machine.

stabilize.

The temperature control panel which contained all the necessary circuitry is shown on the left of the thermoforming machine in Figure 4.1.

4.2.2 Lubrication

In order to facilitate the removal of parts from the thermoforming machine a number of lubricants were investigated.

a) Molycote 'u' paste

This is a molybdenum disulphide compound and was applied with a spatula. This lubricant was considered to be a 'dirty' lubricant and was consequently not applied to the walls of the forming chamber. It was used to lubricate the clamping rings to prevent the sheet 'sticking' in the clamping grooves. The lubricant can be applied before the machine is heated or when the machine is hot. Since the lubricant 'coats' the metal, it was only necessary to reapply the lubricant when the sheet was found to be sticking.

b) Dow Corning 560 Fluid

This is a colourless silicone based lubricant and was used on the sides of the forming chamber. The lubricant does not discolour the surface of the formed part or affect the mould although it is transferred to the surface of the formed part. This lubricant must therefore be reapplied prior

to each forming operation.

c) Spray-kote Bonded Lubricant

This is a similar compound to lubricant (a) but instead of the disulphide being in a paste form it is in suspension and is supplied in an aerosol can. It is extremely dirty and difficult to remove from the formed part and must be applied while the mould is cold. It has the advantage, however, of coating the die and successive applications are not required.

d) Esso GP140 Gear Oil

This is a heavy duty oil and burns at approximately 250°C giving off an unpleasant odour. The oil is deposited on the formed part and must be reapplied prior to each operation. Some difficulty was experienced in removing the oil from the formed parts and from the dies.

The optimum results were obtained using the Molycote u paste, (a), to lubricate the clamping rings and the Dow Corning fluid, (b), to lubricate the walls of the chamber.

4.3 Alloys Used in Experiment

Two alloys of different composition, although based on the eutectoid Zn-Al system, were used in the experiments; these alloys will be designated Alloy A and Alloy B. Processing techniques have been established which render these materials superplastic when rolled into sheet.

The strain-rate sensitivity, 'm', and the constant 'k' in the constitutive equation

$$\sigma = k\dot{\varepsilon}^{m}$$

can be considered as parameters defining each alloy. The value of these parameters vary slightly with each batch of material due to slight differences in the processing technique; they may, however, be considered constant.

The value of the above parameters for the two alloys used are presented in Table 4.1.

4.4 Forming Procedure

The forming procedure for making the part shown in Figure 4.4 was as follows:

a) The lower chamber hot plate was raised to the desired height.

b) A preheated sheet of the superplastic alloy was placed in the machine and clamped between the two chambers using the movable upper chamber.

c) The upper chamber exhaust valve was closed.

d) Nitrogen at the desired pressure was introduced to the upper chamber.

e) After a predetermined time the pressure in the upper chamber was exhausted to atmosphere and the upper chamber retracted.

f) The part was ejected.

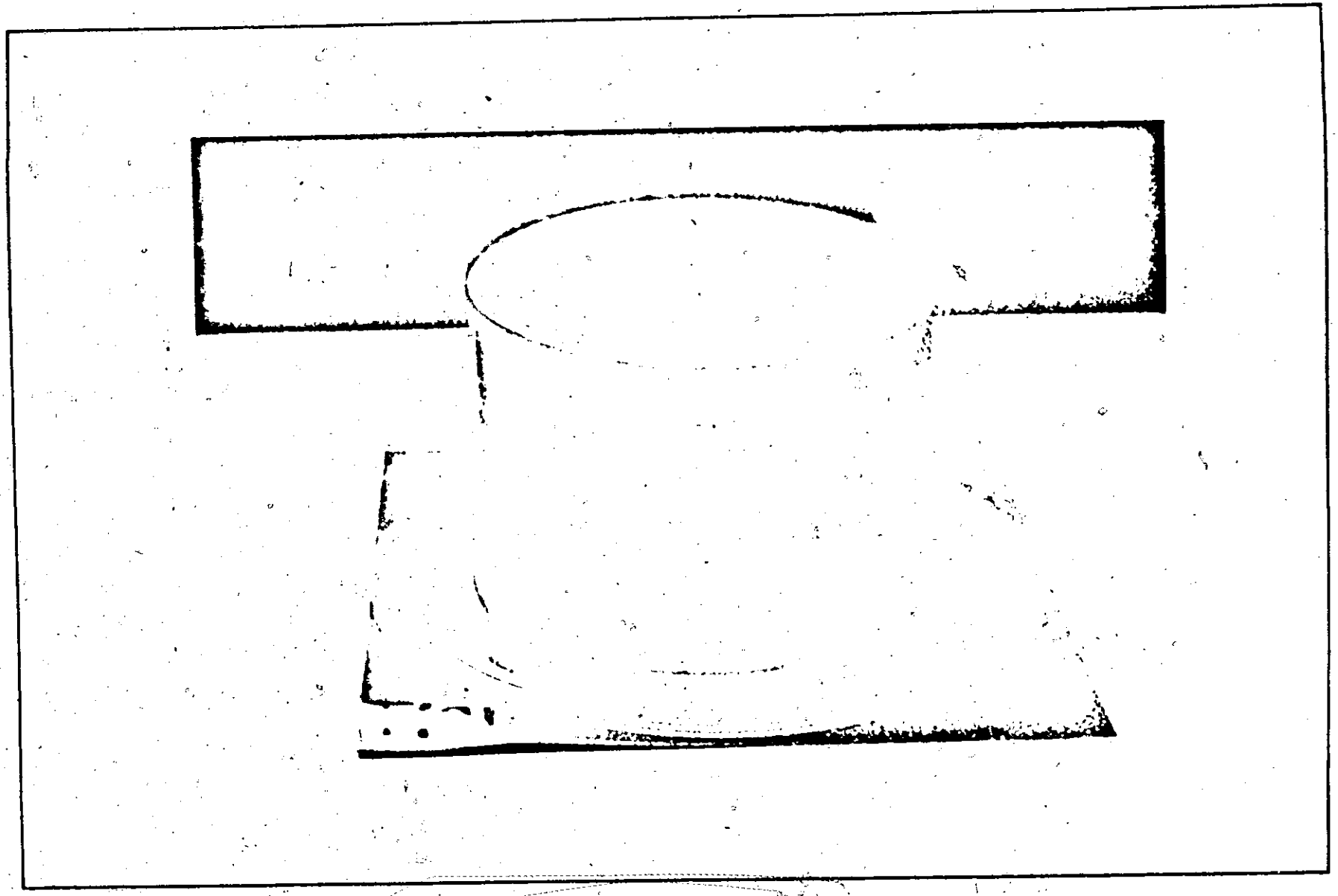

FIGURE 4.4

Photograph of a typical part formed in the flat bottomed cylindrical cavity.

TABLE 4-1

Material Parameters

Alloy	Strain-rate sensitivity m	Constant k ($lb_f/in.^2$ $sec.^m$)
A	0.417	7226
B	0.446	14,710

TABLE 4-2

Results of Forming Time Work

Depth	Alloy	Forming time (sec.)	Forming pressure (psi.)
3"	A	10	150
	B	15	150
5"	A	10	150
	B	25	100
5 3/4"	A	30	100
	B	---	---

Although the forming machine is rated for a safe working pressure of 300 psi, the maximum pressure used was 150 psi.

4.5 Experimental Results

A number of experiments have been performed and the relevant results will be indicated under the appropriate heading.

4.5.1 Forming Time Investigation

These experiments were performed to see if there was any experimental relationship between depth of part and forming time. There was also considerable interest in the minimum forming time since it is widely believed that a serious drawback of the superplastic alloys is the high production cost associated with long cycle times.

In the work described below, the object was to reduce the forming time. This was achieved by increasing the pressure and/or decreasing the forming time until the sheet ruptured or the macroforming was incomplete.

In superplastic forming operations, one is concerned with two types of process, the macroforming and the microforming processes. By definition, macroforming is concerned with the gross change of shape, no quantitative figure however, such as the radius of curvature of the corner of the

formed part, was defined to be the end of the macroforming process.

Due to a rather unscientific approach to the experiments, there were a large number of unsuccessful forming attempts. The reason for this type of approach was that there was no-one experienced with either the equipment or the forming of medium size parts using superplastic alloys.

It was mentioned above that there were a large number of premature sheet failures, these were due to:

a) The applied pressure was too high.

b) The temperature of either the sheet or the thermoforming machine was incorrect.

Figure 4.5 shows a number of failures.

Three different heights, 3, 5 and 5 3/4 inches were arbitrarily chosen and the forming times and pressures for the two alloys to these depths determined.

The tests are incomplete since there was some difficulty experienced with the initial sheet temperature when the last series of tests was being conducted.

The minimum forming times obtained which were reproducable are presented in Table 4.2.

From Table 4.2 it will be seen that the forming times for the 3 and 5 inch deep parts are the same. This may, at first, appear to be incorrect and improbable, but the results were repeatable. A possible explanation for this result is,

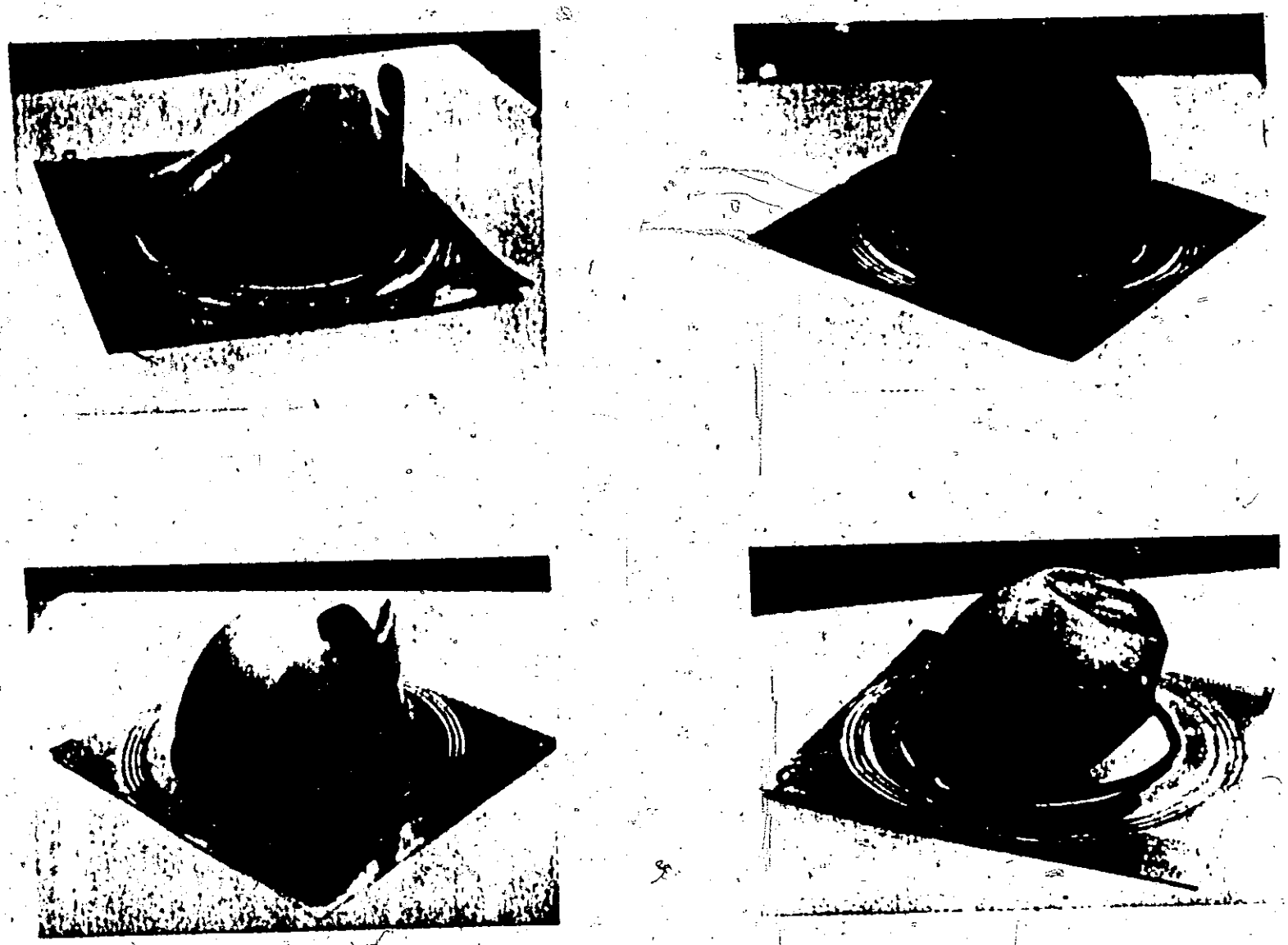

FIGURE 4.5

Photograph showing a number of failures.

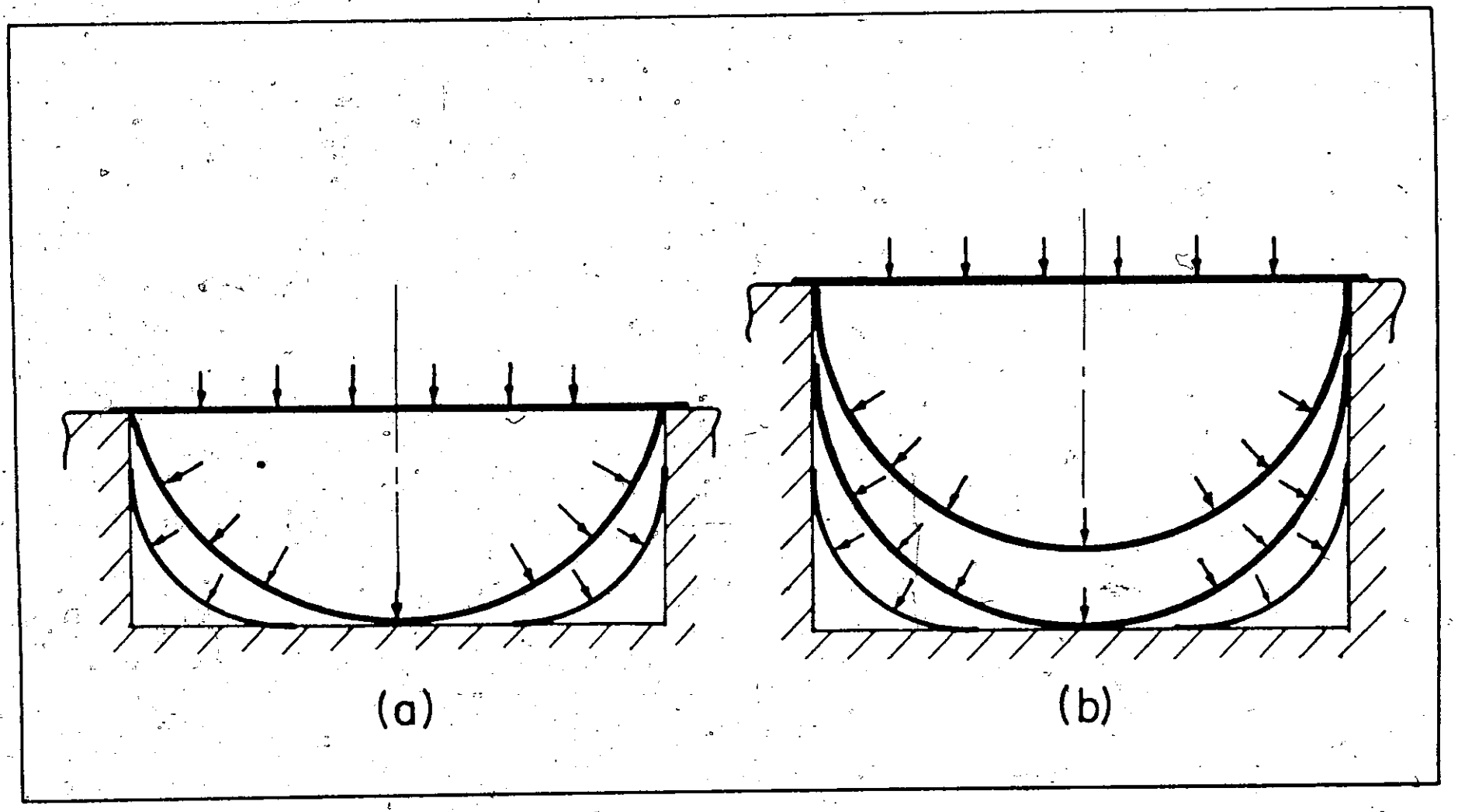

FIGURE 4.6

Schematic diagram of the mechanics of forming into a 3" and 5" deep cylindrical cavity.

as follows.

If one considers the mechanics of deformation, then for forming into a flat bottomed cylindrical cavity which is 8 inches in diameter and 3 inches deep, we have the situation indicated in Figure 4.6 a). It will be seen that initially material adheres to the bottom. After a certain time, material adheres to the sides and to the bottom of the die and the shape of the deforming membrane is part of a toroid of diminishing radius. The flow stress of the material is directly proportional to the surface area of the deforming membrane if the applied pressure is constant; recall that once material touches the die wall deformation in that area ceases.

By virtue of the material forming into the corners of the die, the surface area of the deforming membrane is continually being reduced. The flow stress is consequently being reduced as the process proceeds. The important parameter, however, is the speed of the advance of the deforming membrane into the corner. This is essentially the strain-rate and from Eqn. 2.2 is related to the flow stress;

It is now clear that as the process proceeds, the flow stress and hence the strain-rate, are reduced due to the smaller surface area of the deforming membrane. This reduction of the strain-rate effectively means that the process slows down.

If we consider the case of forming into the same 8

inch diameter cavity with a different depth of 5 inches, as shown in Figure 4.6 b), it is evident that the deforming membrane becomes hemispherical in shape and then moves down into the cavity. As this process proceeds, the material becomes thinner but there is no change in surface area, the flow stress is thus increasing. The strain-rate must also increase and the process advances more quickly. After a certain time the deforming membrane touches the bottom of the die and as deformation continues, the surface area of the membrane becomes smaller. The strain-rate and hence the speed of the process are thus reduced.

Comparing the above case with the case when the depth of the die is 3 inches, we note that the situation is identical in all respects except one, the thickness of the deforming membrane is different. The thickness when forming into the corner starts is approximately 0.030 and 0.020 inches for the 3 and 5 inch deep parts respectively if the initial sheet thickness is 0.075 inches. The geometry and mechanisms of deformation are identical, therefore the flow stress, for the same applied pressure, for the 3 inch part will be 60% of that in the 5 inch part. The strain-rate in the 3 inch part will consequently be about half that in the 5 inch deep part.

It is clear from the above that a forming time versus depth graph would take the form indicated in Figure 4.7. It would be foolish, however, to try to construct the graph from

the results given in Table 4.2.

Little success was achieved with the 5 3/4 inch deep parts. This is not due to any difficulty in forming parts to this depth by the simple blow moulding technique, since parts 6 1/2 inches deep have been produced. Rather this is the consequence of bad temperature control. From work carried out subsequently, it was observed that the temperature gradient in the oven, used to preheat the sheet, could result in the sheet being some 70 to 80°C below the set temperature.

From Table 4.2, the forming times for Alloy B are longer than those for the same depth using Alloy A. This is almost certainly a consequence of the higher 'k' value or steady state flow stress for Alloy B as indicated in Table 4.1.

4.5.2 Conclusions, Forming Time Investigation

Although a number of tests have been conducted, insufficient information has been obtained to permit any definite and accurate conclusions regarding the variation of forming time with depth. It is apparent, however, that the variation will take the form indicated in Figure 4.7. A very careful and complete experimental investigation would be necessary to provide the information to draw this curve accurately, it is debatable whether such an in-depth analysis would justify the expense.

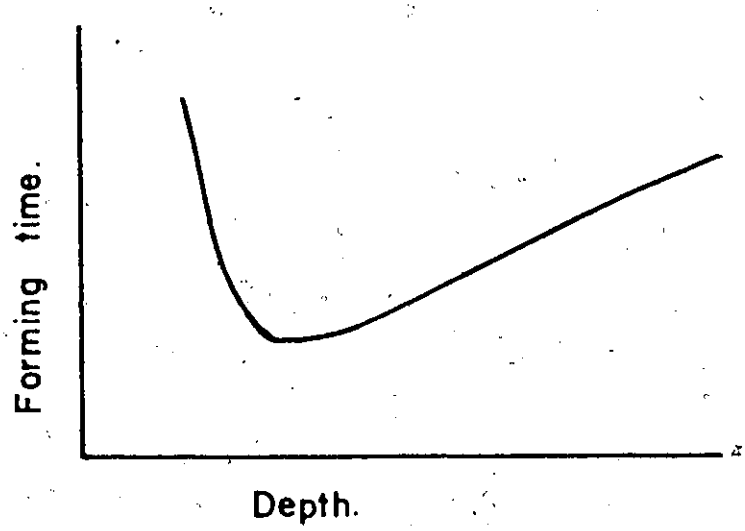

FIGURE 4.7

Schematic diagram of forming time vs. depth graph

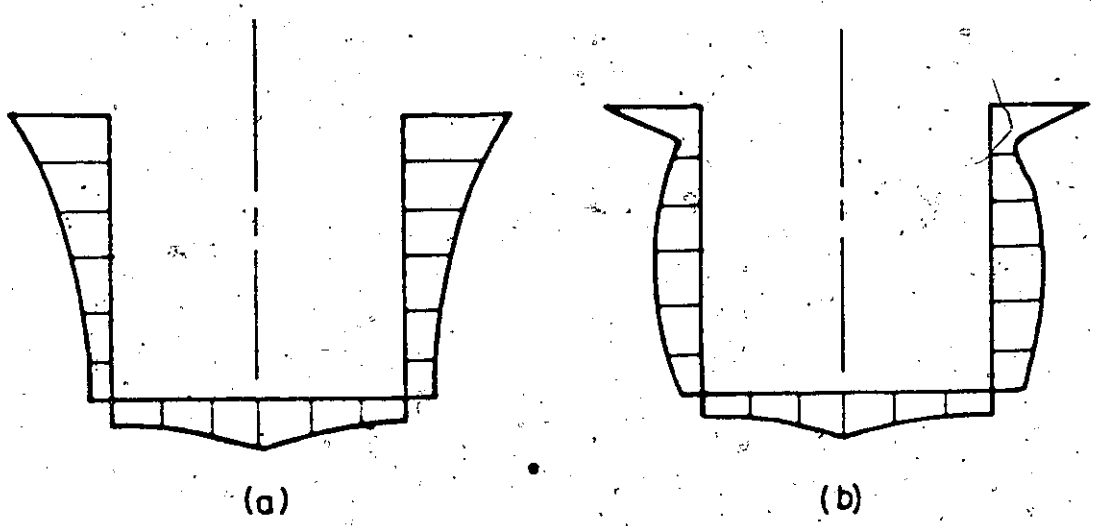

FIGURE 4.8

Two basic types of thickness distribution
a) as expected, and b) unexpected

It has been shown experimentally that the macro-forming time is low, however, the microforming aspect has not been investigated and could increase the cycle time by 100%. Comparable forming operations in the metalworking industry (ie. deep drawing) would take the same time, approximately, if the operation could be conducted in a single step. It is unlikely, however, that this would be possible and a multi-stage process would be needed, especially for the deeper parts.

The forming of materials utilizing the superplastic property of certain alloys would thus appear to be extremely attractive, industrially.

4.5.3 Thickness Distribution Investigation

From an examination of the first few parts made on the thermoforming machine, two definite forms of distribution were evident. These are designated A and B.

Type A.

This is the type of thickness distribution which is expected and is indicated in Figure 4.8 a). This is formed by the sheet bulging uniformly until a hemispherical bulge of radius R is formed. This hemispherical bulge then moves down into the die with material adhering to the walls and, after a certain time, to the bottom of the die. This type of process readily lends itself to a theoretical study.

Type B:

This form of thickness distribution was not initially expected and is indicated in Figure 4.8 b). There is severe thinning at the top near the clamping rings. This type of part is formed due to a temperature gradient within the die or the sheet or by the sheet or die temperature being lower than the superplastic forming temperature (ie. 240°C). Any difference in temperature causes the flow stress of the material to be lower at points where the temperature is higher, preferential deformation consequently takes place in these areas. This type of thickness distribution can probably be analyzed theoretically, it would, however, be a formidable task.

The successfully formed parts from the forming time work were sectioned and the thickness distributions measured. The thickness measurements are presented in Appendix I.

The thickness distributions along the sides of the formed parts for Alloy A and Alloy B are presented in Figures 4.9 and 4.10 respectively. Figure 4.11 illustrates the type B thickness distribution indicated earlier. Also presented on Figures 4.9 and 4.10 is the theoretical curve derived in Chapter Three.

The scatter in the experimental results can be attributed to a number of factors, the most important one being temperature variations. The mechanical properties of the

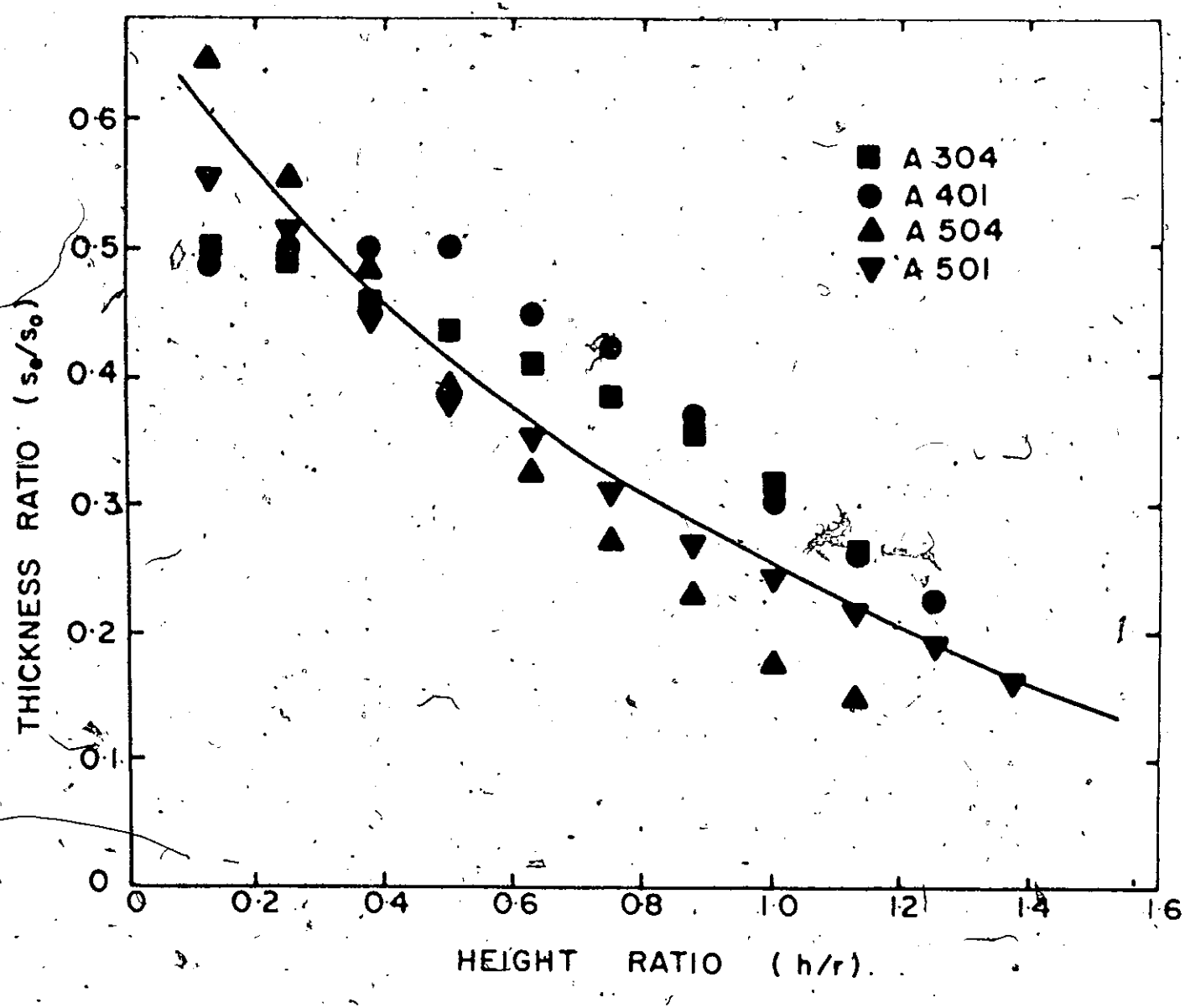

FIGURE 4.9

Experimental thickness distribution along the sides of a part formed into a flat bottomed cylindrical cavity, alloy A.

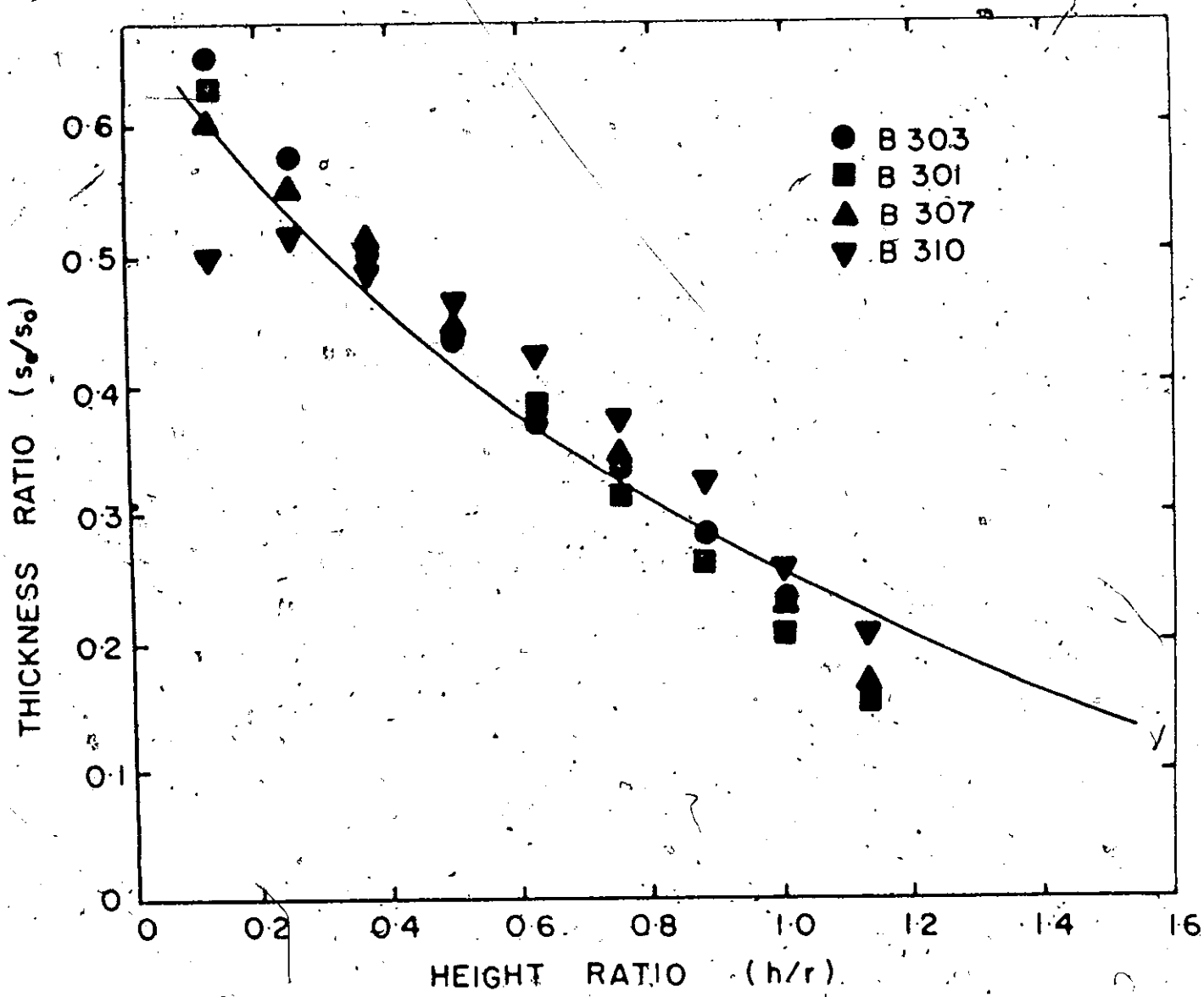

FIGURE 4.10

Experimental thickness distribution along the sides of a part formed into a flat bottomed cylindrical cavity, alloy B.

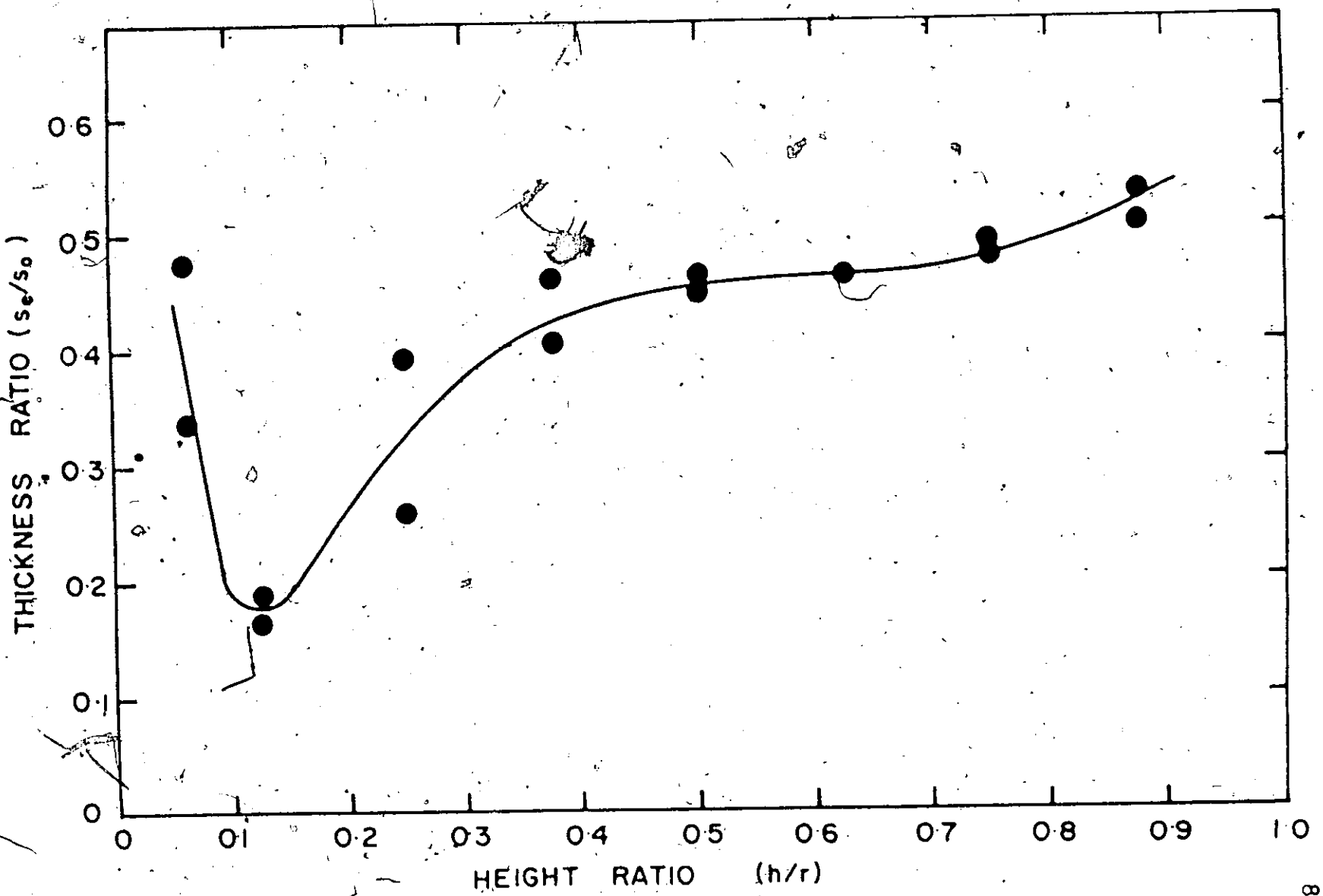

FIGURE 4.11

Type B thickness distribution showing severe thinning near the clamping ring.

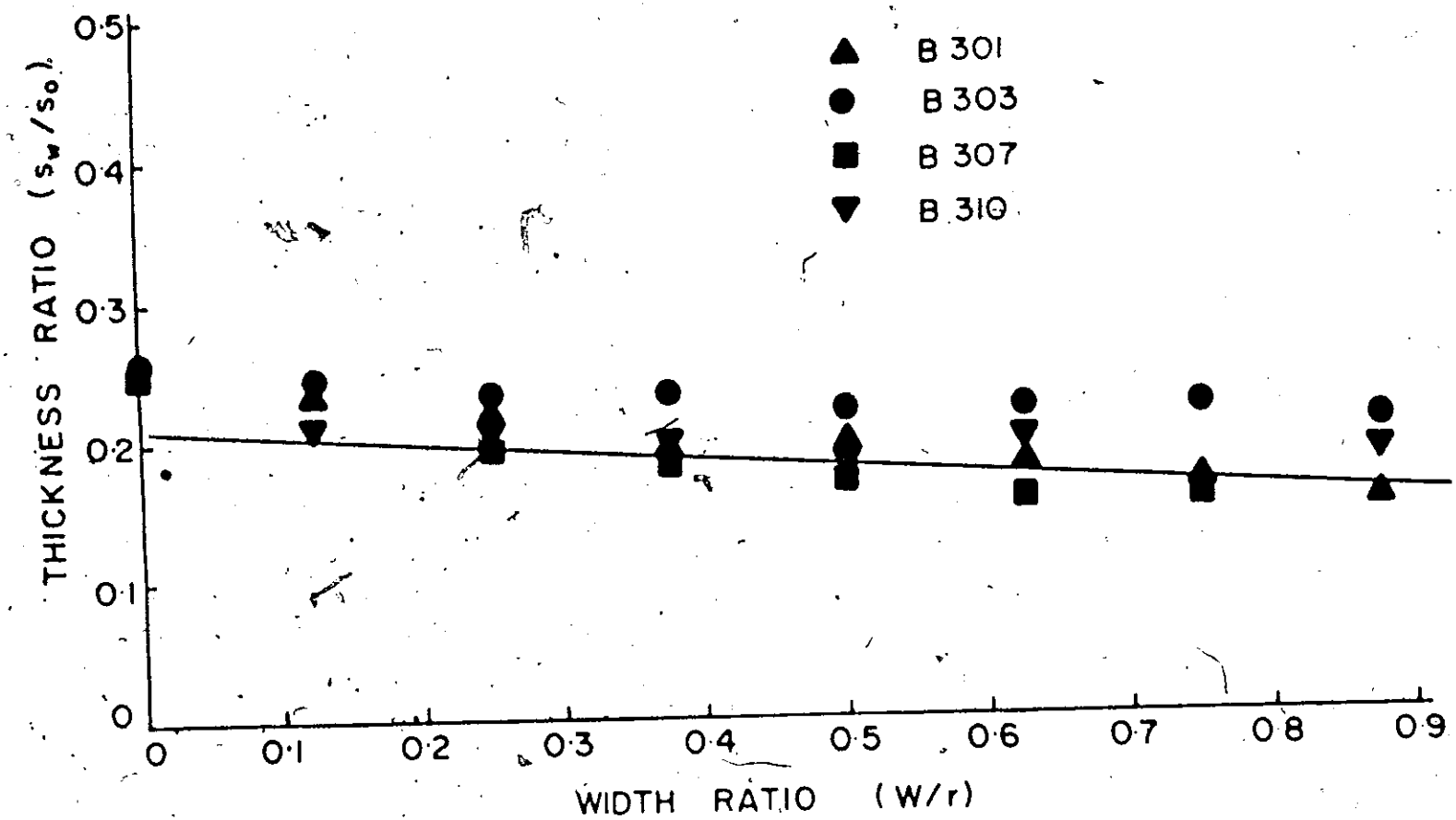

FIGURE 4.12

Thickness distribution across the bottom of parts formed to a depth of 5 inches.

superplastic sheet are appreciably temperature dependent at the forming temperature so that small variations in the temperature along the die walls or across the sheet will lead to thickness variations in the formed part.

A number of thickness distributions across the bottom of the formed part are presented in Figure 4.12 for parts formed to a depth of approximately 5 inches, the theoretical curve is also presented on this figure. The variation between the theoretical and experimental results is to be expected because of the rudimentary nature of the theoretical analysis.

Material Anistropy

To obtain an idea of the isotropy of the material, the thickness distribution of a formed part was measured along and transverse to the rolling direction. The results are presented in Figure 4.13 for the thickness distribution along the sides and in Figure 4.14 for the distribution across the bottom.

It is quite evident from these curves that there is the possibility that there is some degree of anisotropy in the sheet. No attempt was made to measure an 'R' value since previous work tended to indicate that the material was isotropic.

The variation in the results can be attributed to thickness variations within the rolled sheet or slight temperature differences within the forming chambers. The large

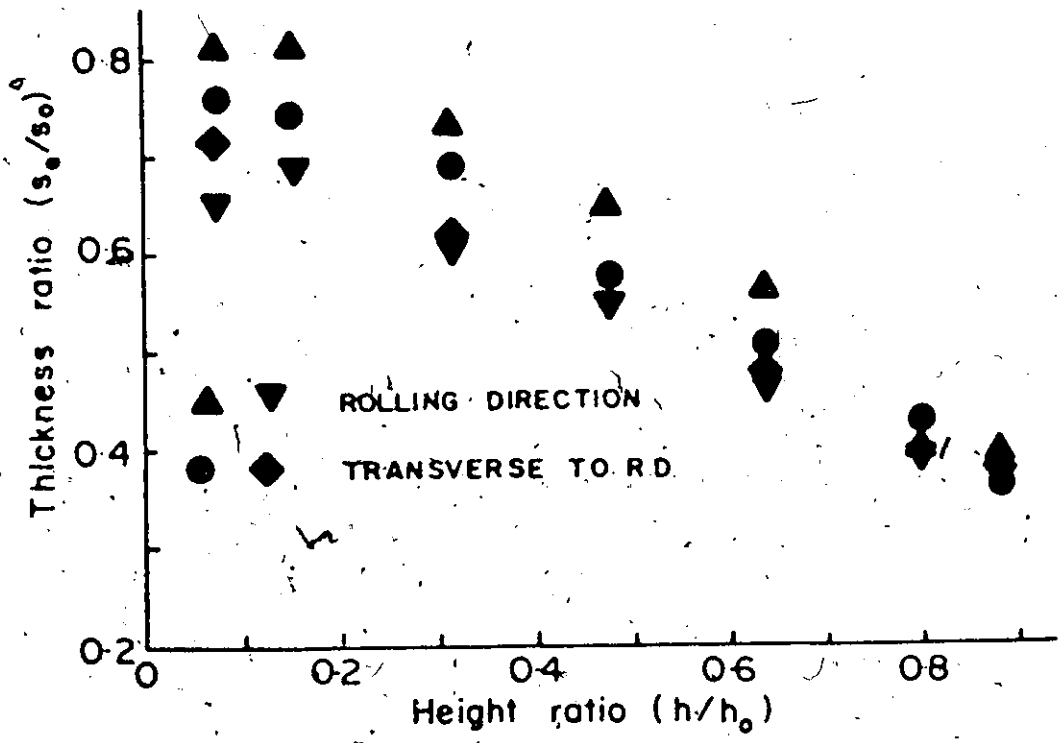

FIGURE 4.13

Thickness distribution along the sides of a part showing the variation of the thickness along and transverse to the rolling direction.

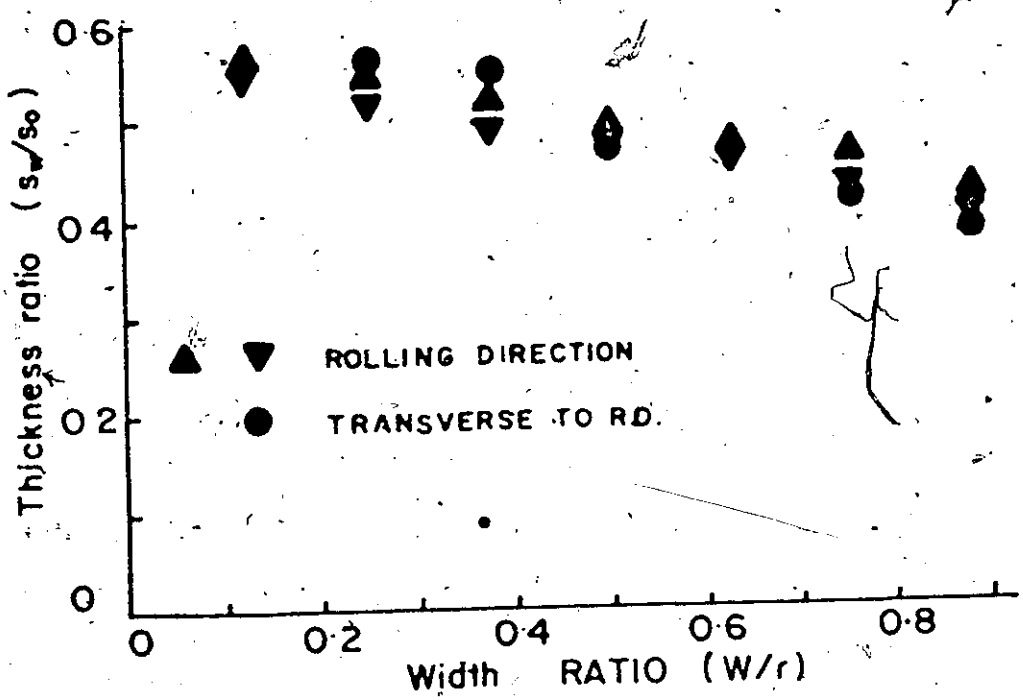

FIGURE 4.14

Thickness distribution along the bottom of a part showing the variation of the thickness along and transverse to the rolling direction.

variation at low values of the height ratio is possibly due to the variation of the friction coefficient around the edge of the die. To prevent tearing of the material, the edge of the die has been radius'd and this causes material to be drawn in from the clamping flang. Slight differences in the friction coefficient will be significant at this stage of the forming operation.

Fracture Thickness

Some forty attempts were made to form parts during the course of the forming time experiments. The successfully formed parts were sectioned and the thickness measured. These measurements provided the data for the preceeding section. Twenty parts, however, can be considered to have failed since the sheet ruptured before forming was complete. There are a number of reasons for the sheet tearing, including an unsuitable temperature distribution and too high a strain-rate. If we assume that the cause of failure is unimportant, then we can examine the fracture thickness.

The fracture thickness was measured for each of the parts which had failed. This was often difficult since the point of initiation of the failure and hence the smallest section is often unknown. The thickness was measured at a number of points along the tear and the smallest measurement taken as the fracture thickness.

The results are tabulated in Appendix II and are

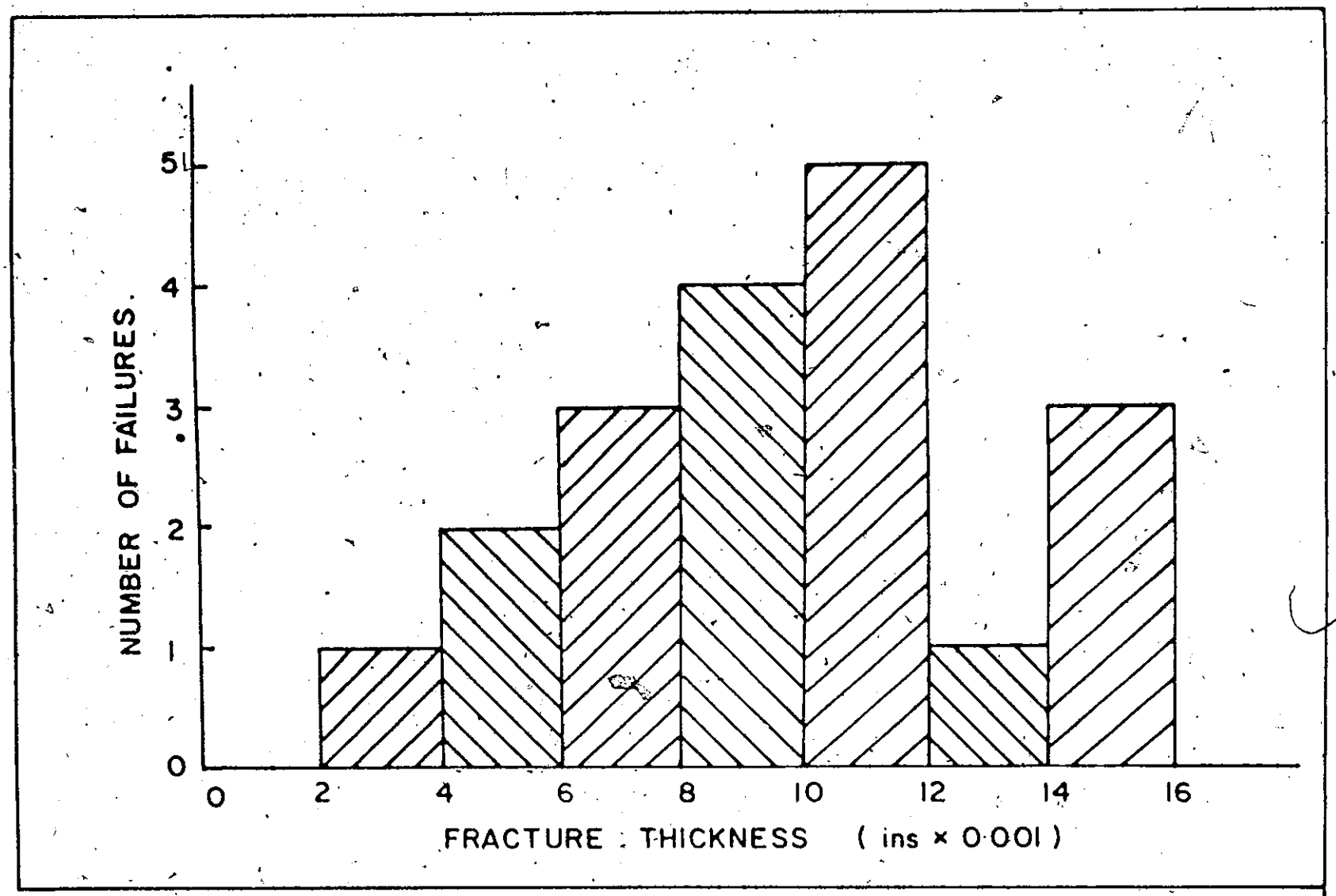

FIGURE 4.15

Column graph of fracture thickness against frequency.

presented in Figure 4.15. This is a column graph of fracture thickness against frequency and shows the sort of normal distribution expected. This curve represents the failure of twenty specimens each slightly different from the others. The initial thickness was not constant, the applied pressure was different in some cases, the temperature distribution was different for each case. It is evident from the results, however, that the fracture thickness is independent of these factors.

This result is the antithesis of that for normal alloys. For a given stress system, a normal alloy will fail, independent of the test piece dimensions. It would appear from Figure 4.15 that a superplastic alloy will deform until the thickness reaches some limiting value. This behaviour is not that extraordinary when one considers the viscous nature of the material at the strain rates encountered in the tests.

From Figure 4.15, it would appear that the probability of failure is increased once the deforming material is thinner than 0.010 inches.

4.5.4 Conclusions - Thickness Distribution Investigation

From the work presented in the previous section, it is evident that the thickness distribution is dependent on a number of factors. The most significant variable is the temperature and this must be controlled to within a degree or

two. It has been suggested that the thickness of a thermoformed part could be controlled by inducing a temperature gradient within the dies. From the above work it would seem that this may be possible, although there may be significant practical difficulties.

The agreement between the experimental results and the theoretical curve presented in Chapter Three is good. The theoretical curves, Figures 3.16 and 3.17, could consequently be used within the design field to test if the thickness variation for a particular part is acceptable.

It has been shown that there is a limiting thickness beyond which the probability of failure is significantly increased. This thickness is 0.010 inches. Using this information and that presented in Figures 3.16 and 3.17, a designer can determine the initial sheet thickness for a particular part.

CHAPTER FIVE

CLOSED-DIE FORGING OF Zn-Al

5.1 Introduction

The superplastic alloys would appear to be extremely suitable for hot forging, since sound forgings have been produced using the conventional techniques of the non-ferrous forging industry. In mechanical and hydraulic press forgings at the usual speeds, the forging loads are approximately the same as in coarse-grained alloys of the same composition. If, however, the strain-rates are reduced to the region in which the rate sensitivity is high, then attractive possibilities exist.

One possible process is a two phase forging cycle. The first part would be a moderately fast stroke to obtain most of the shaping and gross deformation. The second phase of the operation would be a dwell at constant load. In the latter part of the cycle, material can flow slowly at low stresses to fill the die completely and thus obtain a very precise impression. Advantages of such a process would be reduced forging loads, very precise control of dimensional tolerances and excellent reproduction of detail. The disadvantage is that the process must be performed within the

superplastic forming temperature range.

The excellent detail which can be achieved was demonstrated by the short run coining dies described by Saller et al.[42] This is a drop forging operation where advantage was made of the high dynamic yield stresses of superplastic alloys at room temperature. Figure 5.1 indicates the type of detail which can be reproduced.

The most extensive study on superplastic forging which has been published is that by Stewart.[36] The experimental work included both simple upsetting and the forging of a demonstration part having sharp corners and thin webs, as shown in Figure 5.2. From the results of his work, Stewart concluded that,

i) Large deformations can be produced at low stresses.

ii) The optimum forging conditions were achieved with a ram speed of 5 in./min. and at a temperature just below the transformation temperature of 275°C.

iii) Complex shapes can be forged with small draft angles and excellent die fill under relatively low loads.

5.2 Scope of Present Investigation

The aim of the work described in this and the following chapter was to undertake a study of the closed die forging of superplastic alloys. The two phase forging operation mentioned in the introduction was attempted. In order to

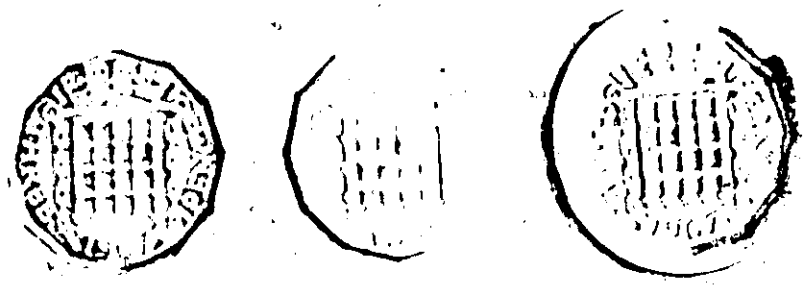

FIGURE 5.1

Photograph of the superplastic stamping die (b), from ref. 42.

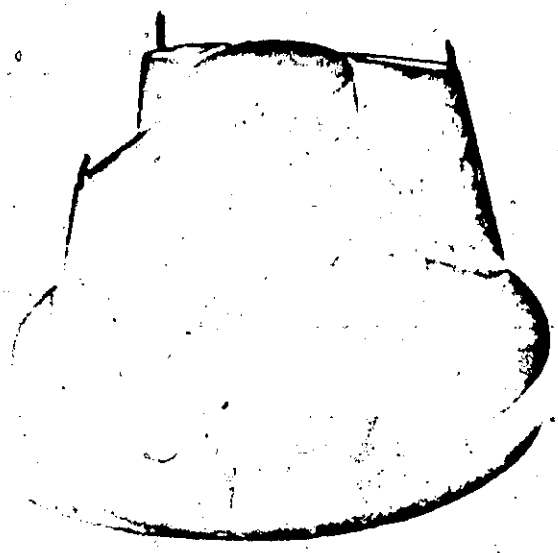

FIGURE 5.2

Photograph of the demonstration part produced by Stewart, from ref. 36.

obtain a measure of the microforming aspect and to produce a part which might have a practical application, it was decided to produce a cap having an internal thread. This was to be accomplished by pressing a threaded punch into a billet of Zn-Al. When the part had been formed it was to be ejected from the die and unscrewed from the end of the punch.

5.3 Equipment Design

The forging die and associated equipment is shown in Figure 5.3. The various ~~parts~~ are described below.

i) Die holder, Figure 5.4

This is a cylindrical block of mild steel, 9 3/4" in diameter and 6 1/2" long. It was originally designed by Jain[37] who used it in his experiments on the backward extrusion and blow molding of superplastic Zn-Al. A cavity had been machined into the block with a 14° taper into which the die was placed.

The block is heated by four cartridge heaters which are situated as shown in Figure 5.4. The temperature was manually controlled using the simmerstats shown in the circuit diagram, Figure 5.5. The temperature at different parts of the die was recorded using the thermocouples indicated in Figure 5.4 and a multipen recorder. By placing a billet, which had a thermocouple imbedded in it into the assembled apparatus, it was possible to note that in the

steady state condition, the temperature of the billet was 250°C when the die block was at 260°C.

To reduce heat losses, the die holder was insulated by wrapping 1/2" asbestos tape around the outside and placing a block of transite between the die holder and the bottom plate, as shown in Figure 5.3.

ii) <u>The die</u>, Figure 5.6

The die was machined from mild steel with the self-locking taper being machined to fit the taper of 14° in the die holder.

To facilitate removal of the formed part, the die cavity was counter bored to 2 1/2" die. This bore was used to guide the punch until the die cavity had been completely closed by the punch.

iii) <u>Punch assembly</u>, Figure 5.7 a) and 5.7 b)

The punch was also machined from mild steel and comprises two parts. The first part is the punch guide into which the punch end is located. This method of assembly had the advantage that the thread continued right up to the shoulder.

The threaded punch end was located in the guide and held using a bolt. This bolt had a left-handed thread so that when the formed part was being unscrewed, the bolt would not become unscrewed. Instead as the part was unscrewed

from the punch end, the bolt was tightened.

iv) Die bottom, Figure 5.8

This is a piece of mild steel machined so that it fitted into the bottom of the die. The top of the die bottom was the base of the die cavity.

It is threaded to accept the ejector rod assembly. The formed part was ejected from the die by pushing the die bottom up using a small hydraulic ejector cylinder which is part of the two hundred ton McMaster-Mand press used in the experiments.

v) Load distributor, Figure 5.9

In order to distribute the load over the bottom of the die holder, the load distributor was made. The die bottom rests on this and the load is thus transferred to the die holder.

vi) Die insulator, Figure 5.10

A 1-3/4" thick block of transite is used to reduce the heat loss from the die block.

vii) Ejector rod assembly, Figure 5.11 a) and 5.11 b)

To eject parts from the die, the ejector cylinder on the press was used. To insulate the hydraulic piston from the die bottom, a hollow stainless steel extension was made as indicated in the figure. This piece was internally

threaded so that the length of the assembly could be adjusted to utilize the maximum ejector rod travel.

viii) Press, Figure 5.12

The two hundred ton McMaster-Mand hydraulic press was used in the experiments. The press is fully automated and has facilities for controlling the displacement, the load and the rate of loading. Figure 5.12 shows the press with the forging apparatus assembled between the plattens.

The equipment described above is held in the press using a piece of 1" plate steel which is placed over the whole apparatus and bolted into the press platten.

An exploded view of the forging equipment is shown in Figure 5.13.

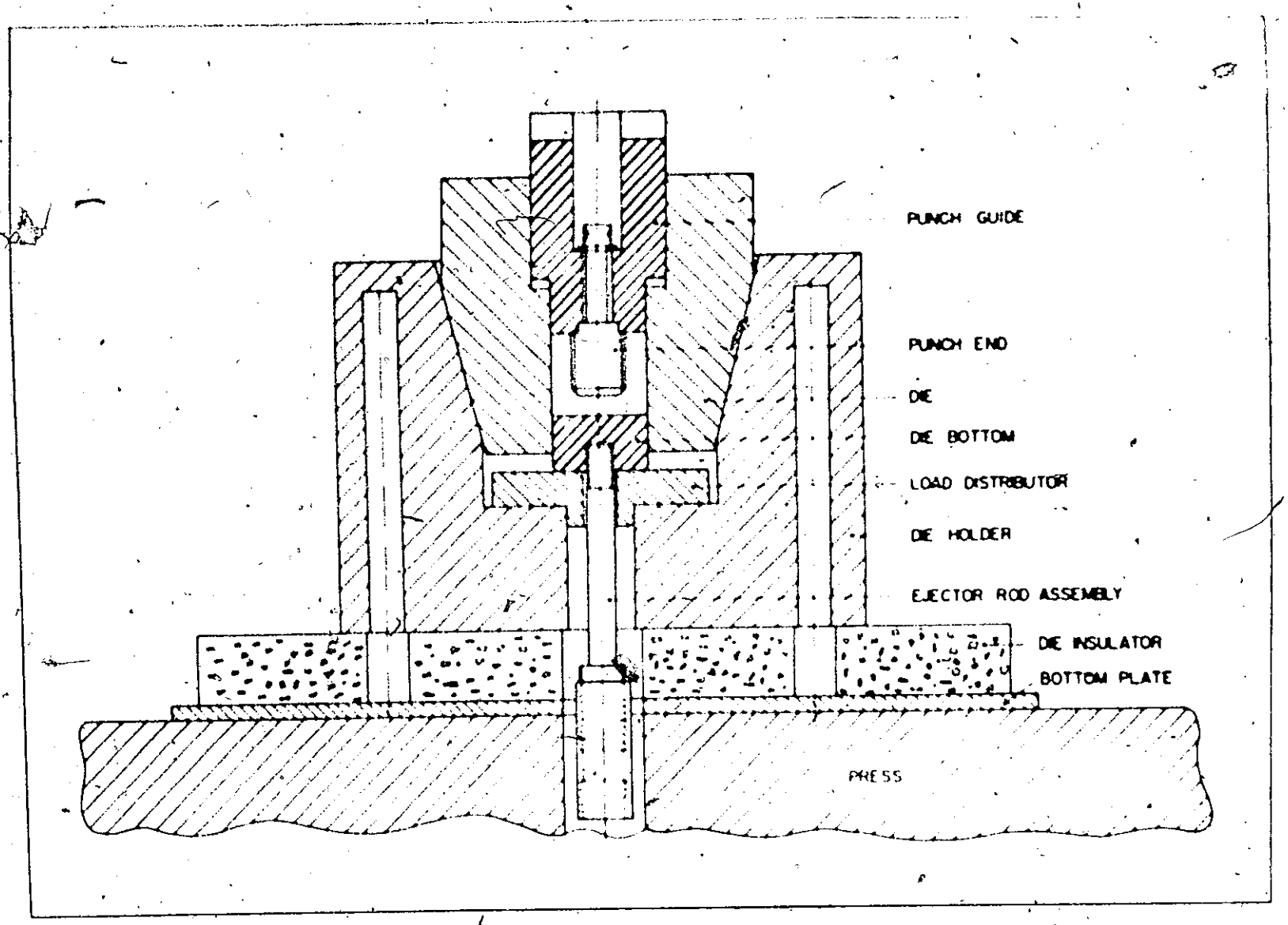

FIGURE 5.3
Forging equipment assembly.

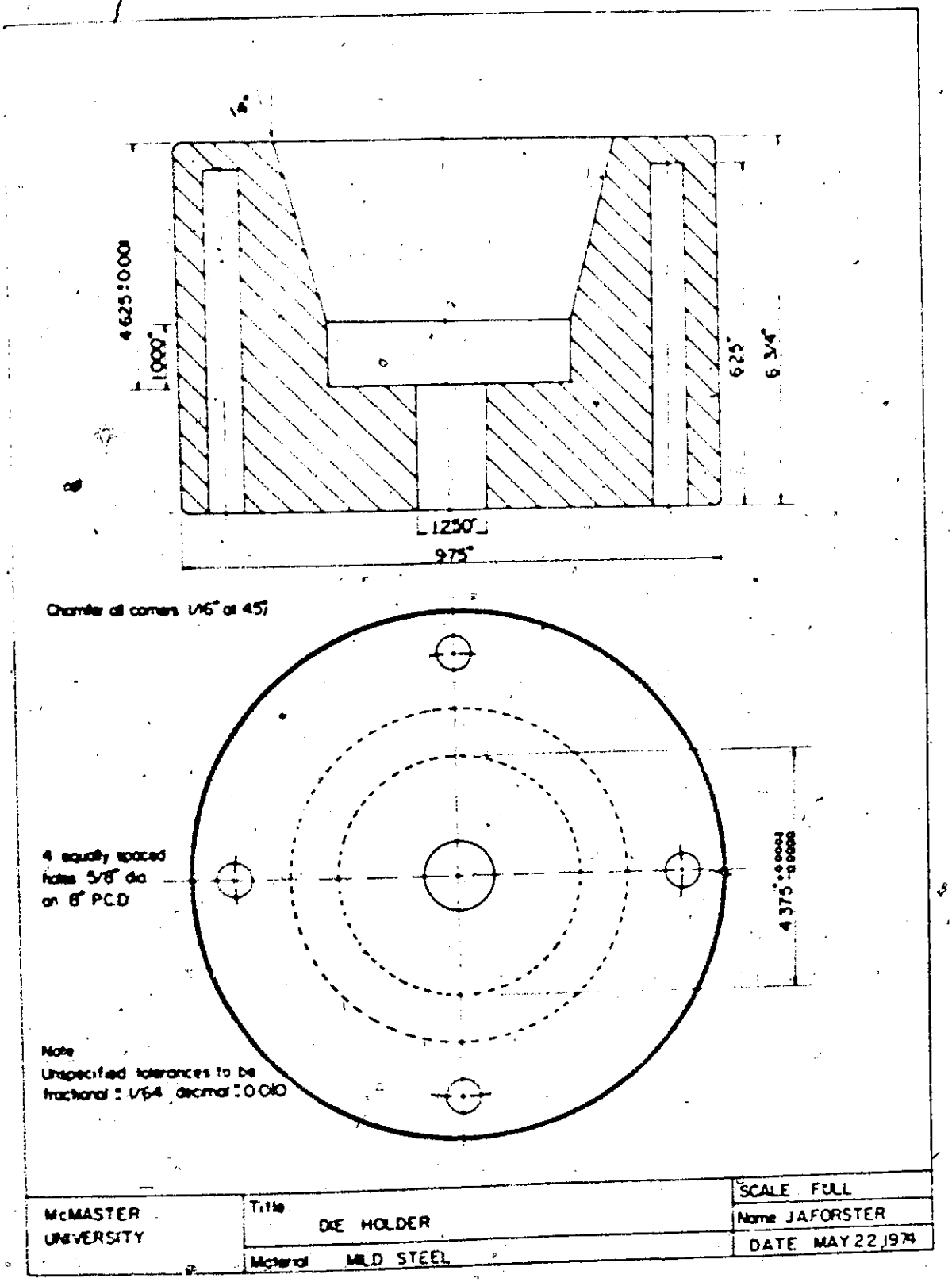

FIGURE 5.4
Die holder.

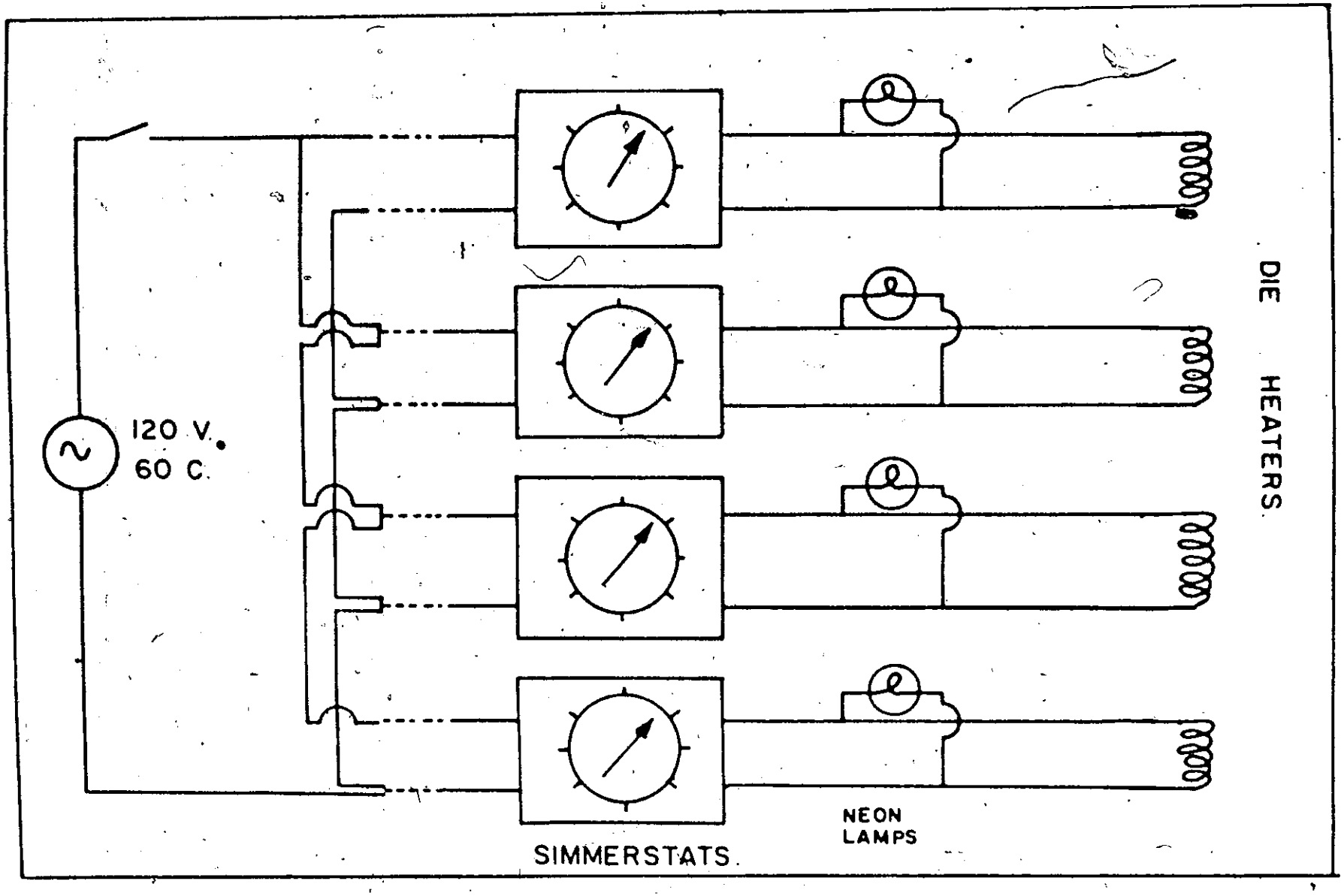

FIGURE 5.5
Circuit diagram of the heater control circuit.

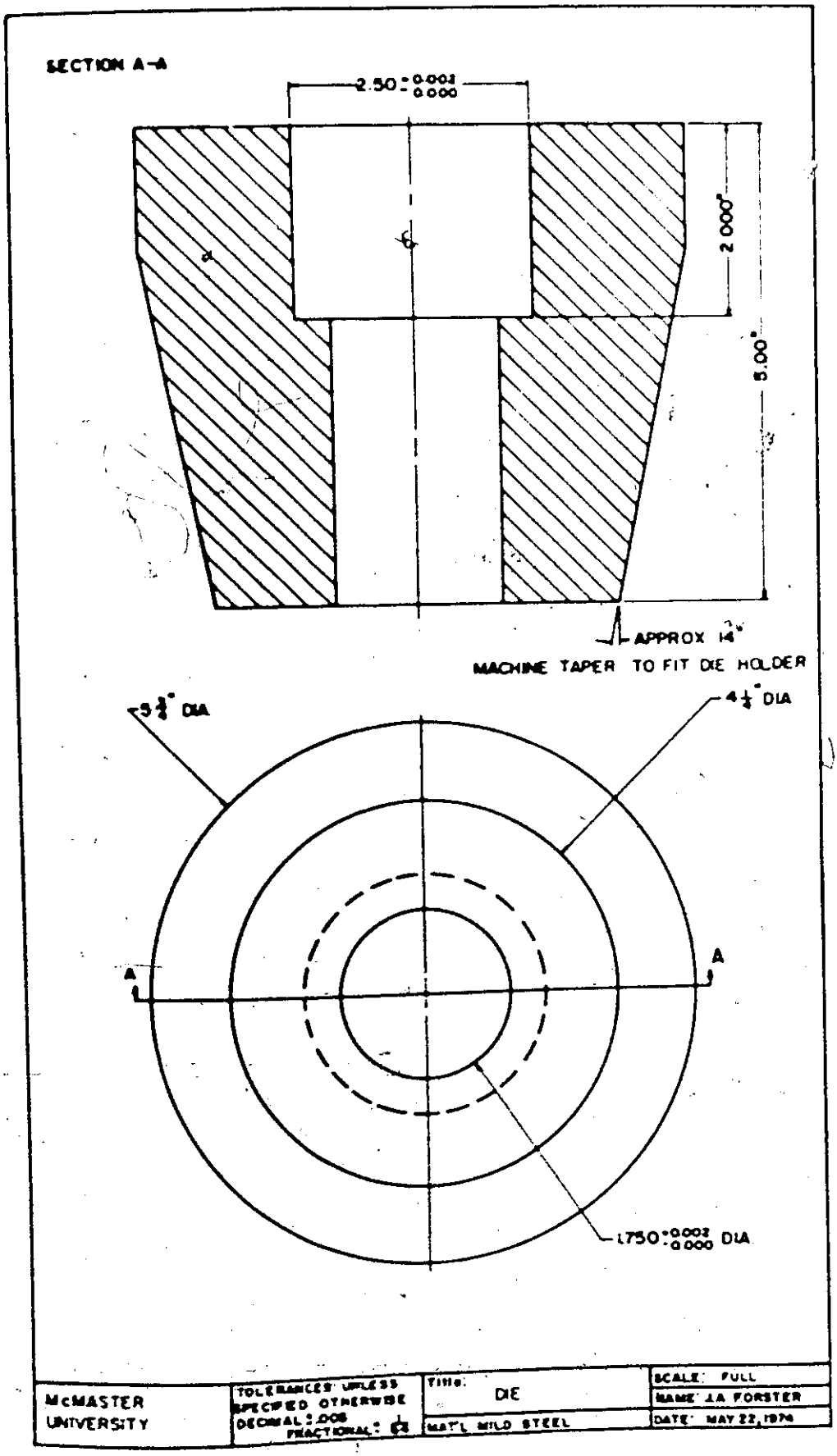

FIGURE 5.6
The die.

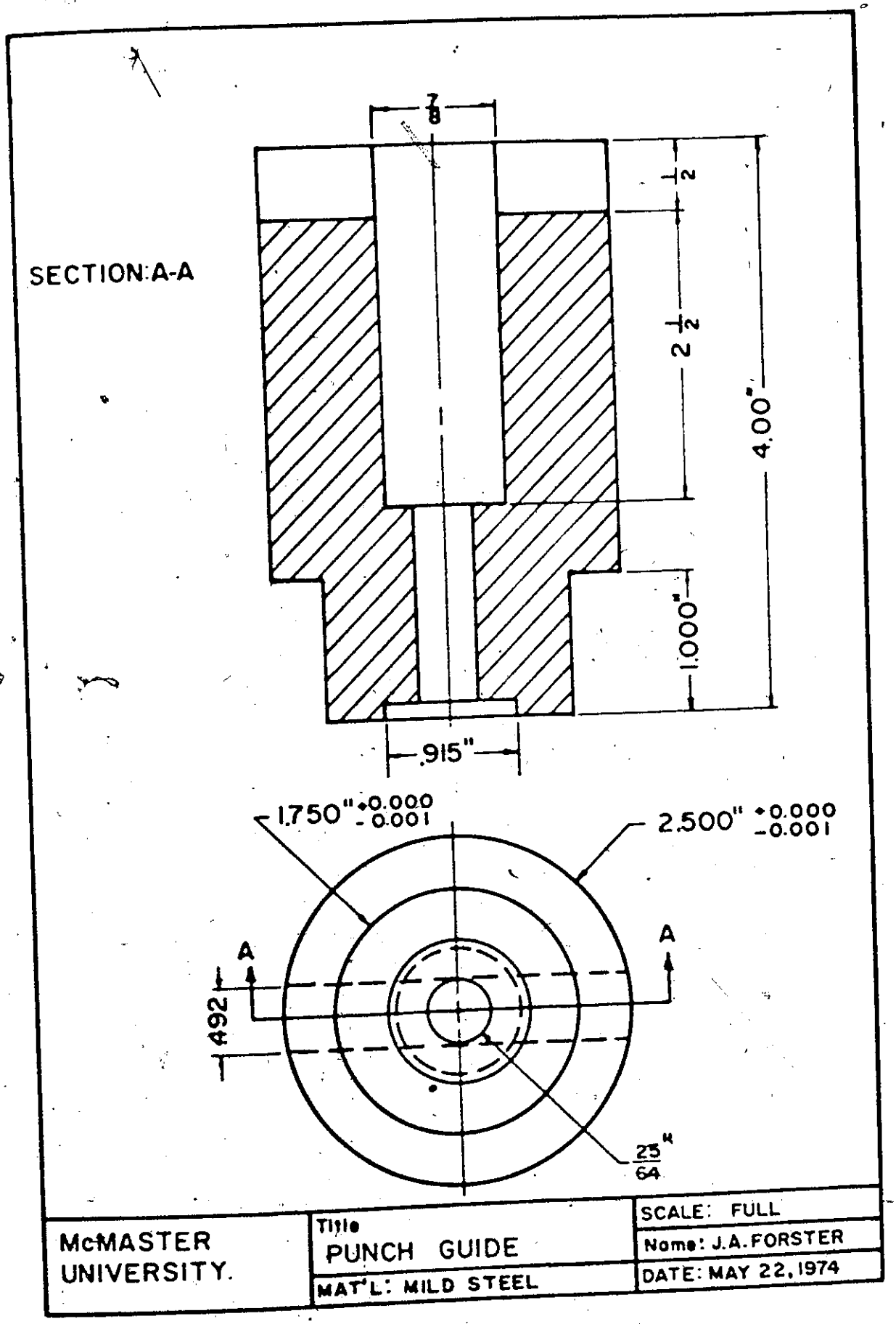

FIGURE 5.7(a)

Punch assembly .... guide.

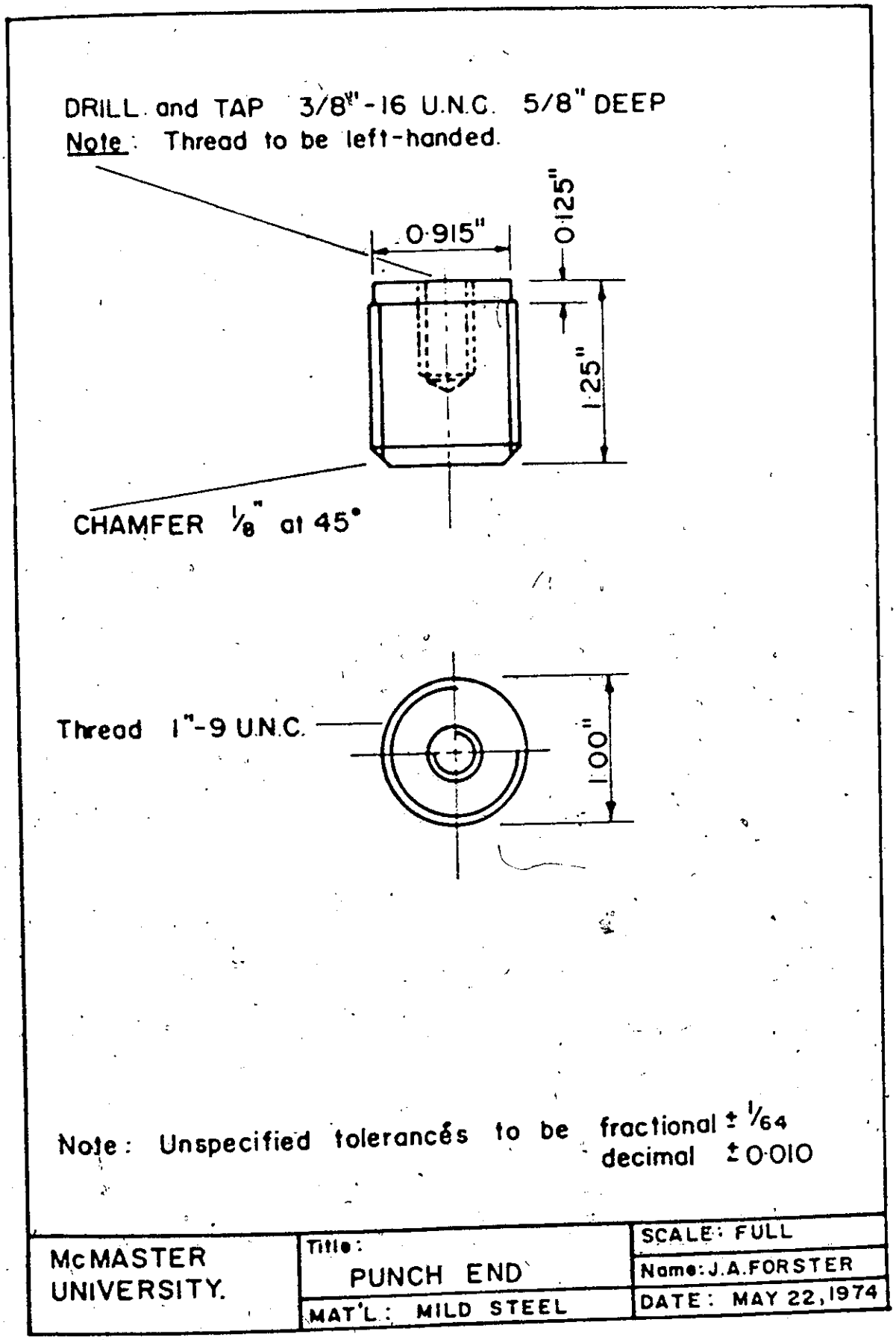

FIGURE 5.7(b)

Punch assembly .... end.

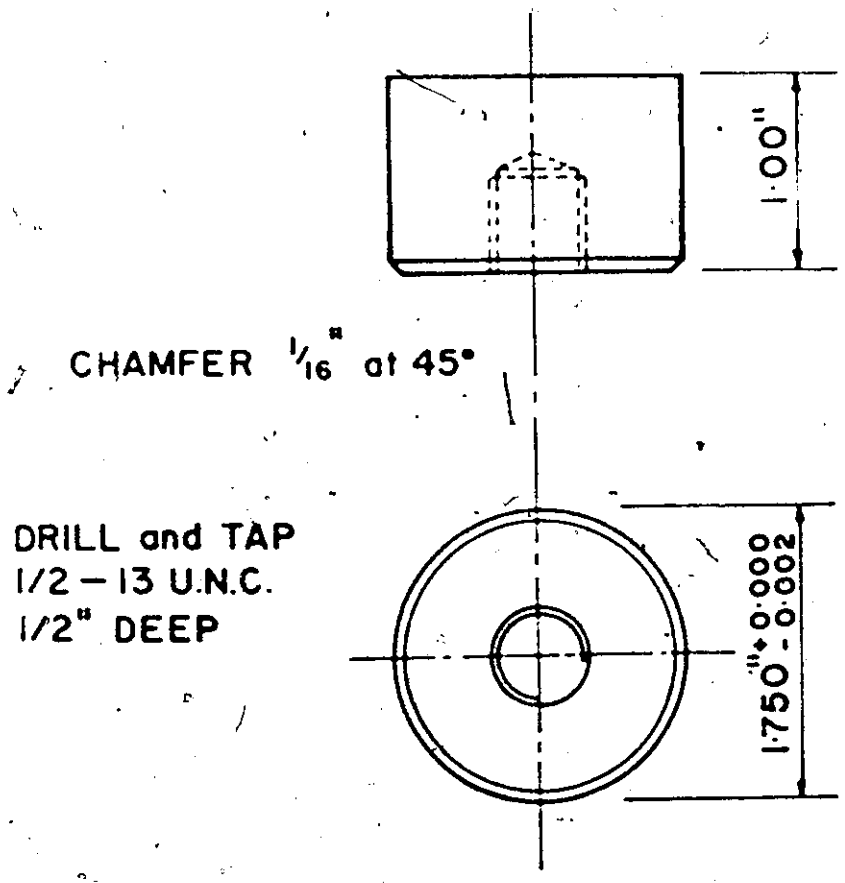

Note: unspecified tolerances to be fractional ± 1/64
decimal ± 0·010

McMASTER UNIVERSITY	Title DIE BOTTOM	SCALE FULL
		Name J.A. FORSTER
	MAT'L MILD STEEL	DATE MAY 21, 1974

FIGURE 5.8

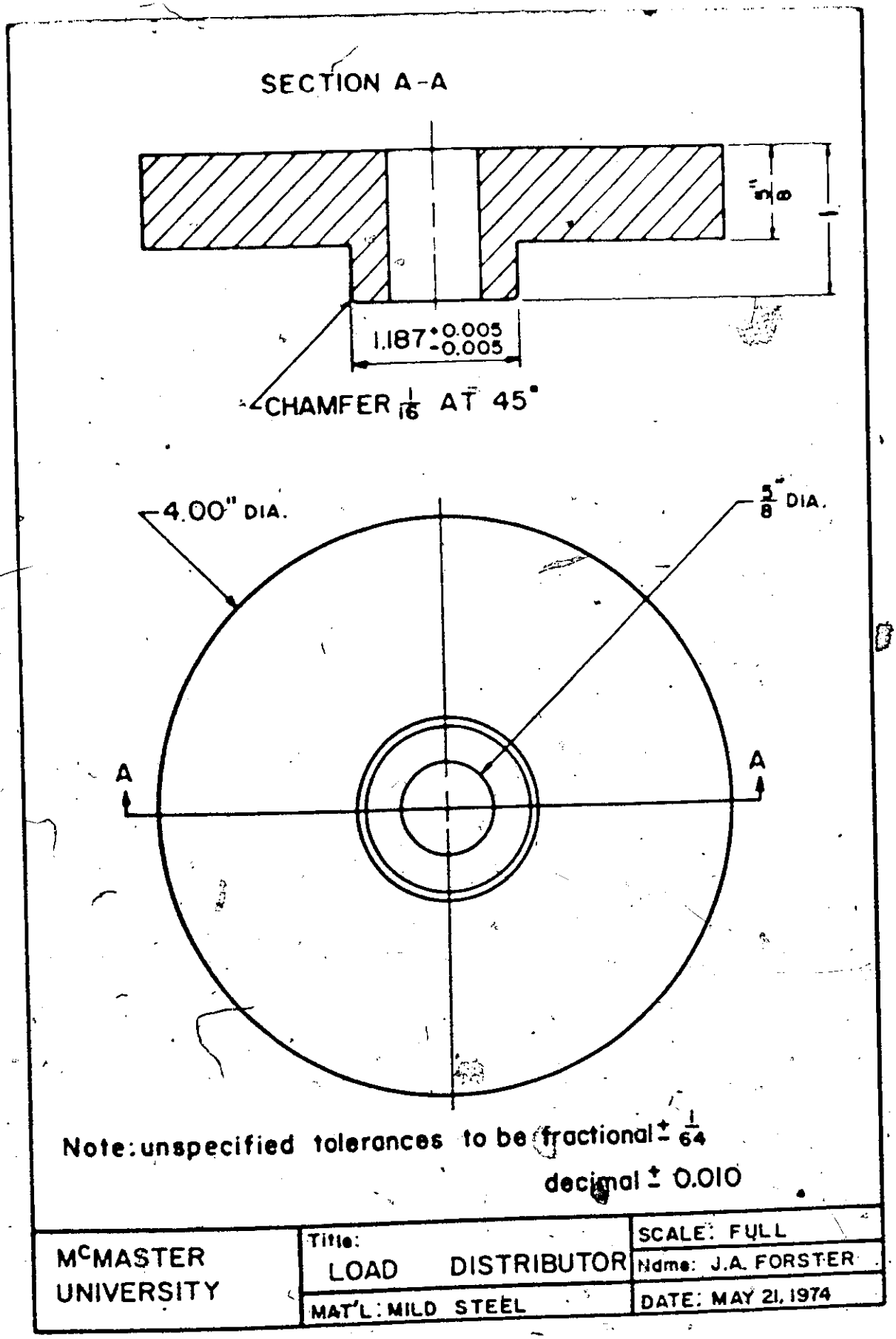

FIGURE 5.9
Load distributor.

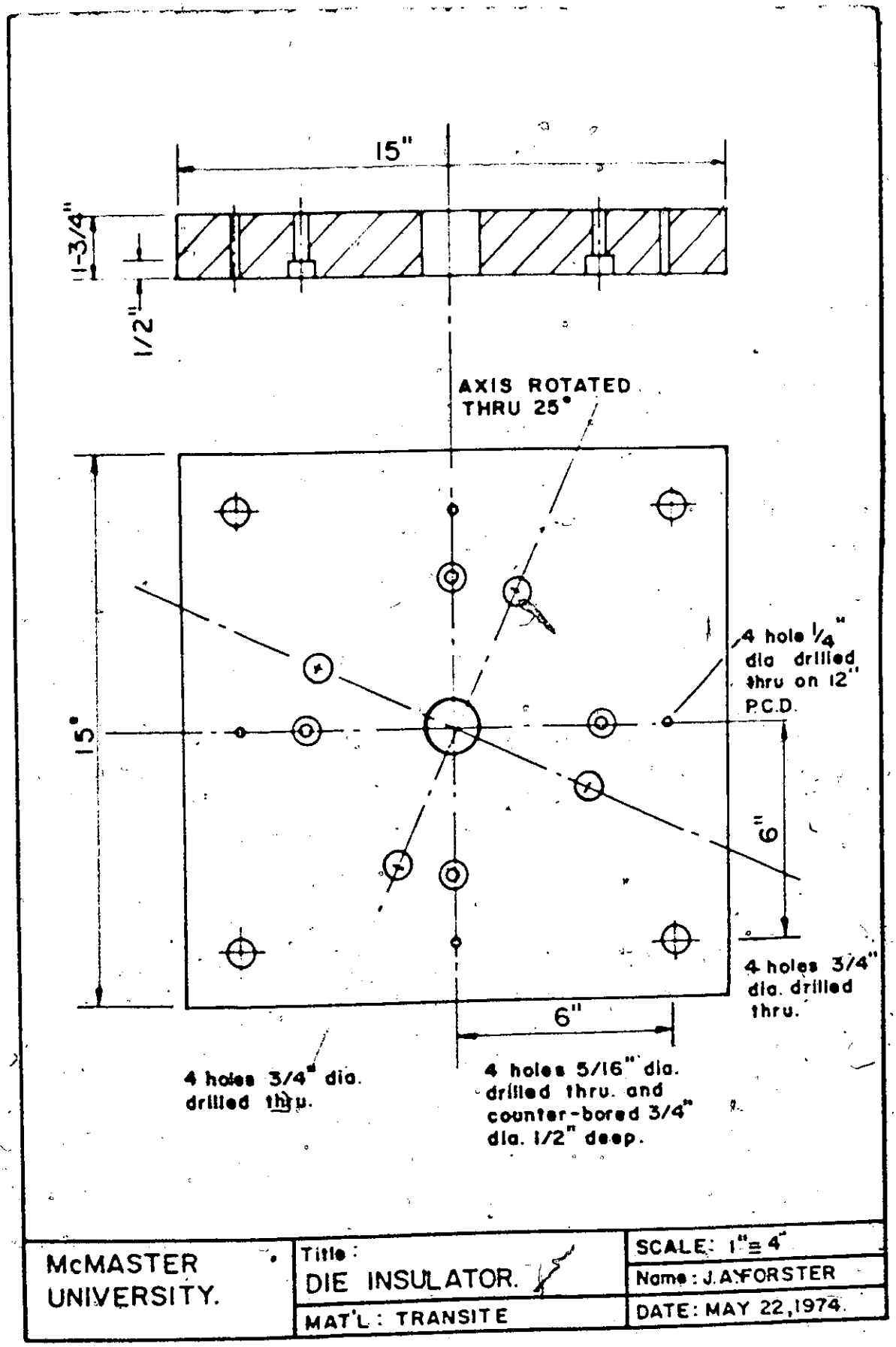

FIGURE 5.10
Die insulator.

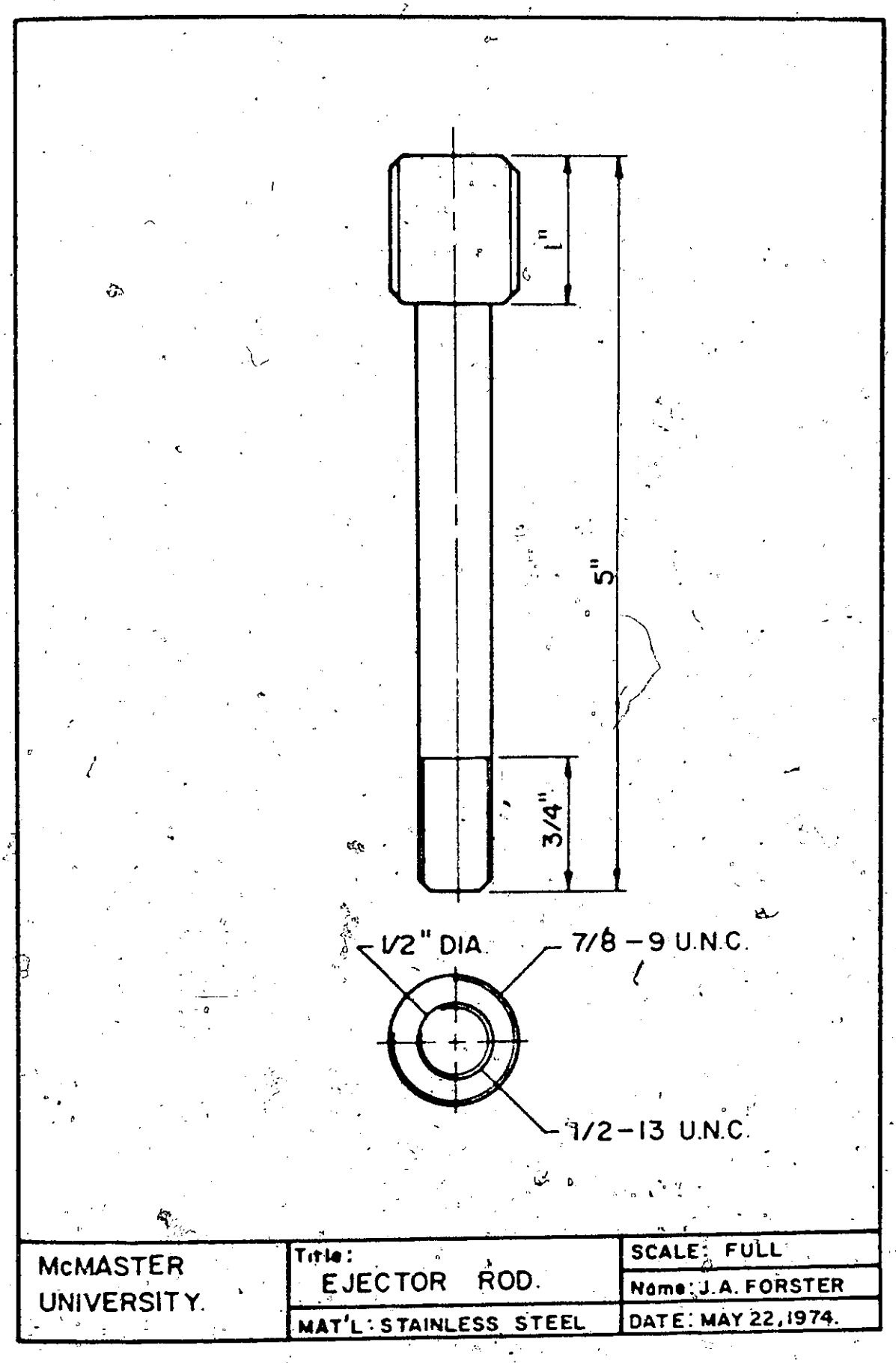

FIGURE 5.11(a)

Ejector rod assembly .... ejector rod.

Note: To be machined from solid stock

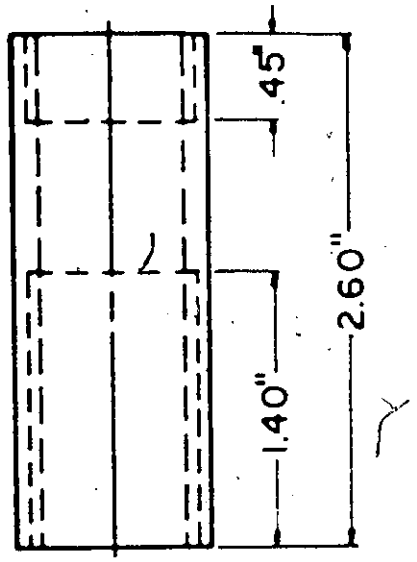

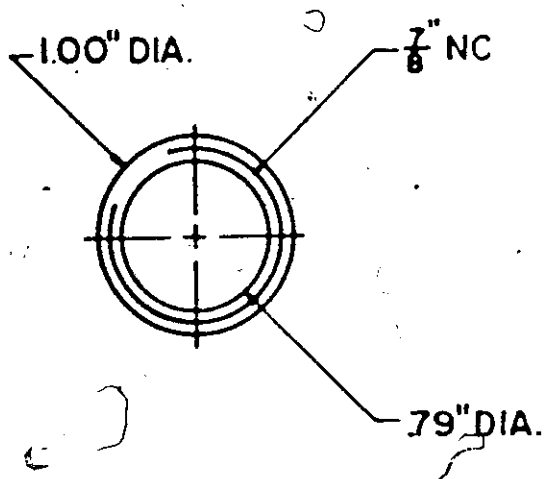

Note: unspecified tolerances to be fractional ± 1/64
decimal ± 0.010

McMASTER UNIVERSITY.	Title: EJECTOR-ROD INSULATOR.	SCALE: FULL
		Name: J. A. FORSTER
	MAT'L: STAINLESS STEEL	DATE: MAY 22, 1974

PIGURE 5.11(b)

Ejector rod assembly .... insulator.

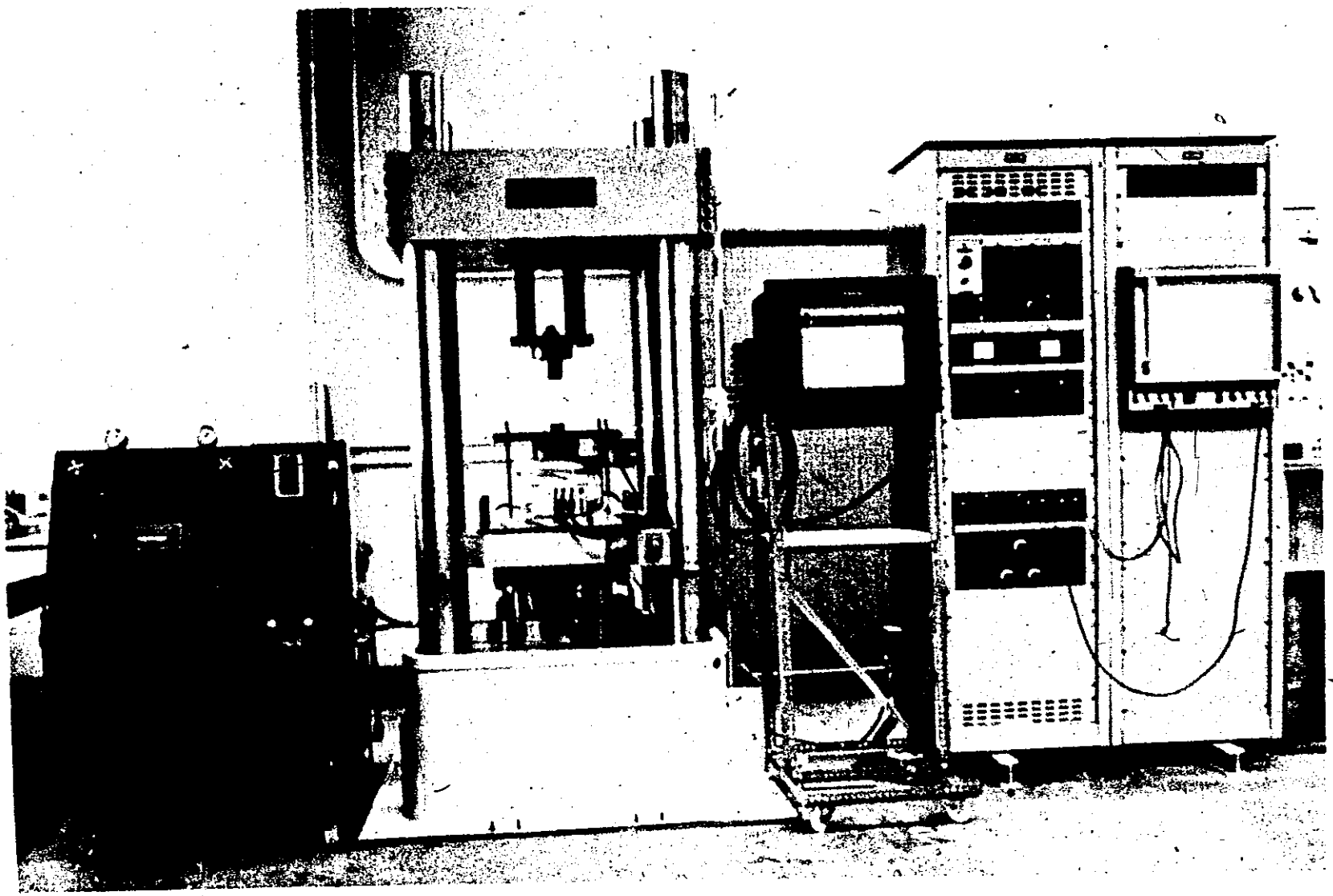

FIGURE 5.12

Photograph of the equipment installed in the press

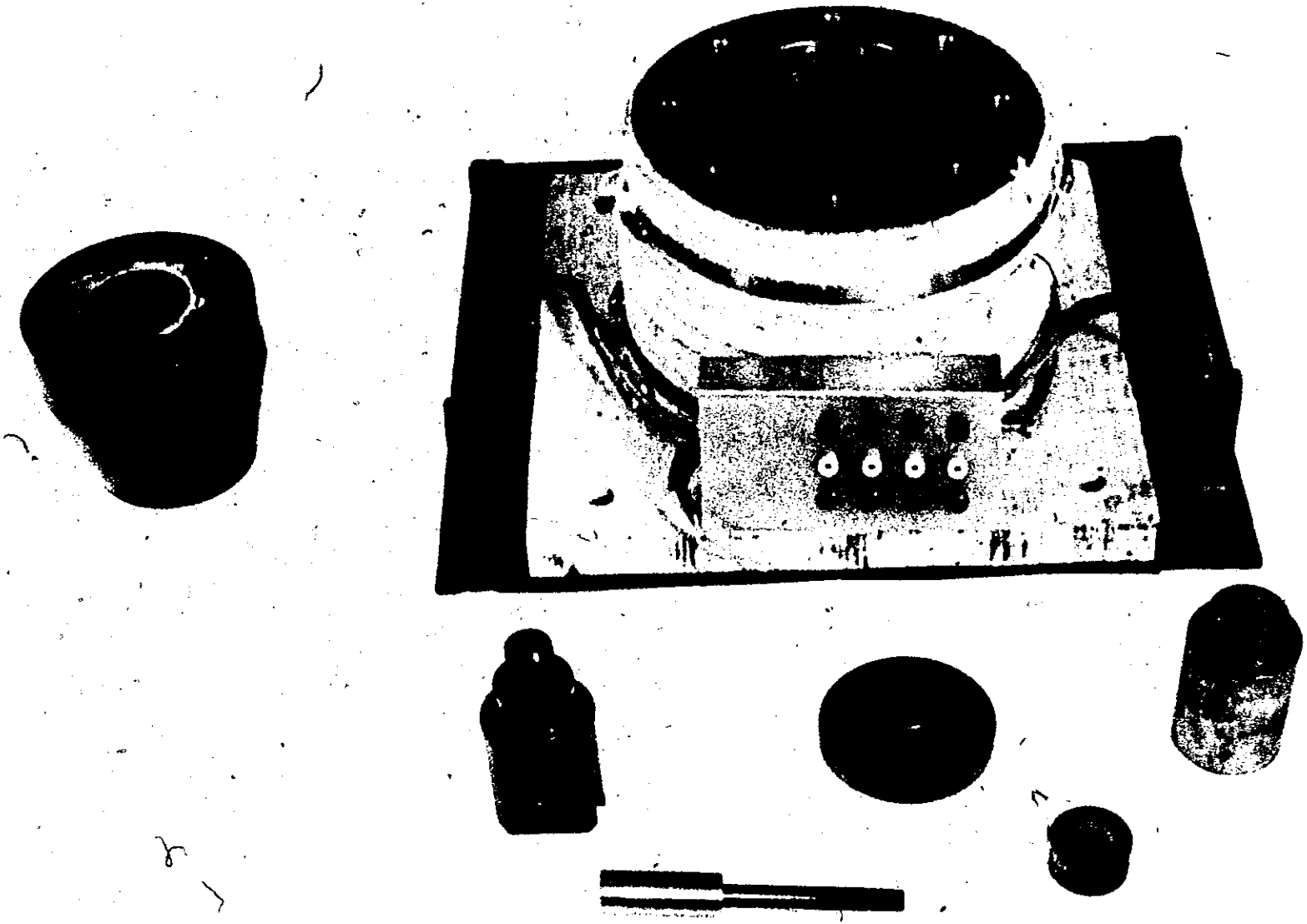

FIGURE 513

Exploded view of the forging equipment

CHAPTER SIX

FORGING TESTS AND RESULTS

6.1 Material Preparation

The eutectic Zn-Al alloy was received in the form of a length of 2 1/4" diameter continuously cast rod and a length of 1 1/4" diameter extruded rod.

The cast billet was machined to 1.75" diameter and cut into 1.5" lengths which were then machined so that the billets were 1.3" long. Eight test pieces were cut from the cast rod and were treated as follows,

i) Three were heated to 350°C for eight hours and quenched in ice-water for thirty seconds.

ii) Three were heated to 350°C for eight hours and air cooled.

iii) Two were left in the as-cast condition.

The heat treatment given in i) above has been reported by Jain[37] as rendering the material superplastic.

The extruded rod was cut into 10 test specimens 3.1" long and 5 of these were subjected to the heat treatment indicated in i) above. The remaining 5 were left in the as-extruded condition.

6.2 Test Procedure

The forging apparatus was assembled on the moving platen of the press and the heaters switched on. The temperature was allowed to stabilize at 260° ± 5°C, the superplastic forming temperature, for a minimum of one hour before any tests were conducted. The billets and the forging punch were preheated in an oven to 250° ± 2°C for an hour prior to testing.

The forging cavity was lubricated with an industrial extrusion lubricant and then the billet, which was also coated with the same lubricant was placed in the cavity. Finally the punch was lubricated and placed in the die.

The press was actuated and the lower platen raised at constant velocity. The load was recorded against platen displacement and when the load was observed to be increasing rapidly, the platen movement was stopped. Figure 6.1 shows a typical load-displacement curve. The load monitoring facility of the press was utilized and a constant load was applied for a given time. Finally, the moving platen of the press was lowered and the formed part ejected with the punch embedded in the billet.

The displacement of the moving platen of the press with respect to time was also recorded so that the forging speed could be calculated, a typical curve is shown in Figure 6.2.

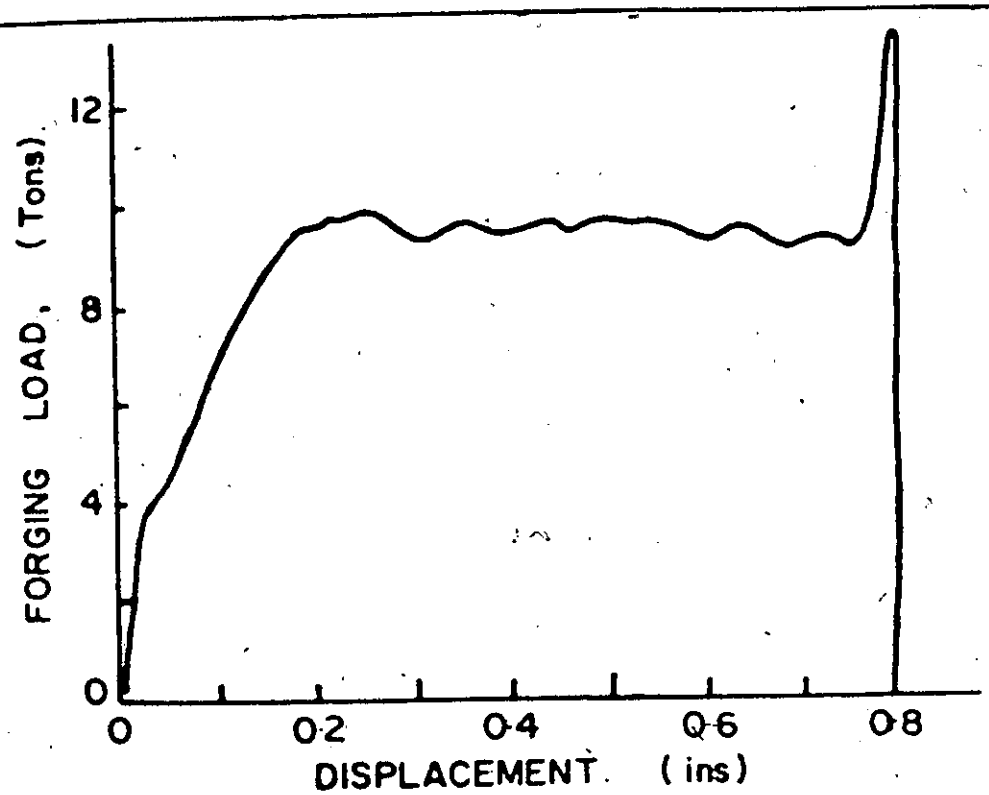

FIGURE 6.1

Typical load-displacement curve from the forging experiments.

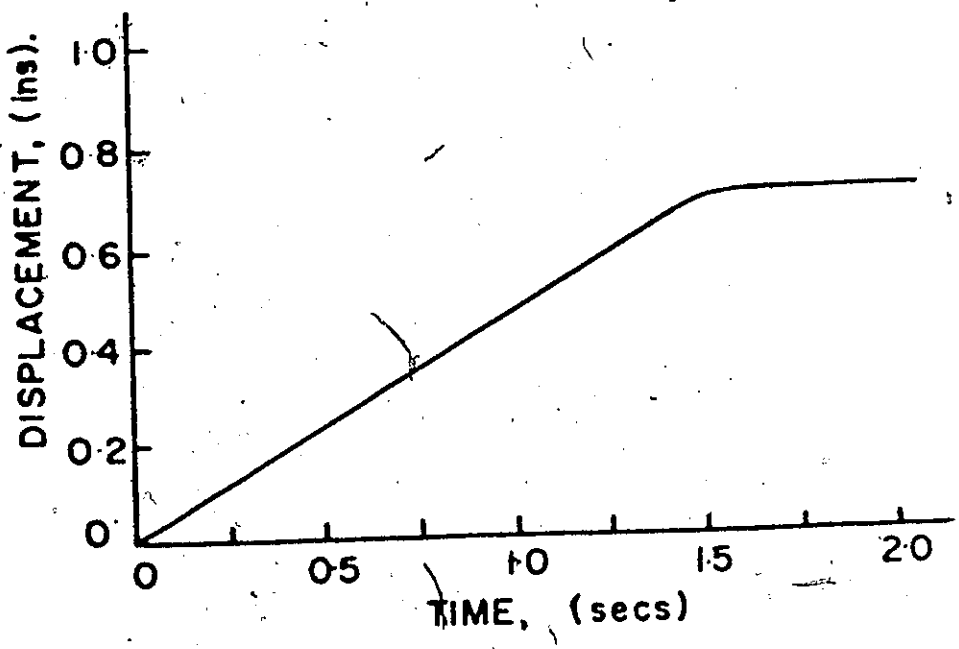

FIGURE 6.2

Typical displacement-time curve from the forging experiments.

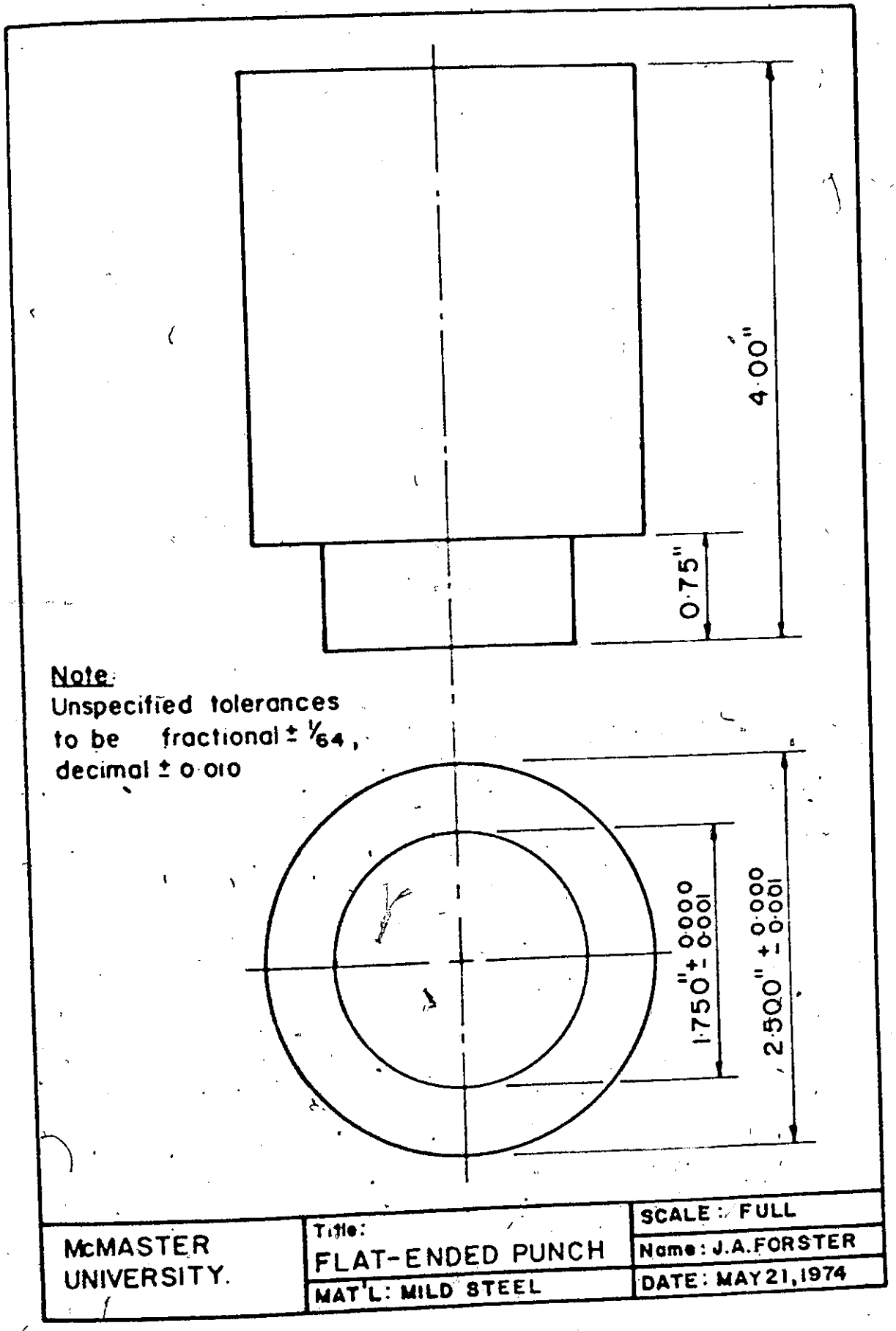

FIGURE 6.3
Flat ended punch.

Having been ejected from the die, the punch and formed part were placed in a bowl of water to cool the formed part, thus imparting some strength to the part. The punch was held using the slot milled across the top and the formed part unscrewed and allowed to cool. The punch, however, was returned to the oven for a few minutes before the next test.

The second set of tests on the extruded bar stock were conducted slightly differently, since it was first necessary to upset the billets to fill the die cavity. A flat-ended punch was made from mild-steel for the upsetting tests and this is shown in Figure 6.3.

The billets and the flat-ended and forging punches were, as before, preheated to 250°C. The billet was initially upset to fill the die cavity and then ejected so that the flat-ended punch could be withdrawn. The forging punch was placed in the die and the tests conducted as before. During this series of tests, a constant load test was attempted, where the control system of the press monitored and controlled the applied load to a preset value, in this case 32 tons.

Figure 6.4 shows the undeformed billets and the parts formed from the cast and extruded materials. The vertical score marks on the sides of the formed part were made when the part was being unscrewed from the punch end using a pipe wrench.

A vertical section was removed from each of the formed

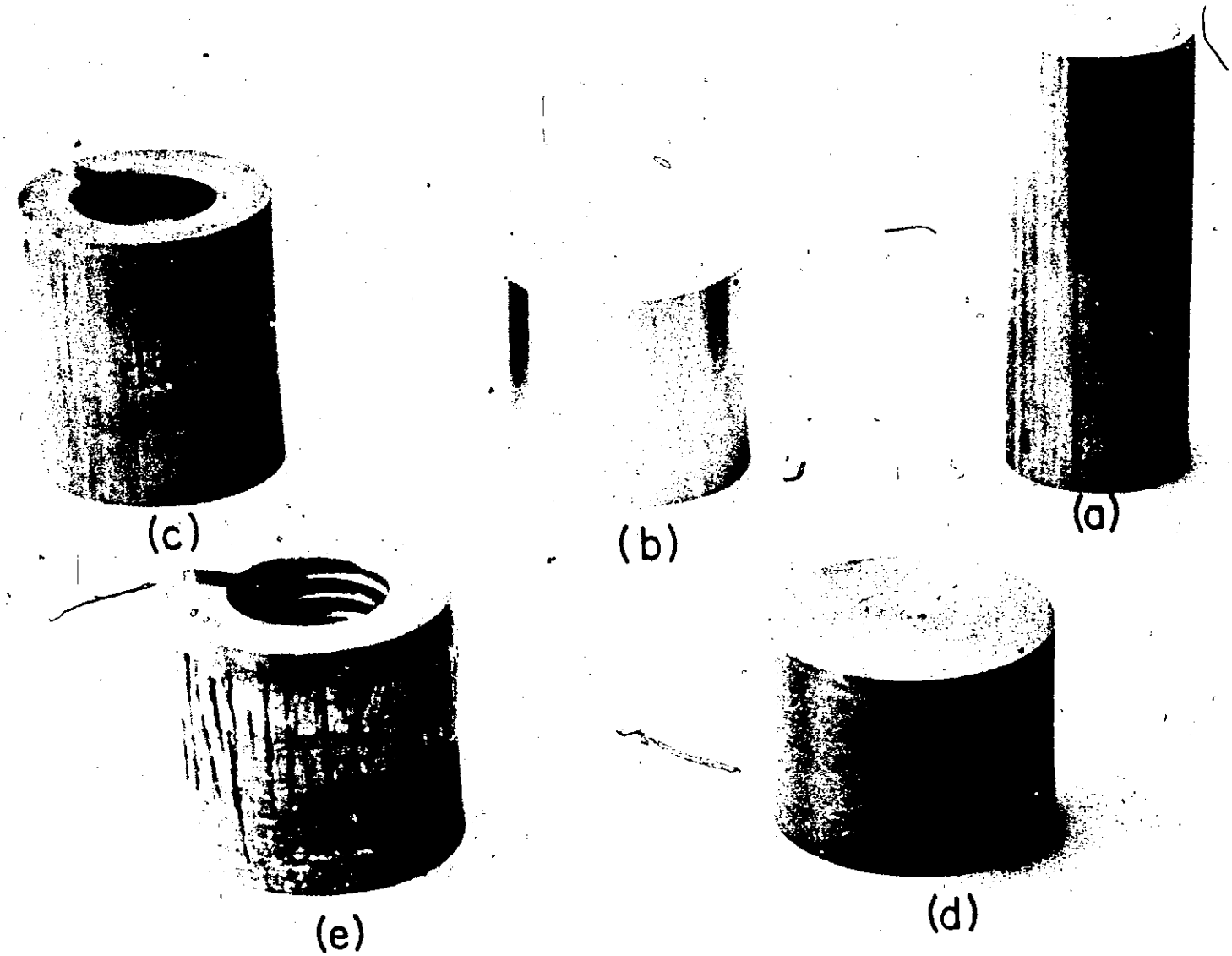

FIGURE 6 4

Photograph of the forged parts, a) undeformed billet of extruded material, b) upset billet, c) forged part, d) undeformed billet of cast material, e) forged part

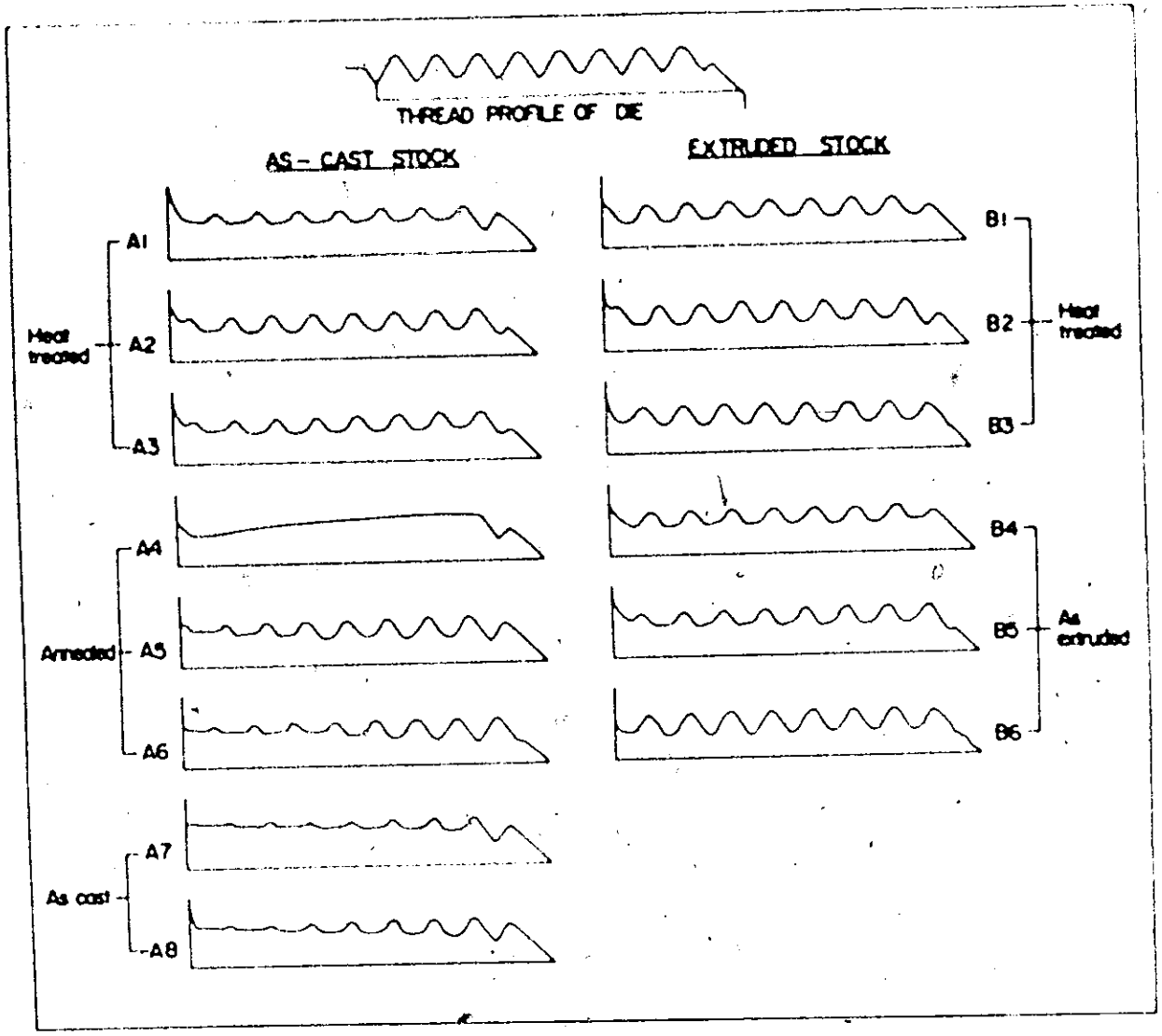

FIGURE 6.5

Thread profiles of parts forged in the experiments.

TEST 1 with as cast, annealed and superplastic material

Test no.	Condition	Ram Velocity	Avg. Load	Hold Load	Hold Time	Area	% of Forming
A1	S	0.06	19	--	--	12.67	80.0
A2	S	0.06	20	24	30	11.64	89.7
A3	S	0.18	28	40	30	11.64	89.7
A4	Ann	0.06	37	40	5	13.05	76.3
A5	Ann	0.02	32	40	30	11.59	90.1
A6	Ann	0.06	36	40	20	11.41	91.8
A7	As cast	0.02	29	40	20	13.29	74.0
A8	As cast	0.06	32	40	20	12.1	83.3

TEST 2 with extruded and heat-treated (superplastic) material

B1	S	0.02	8	32	30	11.28	93.1
B2	S	0.06	12.8	32	30	11.41	91.8
B3	S	0.23	21.2	constant load 64000 lb_f		11.7	89.9
B4	As ext	0.02	15.2	32	30	11.94	86.8
B5	As ext	0.06	21.2	--	--	12.19	84.5
B6	As ext	0.28	32.2	constant load 64000 lb_f		11.36	92.3

UNITS, Ram velocity--ins sec^{-1} Hold time--sec

Average load--$lb_f \times 10^3$ Area--in^2

Hold load--$lb_f \times 10^3$

TABLE 6-1

Results of forging experiments.

parts and the thread profile magnified and traced using an optical comparator. The thread profiles are shown in Figure 6.5.

In order to obtain a quantitative figure to define the extent to which material had flowed into the thread form, the area under the thread profile diagrams was measured using a planimeter. The area of the thread profile of the punch was also measured for comparison and to enable a 'percentage of forming' to be evaluated. The results are presented in Table 6-1.

The results of Table 6-1 should not be viewed in isolation, but should be examined while also noting Figure 6.5. For example, from Table 6-1, the area of the thread-profile diagram of test A6 for the annealed cast material and test B2 for the heat-treated extruded rod are the same. This result is misleading and uninformative since an examination of the thread profiles, Figure 6.5, shows that the thread of B2 is more uniformly formed than that of test A6, which is well formed for the first two threads only.

The best result is that of test B1 where the percentage of forming is 93.1%.

6.3 Quantitative Aspect of the Experiments

During the course of the experiments, a number of observations were made, which must, inevitably, have an effect

on the conclusions regarding this work.

The amount of lubricant applied to the threaded punch should be kept to an absolute minimum since the lubricant tends to collect in the bottom of the thread form, thus preventing complete forming. It may be possible in future work to vent the bottoms of the thread form so that excessive lubricant will be removed as the part is forged. It would probably be an advantage to use a molybdenum disulphide lubricant which can be sprayed onto the threaded punch, thus providing a very thin film of lubricant.

Another observation was made concerning the design of the thread form which, since it was machined on a lathe, had a profile somewhat similar to that shown in Figure 6.6 a). When the first forged part had been unscrewed, it was observed that there were small whiskers of material adhering to the sides of the threaded part and lying in the bottom of the thread form on the punch. It can only be presumed that a process similar to that indicated in Figure 6.7 takes place. As material is being backward extruded, then a small wafer of material is sheared from the advancing material, Figure 6.7 a), in much the same way as the cutting tool of a lathe removes metal. As the process continues, this small wafer is compressed onto the side of the thread form, Figure 6.7 b). To prevent this process, since material was remaining in the bottom of the thread form on the punch, the edges of the

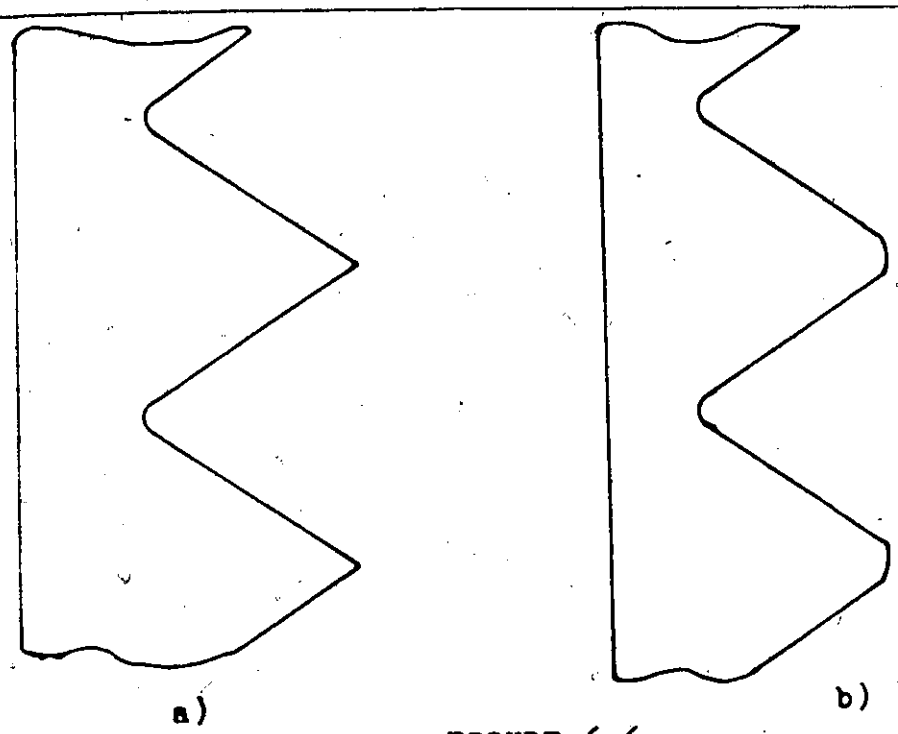

FIGURE 6.6

Thread profiles of punch, a) as initially cut on lathe
b) after modification

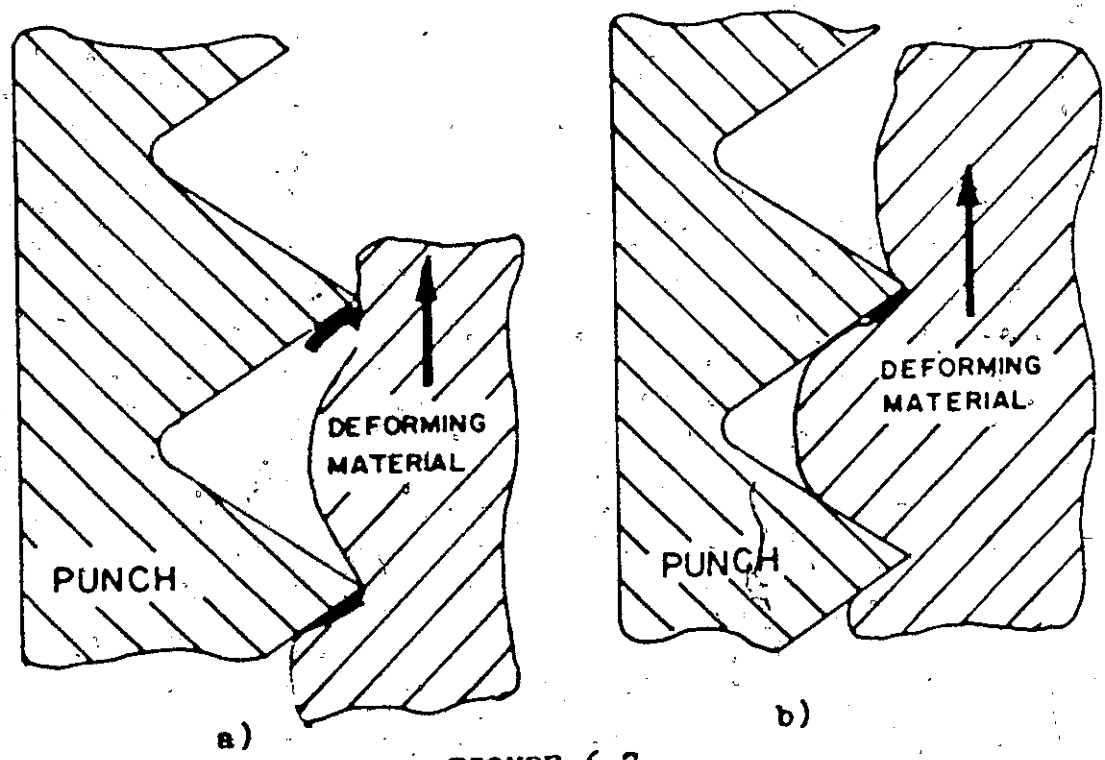

FIGURE 6.7

Possible mechanism of 'whisker' formation,
a) initially material is sheared
b) material compressed onto side of punch.

thread form were rounded, as shown in Figure 6.6 b). This appeared to be reasonably effective at the slower forging speeds, but it made little difference at the higher speeds. It would consequently appear that this effect is a function of thread geometry and of forging speed.

6.4 Discussion of Test Results

For clarity, the results have been separated and are presented below.

6.4.1 Upsetting Tests

The upsetting tests were conducted on the billets of the extruded material. The initial dimensions of the billet were 1.25" in diameter and 3.1" long and this was upset in a closed cavity so that its final dimensions were 1.75" in diameter by 1.58" long.

A typical load-displacement diagram for the test is shown in Figure 6.8 and it can be seen that there is a steady state period during which there is material flow at constant load. If the true stress is plotted against true strain, the stress will clearly decrease with increasing strain since the load was constant. This strain softening effect has been noted by other investigators.[20,38] As material fills the die and the frictional effect increases, the load increases.

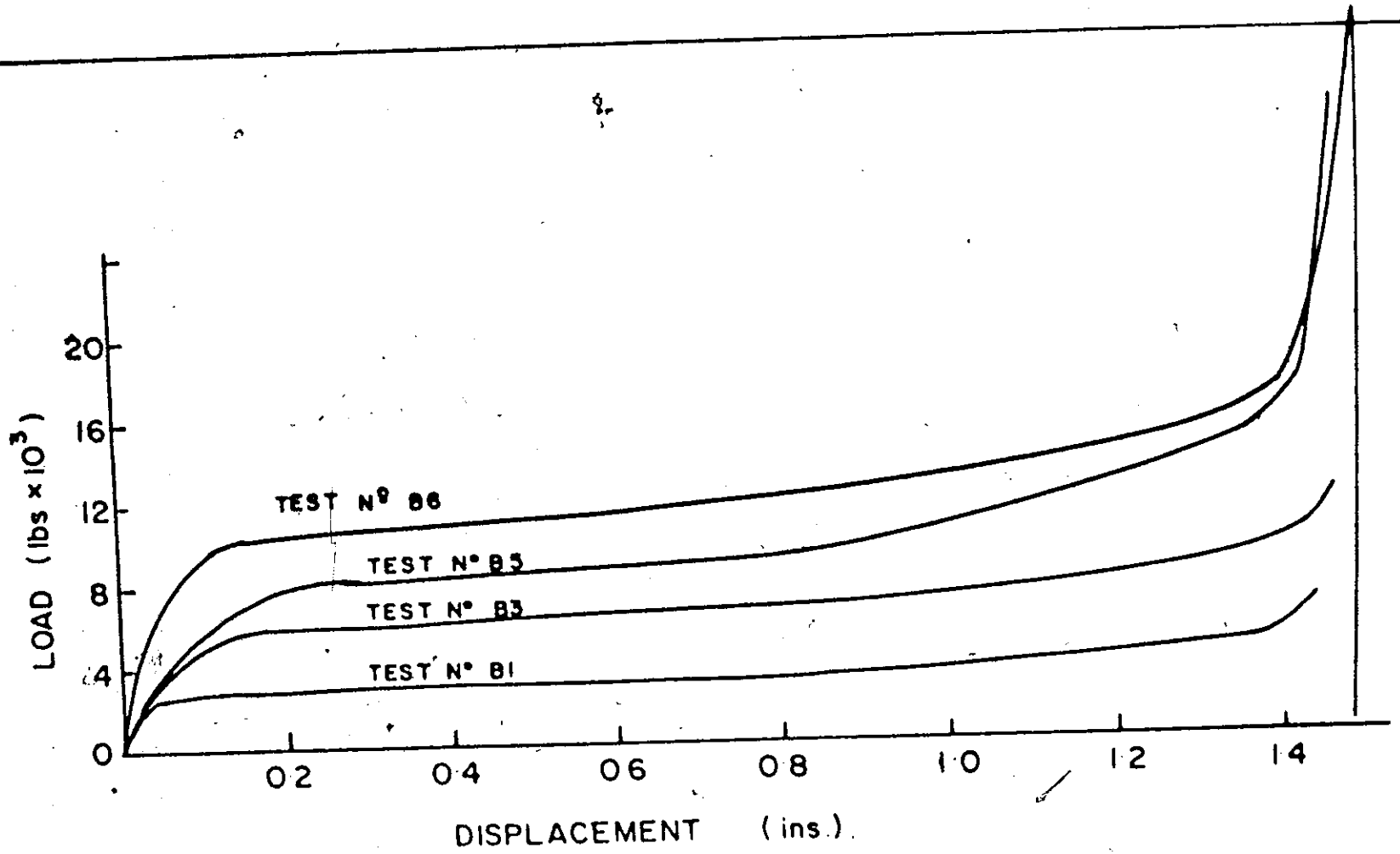

FIGURE 6.8

Typical load-displacement diagrams for the upsetting tests.

Finally, the billet fills the cavity and there is a sharp increase in the applied load.

The strain-rate dependence of the material is clearly observed in Figure 6.8, where the higher flow stresses are associated with the higher forging speeds.

Material Parameters

The value of the strain-rate sensitivity, m, and the constant, k, in the constitutive equation

$$\sigma = k\dot{\varepsilon}^{m}$$

can be obtained from the results of the upsetting tests.

Assuming that there is no barrelling of the specimen, then the stress and strain-rate at several points during the test can be found from the load-displacement diagram. This has been done and the results are given in Appendix III and are presented logarithmically on Figure 6.9. From this figure the 'm' and 'k' values can be determined and are presented in Table 6-2. Also presented in this table are the material parameters for the continuously cast material from Ref. 38.

Material	Condition	k $lb_f\ inch^{-2}\ sec^m$	m
continuously cast	as cast superplastic	13,550 13,580	0.184 0.360
extruded	as extruded superplastic	11,000 5,050	0.48 0.48

TABLE 6-2, Material Parameters

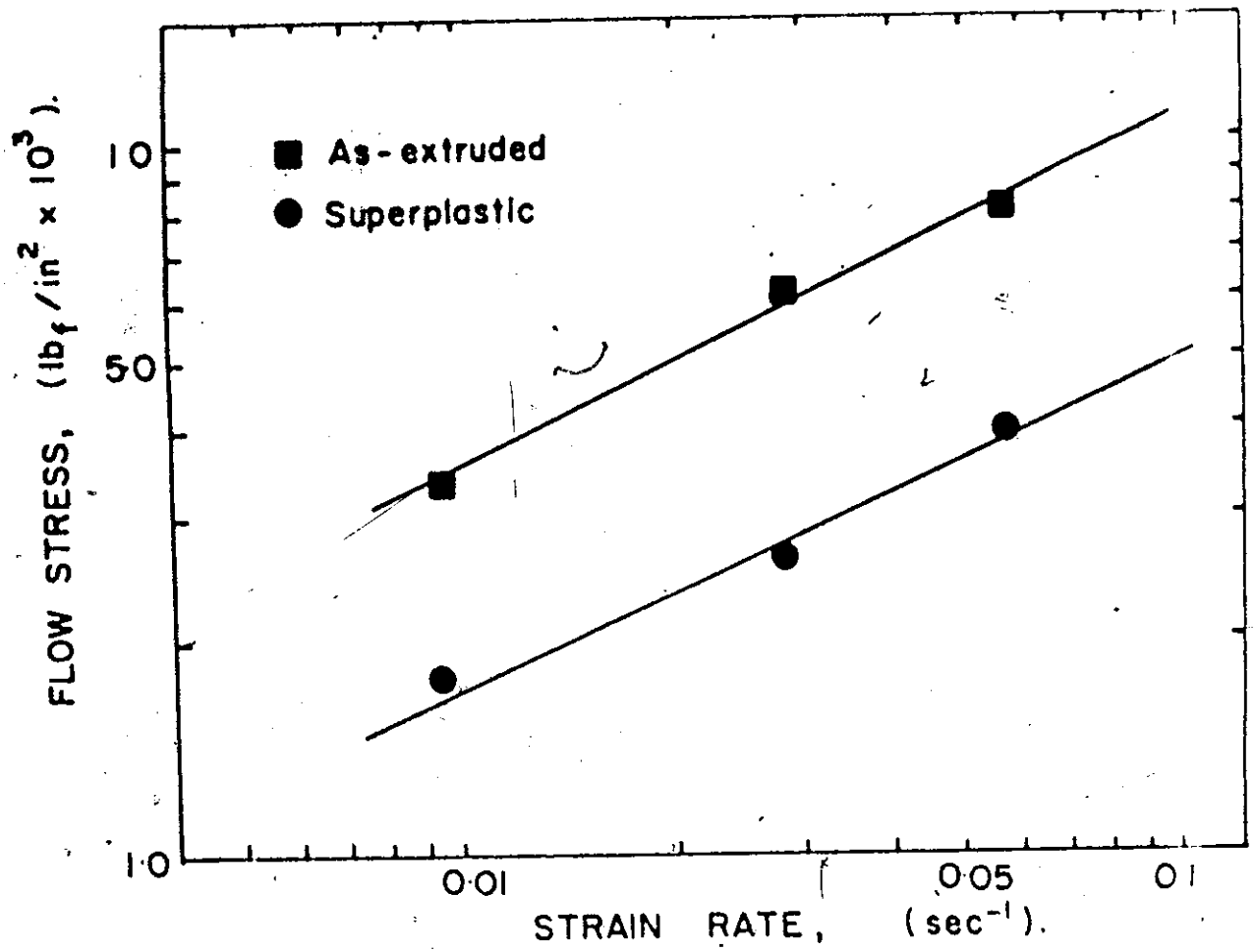

FIGURE 6.9

True stress and strain rate curves for the upsetting of the initial billet. ($\varepsilon = 0.3$)

It should be noted that the material, although both based on the eutectic Zn-Al, have different compositions. The continuously cast material is of the eutectic composition ie. 78% Zn - 22% Al, while the extruded rod contains 0.1% copper. This copper is added to improve the creep properties of the material.(43)

Micro-structure of the Alloys

Following the experiments, sections were cut from a number of the formed parts and the micro-structure examined. These photographs are presented in Figure 6.10 for the continuously cast material. Figure 6.10 a) is a photograph of the micro-structure of the heat treated specimen and the fine grain structure associated with the superplastic alloys is clearly visible. This compares with that of Figure 6.10 b) where the lamellar of the zinc rich phase are evident.

Figure 6.11 shows the micro-structure of two parts formed from the extruded material. Figures 6.11 a) and b) are for the heat treated sample in the direction of extrusion a) and transverse to the extrusion direction, b). It will be seen that there is no preferential grain orientation with respect to the extrusion direction. This is in contrast to Figures 6.11 c) and d) which are micrographs of the as-extruded material. Figure 6.11 c) is along the direction of extrusion and the elongation of the grains in the extrusion direction can be seen when this micrograph is compared with

Figure 6.11 a). Figure 6.11 d) is transverse to the rolling direction and this micro-structure is quite similar to that observed for the heat treated sample, Figure 6.11 b).

The directionality of the material properties of the as-extruded material is again indicated in the sequence of figures, 6.12, 6.13, 6.14, and 6.15. These photographs have been taken of the formed teeth from a number of parts.

Figure 6.12 is for the annealed cast material and Figure 6.13 is for the heat treated extruded material. The uniform deformation of the superplastic alloys can be seen from this comparison, where the grains of the annealed structure are shown deformed, while the grain structure of the superplastic alloy is unchanged. Figure 6.13 demonstrates that the micro-structure of the superplastic alloys is unaltered by deformation which is in direct contrast to that of the annealed or conventional alloy.

Figures 6.14 and 6.15 are for the extruded alloy and these photographs pose some very interesting questions concerning the mechanism of deformation and the nature of material flow.

6.4.2 Forging Tests

The results of the forging tests have been presented in Table 6-1. The load displacement diagram indicates that during the forging process there is a steady state during

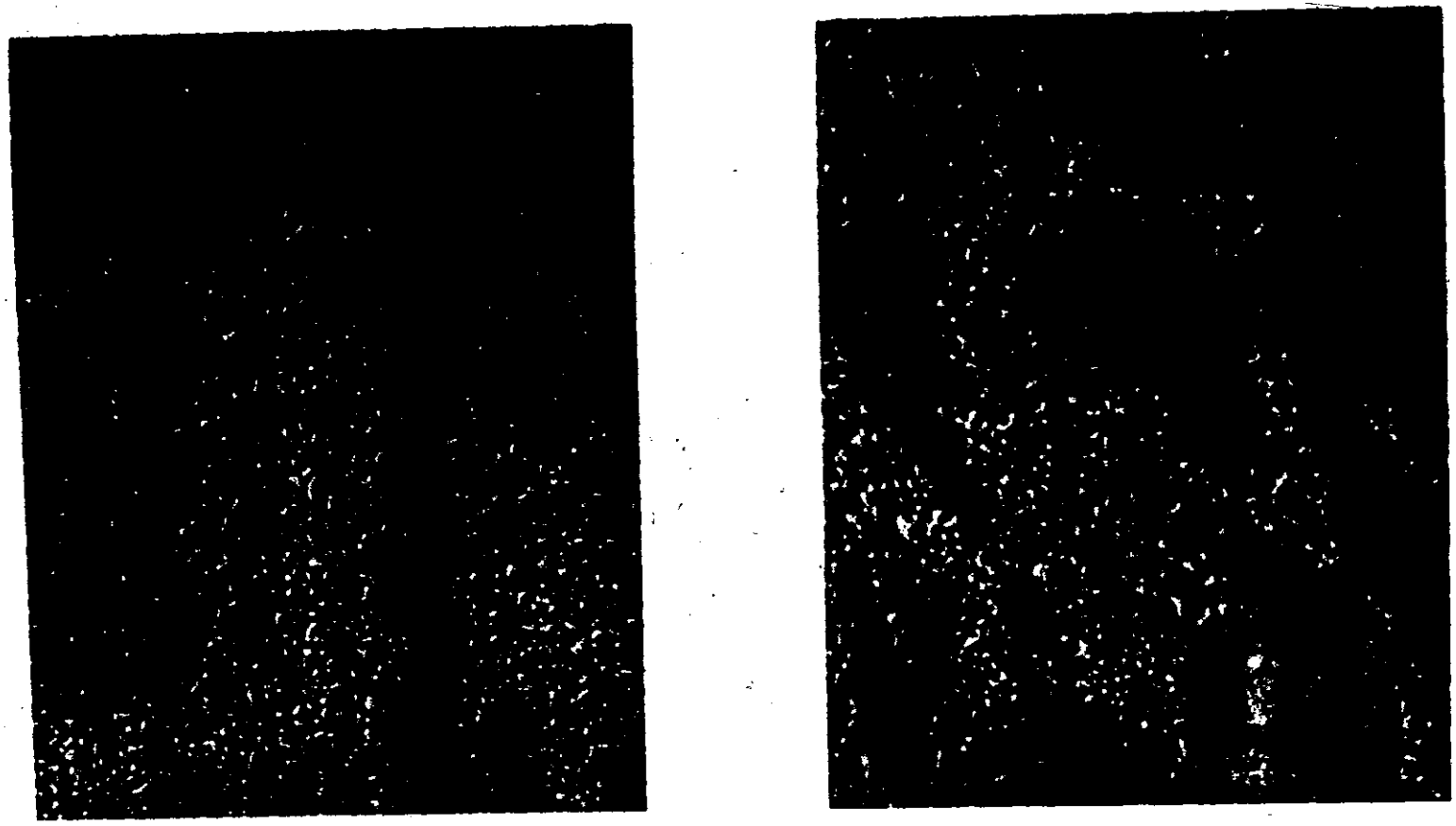

a) Superplastic.

10μ

b) As-cast.

FIGURE 6.10

Microstructure of the continuously cast material. (x 1000)

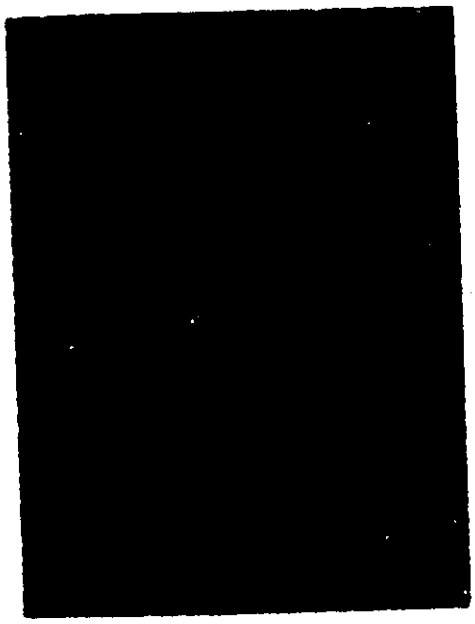

(a)

(b)

(C)

(d)

FIGURE 6 11

Microstructure of the extruded material (× 1000)

a) Superplastic – extrusion direction, b) Superplastic — transverse to the extrusion direction; c) As extruded – extrusion direction; d) As extruded — transverse to the extrusion direction.

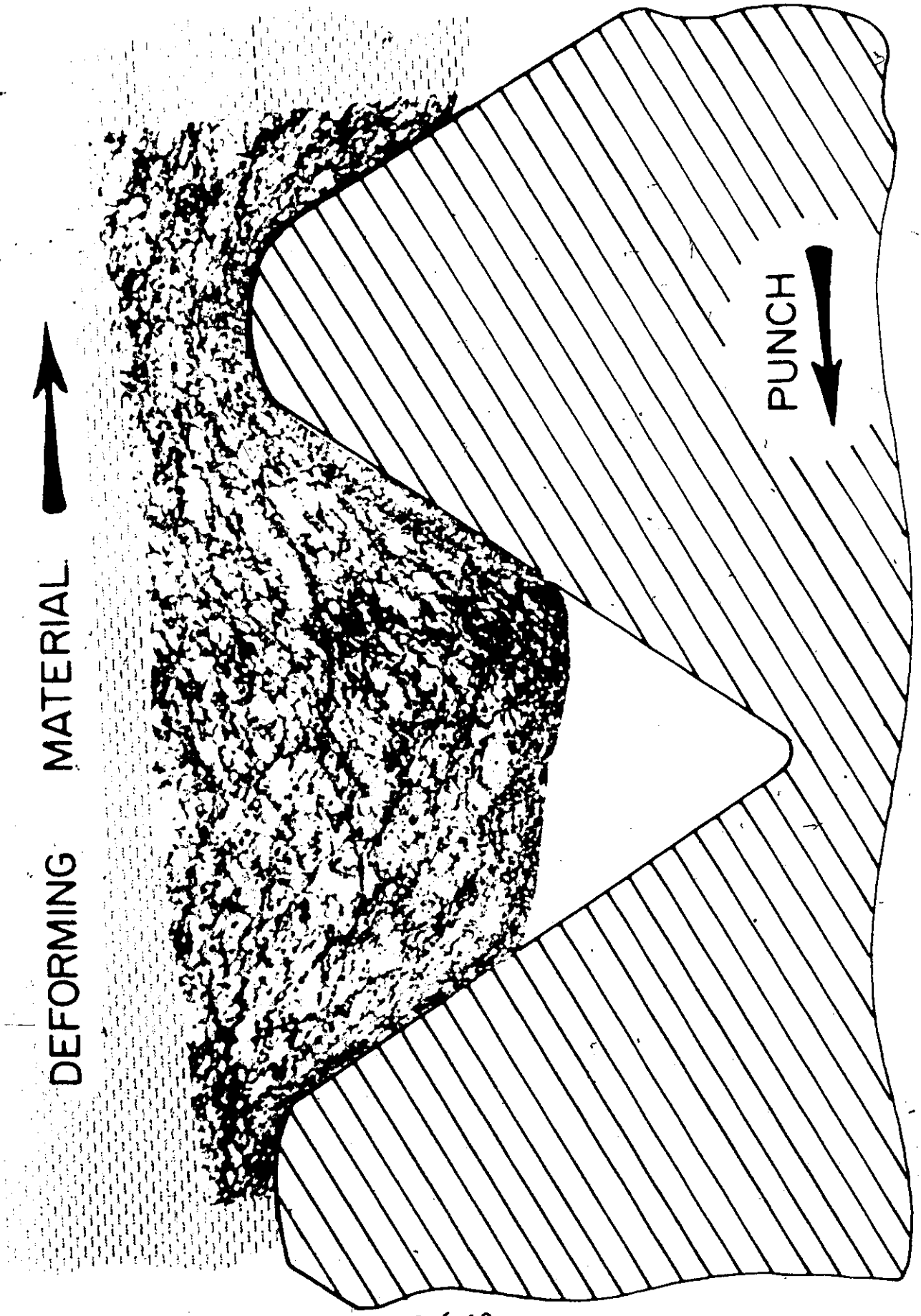

FIGURE 6.12

Micrograph of a forged tooth for the annealed material. (x50)

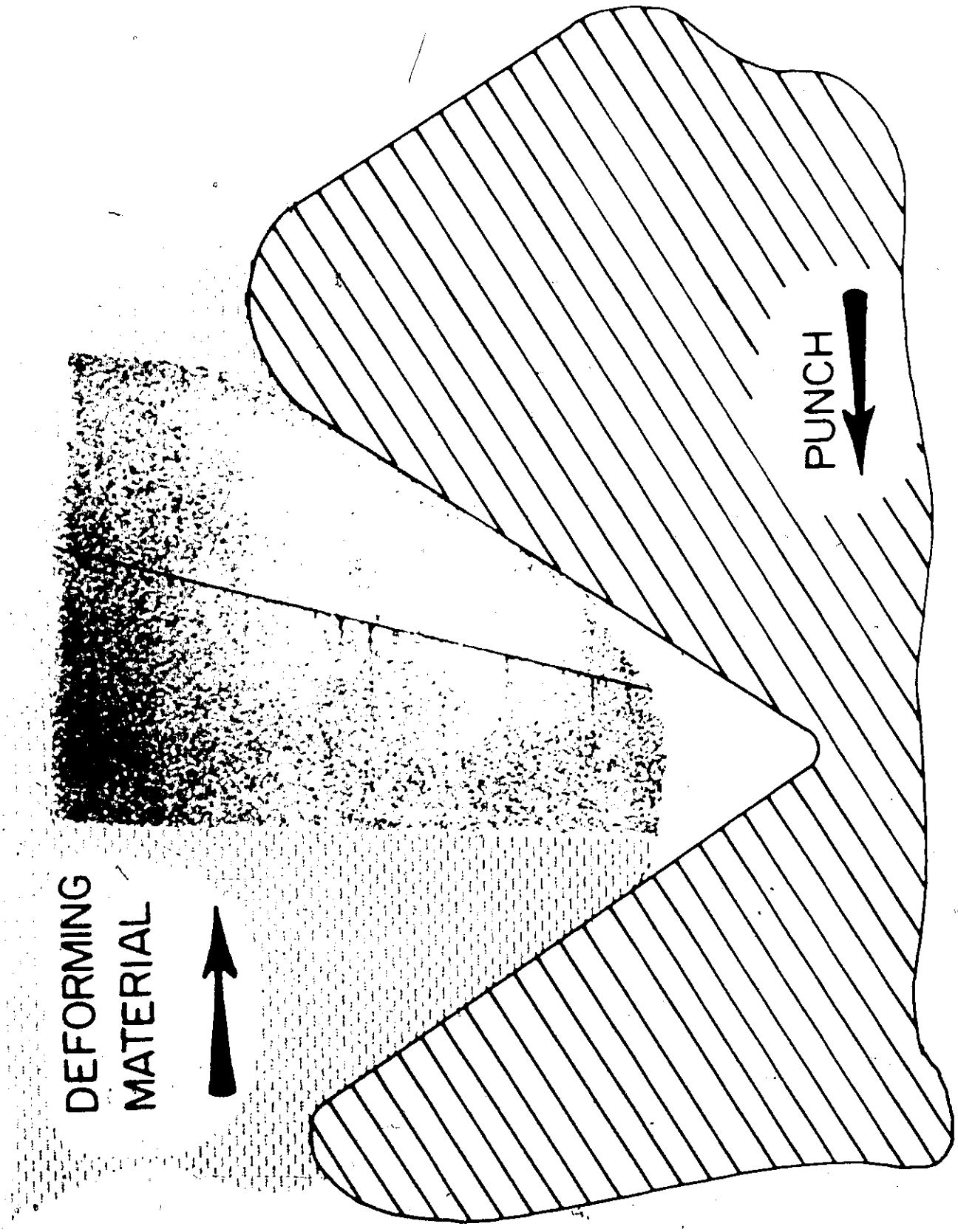

PIGURE 6.13

Micrograph of a forged tooth for the superplastic extruded material. (x50).

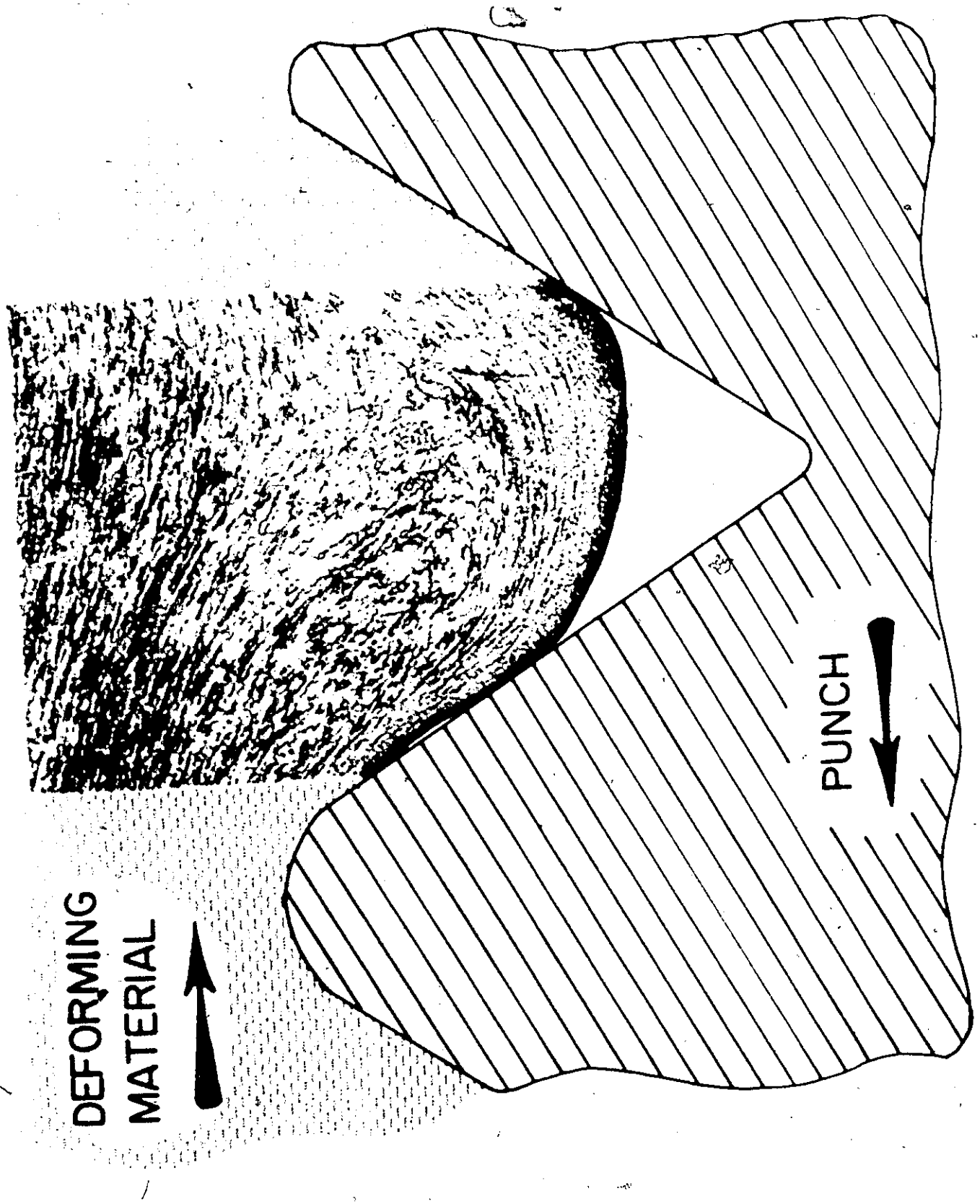

FIGURE 6.14

Micrograph of a forged tooth for the as-extruded material. (x50)

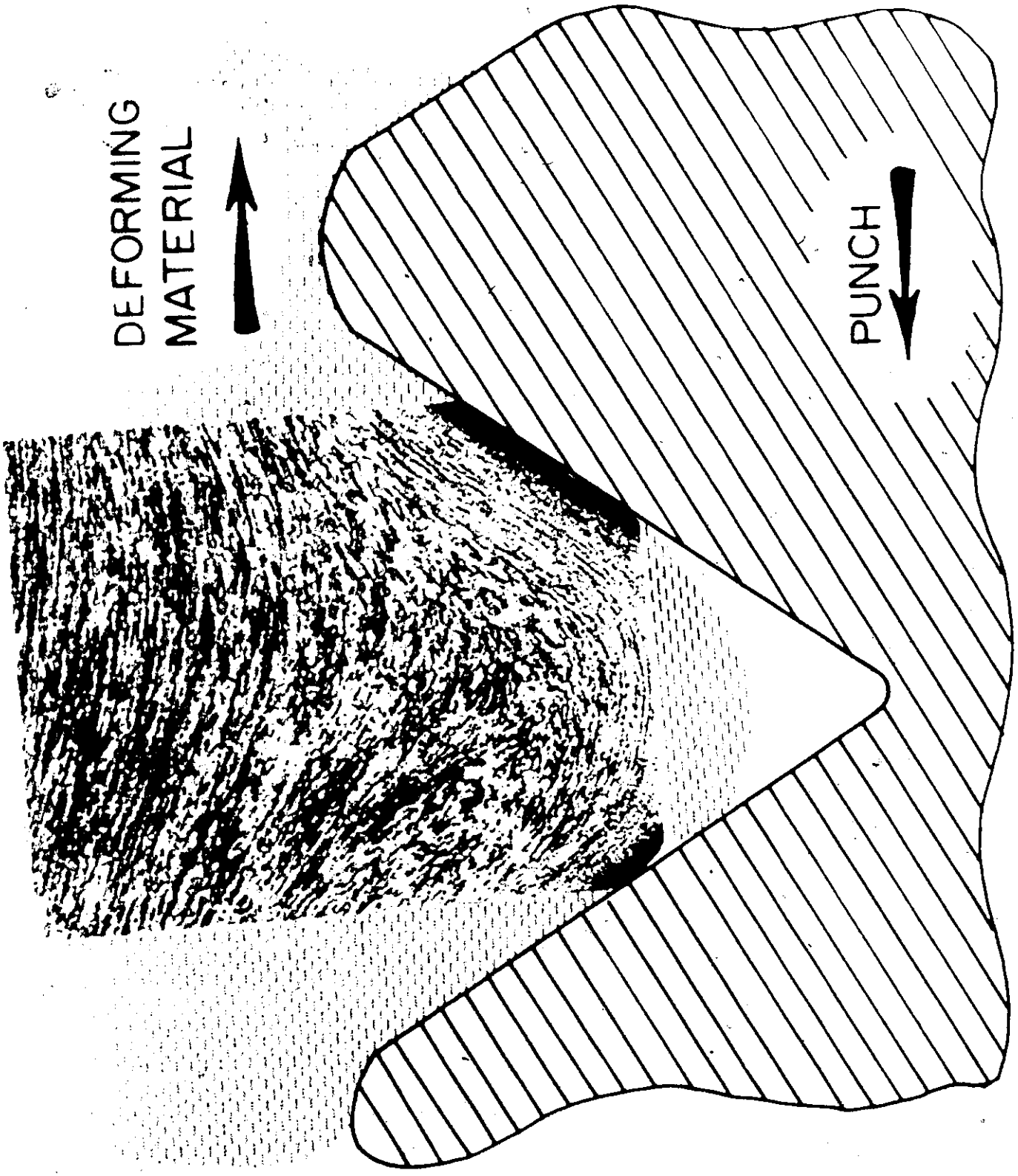

FIGURE 6.15

Micrograph of a forged tooth for the as-extruded material.(x50)

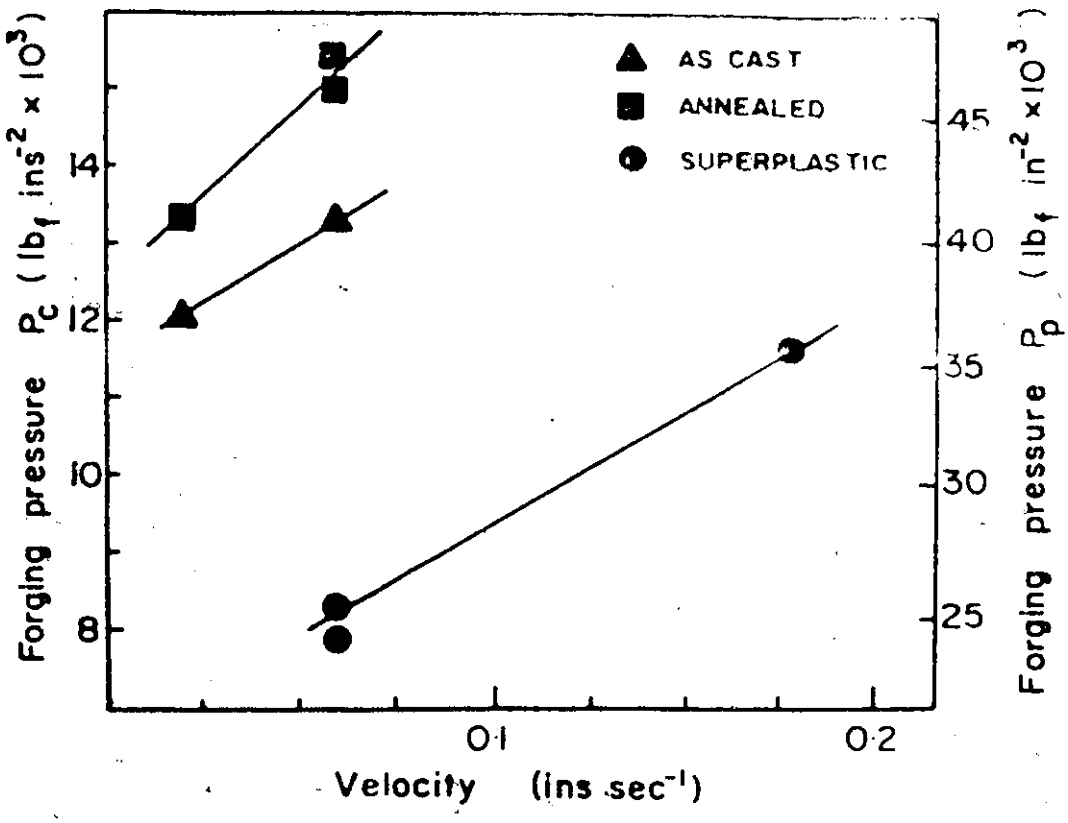

FIGURE 6.16

Forging pressure v's velocity for the cast material.

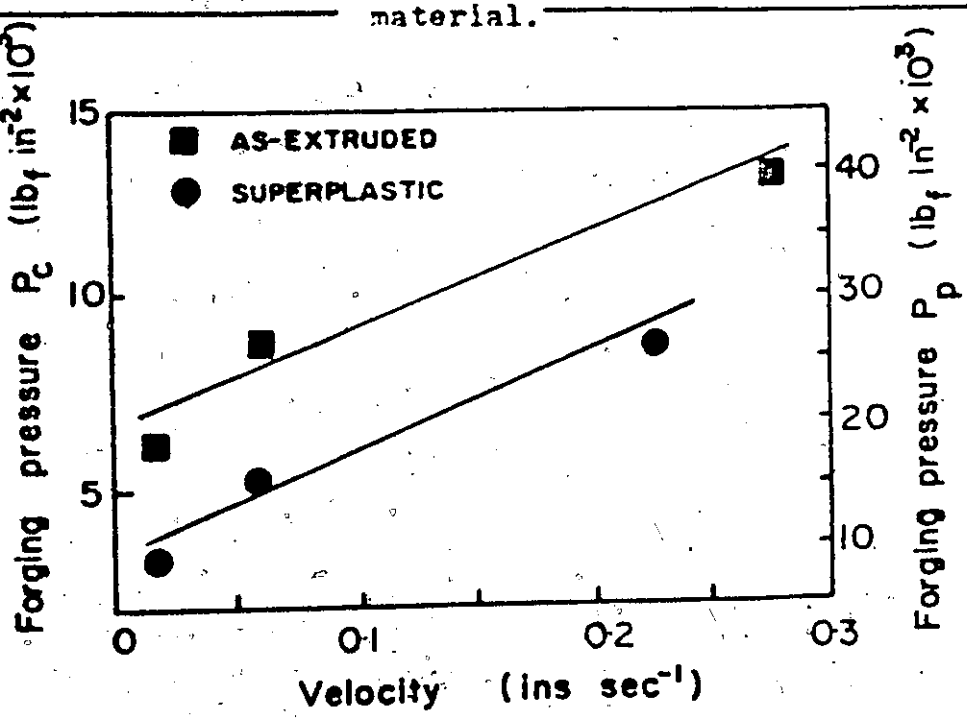

FIGURE 6.17

Forging pressure v's velocity for the extruded material.

which there is material flow under a constant load. This steady state has been observed by previous investigators.[38]

The steady state forging pressure can be defined in two ways dependent upon which area is taken,

$$P_c = \frac{\text{steady state load}}{\text{cross-sectional area of container}}$$

or

$$P_p = \frac{\text{steady state load}}{\text{cross-sectional area of punch}}$$

The forging pressure derived from the steady state portion of the load-displacement curves is plotted against punch velocity in Figure 6.16 for material from the cast stock and Figure 6.17 for material from the extruded stock. From these figures it can be seen that there is a significant difference between the forging pressures of the superplastic and annealed material. If the material is extruded and then heat treated, the percentage reduction of forging pressure compared with the forging pressure of the cast material which has been annealed is 300%.

It has been suggested that in the backward extrusion of superplastic alloys there exists a dimensionless extrusion parameter of the form

$$\phi = \frac{\bar{p}}{k\left\{\frac{v_e}{b}\right\}^m}$$

where v_e is the extrusion velocity

b is the depth of the billet at some instant

$\bar{p}$ is the mean extrusion pressure

k is the constant of the equation $\sigma = k\dot{\epsilon}^m$

m is the strain-rate sensitivity.

If the assumption is made that the mean value of the equivalent total strain is independent of the forging rate, then it has been shown[38] theoretically that this extrusion parameter, ϕ, is dependent only on the geometry of the die and the rate-sensitivity index.

Figures 6.18 and 6.19 are graphs of the extrusion parameter against the extrusion velocity. It would appear from the results that the extrusion parameter, ϕ, is not independent of the forging velocity and that, consequently, the total equivalent strain is not independent of the forging rate. That is, the initial assumption is incorrect and that the total equivalent strain is dependent on the extrusion rate, ie.

$$\varepsilon = f(v_e)$$

or

$$\varepsilon = f(\dot{\varepsilon})$$

This must mean that the mechanisms of deformation during the process are changing and that this must cause a change in the material parameters.

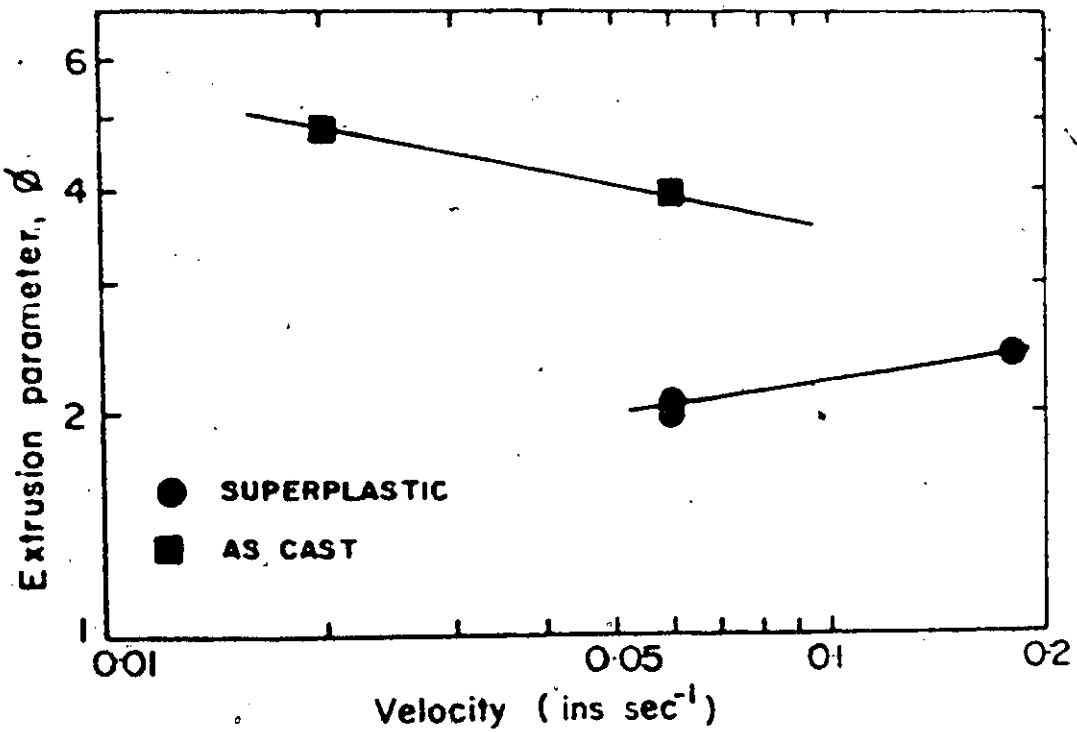

FIGURE 6.18

Variation of the extrusion parameter, Ø, with velocity for the cast material.

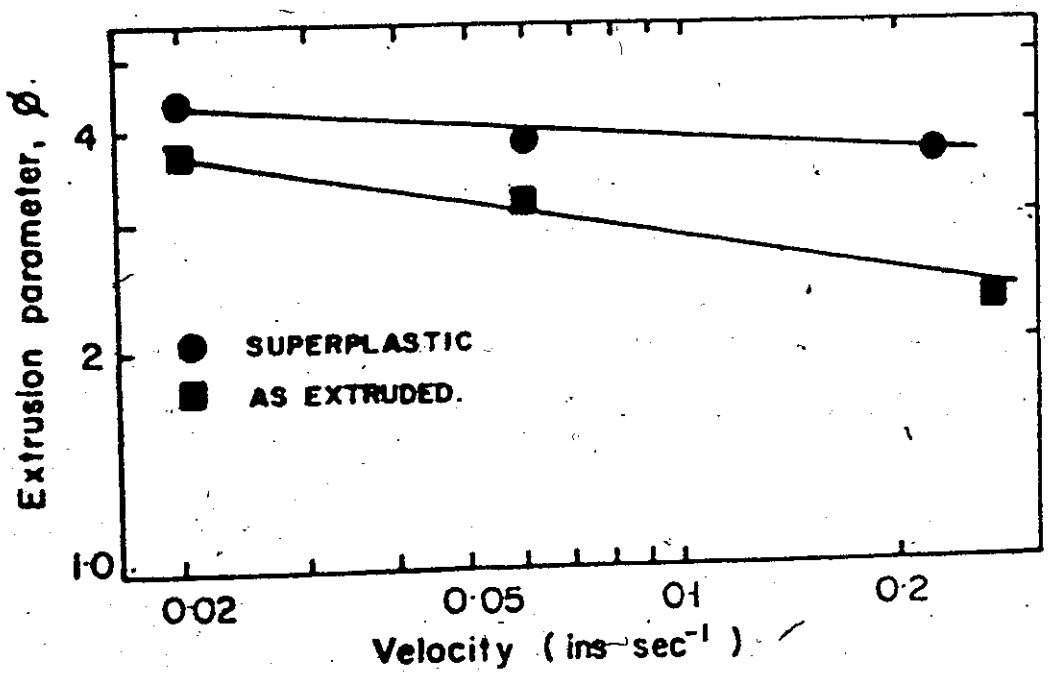

FIGURE 6.19

Variation of the extrusion parameter, Ø, with velocity for the extruded material.

6.5 Conclusions

From the work presented in this chapter it may be concluded that the two phase forging cycle could be of industrial importance in the forming of superplastic alloys. A very simple part has been produced and the results tend to illustrate that fine detail can be reproduced fairly quickly.

There are substantial reductions of the forging load. the industrial significance of this is that larger parts can be forged on existing presses without exceeding the capacity of the machine. This could prove especially usefull in the aircraft industry where precision forgings are produced from the exotic titanium alloys.

It has been shown that the extrusion parameter ϕ is not independent of the forging velocity as previously suggested(38). This would tend to indicate that the mechanics of deformation are dependent upon the rate of deformation.

The photographs of the microstructure of the parts produced from the as-extruded material have posed some interesting questions regarding the nature of the metal flow. Figure 6.14 is especially interesting in that there appears to be a vortex and associated flow stagnation. This type of flow is usually associated with the flow of viscous fluids. Whether this is a 'freak' occurrence or a genuine result for the forging is an obvious question. It would be interesting to examine a series of micrographs taken along a

complete section of forged thread to produce an exact picture of the metal flow. The flow visulization afforded by the extruded material could prove to be a usefull tool in the visulization of metal flow.

CHAPTER SEVEN

GENERAL CONCLUSIONS

The reader is referred to the latter sections of each chapter for a detailed analysis of the results. The following is a brief summary of the results presented in previous chapters.

The forming of a sheet of superplastic material into a long rectangular trough has been considered and a simplified analysis presented. Theoretical thickness distributions, dependent on the initial height to width ratio, have been presented in figures of the thickness ratio against an appropriate height parameter.

The forming of a sheet of superplastic material into a flat bottomed cylindrical cavity has been considered. The results of Cornfield and Johnson have been used in a semi-empirical analysis of the problem. The theoretical thickness profiles are compared with the results of experiments on parts which have been superplastically formed in zinc-aluminum sheet. The agreement between the theoretical and experimental distributions was close.

The forging of zinc-aluminum has been examined and experiments performed on the closed die forging of a simple part. Results have indicated that there are significant

load reductions if the material is superplastic. The forging is similar to the backward extrusion of a cup and it has been shown that the total equivalent strain in such a process is not independent of strain-rate, as previously thought.

A two-phased forging cycle was attempted where the bulk of deformation was achieved in a constant velocity stroke. This was followed by a period at constant load when material flowed into the detail of the die. The results indicate that such a process does improve the overall degree of forming, as expressed in the 'percentage of forming' of Table 6-1.

REFERENCES

1. W.A.Backofen, I.R.Turner and D.H.Avery, Trans. A.S.M. 57, 980 (1964)

2. J.L.Duncan, Metalworking Research Report No. 8, McMaster University, Hamilton (1973)

3. W. Rosenhein, J.K.Haughton and K.E.Bingham, J. Inst. Metals 23, 261 (1920)

4. C.E.Pearson, J. Inst. Metals 54, 111 (1934)

5. A.A.Bochvar and Z.A.Sviderskaya, Izu. Akad. Nauk SSSR 9, 821 (1945)

6. A.A.Presnyakov and V.V.Chervyakova, Izu. Akad. Nauk SSSR 3, 92 (1960)

7. A.A.Presnyakov and V.V.Chervyakova, Fiz. Mer. i Metallovedenia 8, 114 (1959)

8. The reader is referred to the paper by Underwood for a more complete listing of the Russian work.

9. E.E.Underwood, J. of Metals 14, 914 (1962)

10. D.H.Avery and W.A.Backofen, Trans. A.S.M. 58, 551 (1965)

11. D.L.Holt and W.A.Backofen, Trans. A.S.M. 59, 755 (1966)

12. P.J.Martin and W.A.Backofen, Trans A.S.M. 60, 352 (1967)

13. S.W.Zehr and W.A.Backofen, Trans. A.S.M. 61, 300 (1968)

14. R.H.Johnson, Met. Rev. 146, 115 (1970)

15. A.Ghosh and J.L.Duncan, Int. J. Mech. Sci. 12, 499 (1970)

16. T.H.Alden, Acta Metallurgica 15, 469 (1967)

17. C.M.Packer and O.D.Sherby, Trans. A.S.M. 60, 21 (1967)

18. F.Jovane, A.H.Shabaik and E.G.Thomson,
Trans A.S.M.E., 680 (1069)

19. L.T.Peng, Paper presented at Automotive Engineering Congress, Detroit (1970)

20. K.Nuttall, J. Inst. Metals 100, 114 (1972)

21. K.Nuttall, J. Inst. Metals 99, 291 (1971)

22. C.M.Packer, R.H.Johnson and O.D.Sherby,
Trans. Metall. Soc. A.I.M.E. 242, 2485 (1968)

23. J.A.Forster, S.R.Mogford, J.Grach and J.L.Duncan,
Metalworking Research Report No. 20 (1973)

24. D.Oelschlagel and V.Weiss,
Trans. A.S.M. 59, 143 (1966)

25. W.B.Morrison, Trans. A.S.M. 61, 423 (1968)

26. C.M.Packer and O.D.Sherby,
Trans. A.S.M. 60, 21 (1967)

27. D.Lee and W.A.Backofen,
Trans. Metall. Soc. A.I.M.E. 236, 1637 (1966)

28. N.J.Petch, J.I.S.I. 174. 25 (1953)

29. T.H.Thomsen, D.L.Holt and W.A.Backofen,
Metals Eng. Quart. 1, May (1970)

30. F.Jovane, Int. J. Mech. Sci. 10, 403 (1968)

31. D.L.Holt, Int. J. Mech. Sci. 12, 491 (1970)

32. G.C.Cornfield and R.H.Johnson,
Int. J. Mech. Sci. 12, 479 (1970)

33. J.Hestbech, E.W.Langer and A.Rosen,
J. of Inst. of Metals 99, 306 (1971)

34. T.Y.M.Al-Naib, Superplastic Forming of Zn-Al, Ph.D. Thesis
Univ. Manchester Inst. Sci. and Tech. (1971)

35. W.Johnson, T.Y.M.Al-Naib and J.L.Duncan,
J. Inst. of Metals 100, 45 (1972)

36. M.J.Stewart, Canadian Met. Quarterly 12, 2(1973)

37. K.K.Jain, M.Eng. Thesis McMaster University, Hamilton Canada (1972)

38. A.R.Ragab, Ph.D. Thesis McMaster University, Hamilton Canada (1973)

39. SPZ Mouldings In Focus, Publicity brochure by I.S.C. Alloys Ltd., Great Britain (1973)

40. I.B.M. Design Guide, The Promise of Superplasticity, Doc. EN.20.0276 July (1972)

41. A.R.Ragab and J.L.Duncan, to be published Int. J. Mech Sci.

42. R.A.Saller and J.L.Duncan, J. Inst. Metals 99, 173 (1971)

43. H.Naziri and R.Pearce, Int. J. Mech. Sci. 12, 513 (1970)

44. D.Lee, Acta Metallurgica 17, 1057 (1969)

45. R.C.Gifkins, J. Inst. Metals 95, 373 (1967)

46. R.H.Johnson, Metal Review 146, 115 (1970)

47. J.L.Duncan, Proc. Symp. "Fundamentals of Plasticity", Polish Academy of Sciences, Warsaw (1972)

48. W.A.Backofen, I.R.Turner and D.H.Avery, Trans. A.S.M. 57, 980 (1964)

49. G.J.Davies, J.W.Edington, C.P.Culter and K.Padmanabhan, J. of Mat. Sci. 5, 1091 (1970)

APPENDIX I

THICKNESS DISTRIBUTION RESULTS

Notation

h--current height

r--radius of die

h/r--height ratio

s_o--original thickness

s_e--edge thickness

s_e/s_o--thickness ratio

TEST NO. A304

Initial sheet thickness--0.076"

h	0.5	1	1.5	2	2.5	3	3.5	4	4.5
s_e	38	37	35	33	31	29	27	24	20
s_e/s_o	.5	.487	.461	.434	.408	.382	.355	.316	.263
h/r	.125	.25	.375	.5	.625	.75	.875	1.0	1.125

TEST NO. A401

Initial sheet thickness--0.076"

h	0.5	1	1.5	2	2.5	3	3.5	4	4.5	5
s_e	37	38	38	38	34	32	28	23	20	17
s_e/s_o	.487	.5	.5	.5	.447	.421	.368	.302	.263	.224
h/r	.125	.25	.375	.5	.625	.75	.875	1.0	1.125	1.25

TEST NO. A501.

Initial sheet thickness--0.074"

h	0.5	1	1.5	2	2.5	3	3.5	4	4.5	5	5.5
s_e	41	38	33	28	26	23	20	18	16	14	12
s_e/s_o	.554	.514	.446	.378	.351	.311	.270	.243	.216	.189	.162
h/r	.125	.25	.375	.5	.625	.75	.875	1.0	1.125	1.25	1.375

TEST NO. A504

Initial sheet thickness--0.074"

h	0.5	1	1.5	2	2.5	3	3.5	4	4.5
s_e	48	41	36	29	24	20	17	13	11
s_e/s_o	.649	.554	.486	.392	.324	.270	.230	.176	.149
h/r	.125	.25	.375	.5	.625	.75	.875	1.0	1.125

TEST NO. B301

Initial sheet thickness--0.073"

h	0.5	1	1.5	2	2.5	3	3.5	4	4.5
s_e	46	40	36	32	28	23	19	15	11
s_e/s_o	.630	.548	.493	.438	.384	.315	.260	.205	.151
h/r	.125	.25	.375	.5	.625	.75	.875	1.0	1.125

TEST NO. B303

Initial sheet thickness--0.078"

h	0.5	1	1.5	2	2.5	3	3.5	4
s_e	51	45	39	34	29	26	22	18
s_e/s_o	.654	.577	.5	.436	.372	.333	.282	.231
h/r	.125	.25	.375	.5	.625	.75	.875	1

TEST NO. B307

Initial sheet thickness--0.078"

h	0.5	1	1.5	2	2.5	3	3.5	4	4.5
s_e	47	43	40	35	30	27	22	18	13
s_e/s_o	.603	.551	.513	.449	.385	.346	.282	.231	.167
h/r	.125	.25	.375	.5	.625	.75	.875	1.0	1.125

TEST NO. B310

Initial sheet thickness--0.078"

h	0.5	1	1.5	2	2.5	3	3.5	4	4.5
s_e	39	40	38	36	33	29	25	20	16
s_e/s_o	.5	.512	.487	.462	.423	.372	.321	.256	.205
h/r	.125	.25	.375	.5	.625	.75	.875	1.0	1.125

A P P E N D I X II

FRACTURE THICKNESS RESULTS

Part No.	Original Thickness (Thou.)	Fracture Thickness (Thou.)	$\frac{t \text{ failure}}{t \text{ original}}$
A301	73	8	.110
A302	74	7	.095
A305	74	11	.149
B302	77	11	.143
B304	77	8	.104
B305	77	11	.143
B308	78	14	.179
B309	76	12	.158
A402	76	10	.132
A403	76	16	.211
A404	76	12	.157
B402	73	6	.082
B403	74	5	.068
B404	75	4	.053
A405	77	15	.195
A406	78	9	.115
A409	78	15	.192
A410	77	9	.117
A411	73	9	.123

A P P E N D I X III

UPSETTING RESULTS FROM LOAD DISPLACEMENT CURVES

B1

Displacement	0	0.2	0.4	0.6	0.8	1.0	1.2	1.4
Load lb_f	0	2400	2800	2400	2800	3200	4000	5600
Area in^2	1.23	1.31	1.41	1.52	1.65	1.81	2.0	2.24
Stress lb/in^2	0	1832	1986	1579	1697	1768*	2000	2500

B2

Load lb_f	0	3600	4000	4000	4400	4800	6000	8400
Stress lb/in^2	0	2748	2837	2632	2667	2652*	3000	3750

B3

Load lb_f	0	6400	6400	6600	6800	7200	8800	10400
Stress lb/in^2	0	4885	4539	4342	4121	3978*	4400	4643

B4

Load lb_f	0	4400	4800	4800	5200	6000	7200
Stress lb/in^2	0	3358	3404	3158	3152	3315*	3600

B5

Load lb_f	0	8000	8000	8800	9200	11200	13200	17600
Stress lb/in^2	0	6107	5674	5789	5576	6188*	6600	6929

B6

Load lb_f	0	10400	10800	11200	12000	12800	14400	16800
Stress lb/in^2	0	7939	7659	7368	7273	7072*	7200	6614

* These values of the stress and strain rate used in Figure 6.9.